Charles University

Faculty of Science

Molecular and Cellular Biology, Genetics and Virology

MSc. Diana Lustyk

Mouse hybrid sterility genes linked to chromosome X

Myší geny hybridní sterility vázané na chromozomu X

Doctoral thesis

Supervisor: Ing. Petr Jansa, CSc.

Prague, 2024

Declaration

I hereby declare that I wrote this thesis by myself, with all information sources and literature properly cited. Furthermore, I confirm that the entire content of this thesis, or any substantial part of it, has not been previously used to obtain the same or any other academic degree. I confirm that AI was used solely to enhance readability and language clarity.

Prague, 18 November 2024

Acknowledgements:

I am deeply grateful to my supervisor, Petr Jansa, for his invaluable patience, wisdom, and unwavering support, which have guided me through every stage of my scientific journey. His mentorship has been instrumental in shaping my skills and confidence as a researcher, and I am privileged to have learned from him.

This journey would not have been possible without the generosity and encouragement of Jiri Forejt, who welcomed me into his exceptional scientific team and shared his profound knowledge and insights.

My thanks also go to the entire Laboratory of Mouse Molecular Genetics and my colleagues from the BIOCEV Division - for making this journey so much more enjoyable.

Words cannot express my gratitude to my mother, Urszula, without whom I would not be who I am today. She stood by my side, believing in me and supporting me.

Finally, I am incredibly grateful to my husband, Ondrej, for his unwavering support through difficult times, and to my children, Natalie and Elliot, for their love.

Abstract

Speciation is the process by which new species arise. Allopatric speciation, the most common form of speciation, occurs when populations become geographically isolated, leading to reproductive isolation. One well-known example of an early postzygotic reproductive isolation mechanism is the Hybrid Sterility (HS). Hybrids between *Mus musculus domesticus (Mmd)* and *Mus musculus musculus (Mmm)* create a narrow hybrid zone across central Europe. The PWD wild-derived inbred strain (representing *Mmm*) and the B6 laboratory inbred strain (representing *Mmd*) provide a well-defined model for studying hybrid sterility. The (PWD x B6)F1 hybrid males are completely sterile, exhibiting smaller testes, no sperm in the epididymis, meiotic pachytene arrest, and high rates of asynapsed autosomes. The first hybrid sterility locus in vertebrates was mapped to chromosome 17 and named *Hybrid sterility 1 (Hst1)*, which was later identified as *Prdm9* gene. The *Prdm9*-interacting hybrid sterility locus, named the *Hstx2*, was mapped in (PWD x B6)F1 hybrids to a 4.7 Mb critical region (chr X: 64.88 – 69.58 Mb) on chromosome X. *Hstx2* harbors two additional factors responsible for spermiogenesis (*Hstx1*) and meiotic recombination rate (*Meir1*).

In this work, we aimed to contribute to the identification of the *Hstx2* candidate by developing new subconsomic strains containing only the minimal functional *Hstx2* region from the PWD strain on the genetic background of the B6 strain. We used classical genetic backcrossing and targeted recombination approach using the CRISPR-Cas9 system. The recombinant event narrowed the $Hstx2^{PWD}$ locus to 2.70 Mb region (chr X: 66.51 – 69.21 Mb). This redefined *Hstx2* locus remains the primary X-linked determinant of F1 hybrid sterility, regulating meiotic chromosome synapsis and meiotic recombination rates. However, even after extensive backcrossing, the 2.70 Mb $Hstx2^{PWD}$ interval behaved as a recombination cold spot.

We investigated the role of two *Hstx2* candidate protein-coding genes, *Fmr1nb* and *Fmr1* and microRNA Mir465. The newly generated knockout and transgenic models showed the importance of *Fmr1nb* in sperm development, particularly as a modifier of sperm head morphology. Additionally, we have revealed that *Fmr1* plays a key role in regulating meiotic crossover rate. Notably, neither *Fmr1* nor *Fmr1nb* alter the male sterility phenotype associated with meiotic arrest of the (PWD x B6)F1 hybrids. Overall, our findings, including microRNA expression profiling, suggest that the *Mir-465* cluster may be a major regulatory element within the *Hstx2* locus responsible for hybrid sterility of (PWD x B6)F1 males.

Abstrakt

Speciace je proces, kterým vznikají nové druhy. Alopatrická speciace, nejběžnější forma speciace, nastává, když se populace geograficky izolují, což vede k reprodukční izolaci. Dobře známým příkladem raného postzygotického mechanismu reprodukční izolace je hybridní sterilita (HS). Hybridi mezi poddruhy myši domácí *Mus musculus domesticus* (*Mmd*) a *Mus musculus musculus* (*Mmm*) vytvářejí úzkou hybridní zónu napříč střední Evropou. Inbrední kmen PWD odvozený z divokých populací (reprezentující *Mmm*) a laboratorní inbrední kmen B6 (reprezentující *Mmd*) poskytují dobře definovaný model pro studium samčí hybridní sterility. Samci hybridů (PWD × B6)F1 jsou zcela sterilní, mají menší varlata, žádné spermie v nadvarlatech, meiotickou pachytenní zástavu a vysokou míru nesynapsovaných autosomů. První lokus hybridní sterility obratlovců byl zmapován na chromozom 17 a pojmenován *Hybrid sterility 1* (*Hst1*), později pak byl identifikován jako gen *Prdm9*. *Prdm9* interagující lokus hybridní sterility, pojmenovaný *Hstx2,* byl zmapovaný u hybridů (PWD × B6)F1 do kritické oblasti o velikosti 4,7 Mb (chr X: 64,88 – 69,58 Mb.) na chromozomu X. *Hstx2* lokus obsahuje dva další genetické faktory odpovědné za spermiogenezi (*Hstx1*) a za míru meiotické rekombinace (*Meir1*).

Cílem této práce bylo přispět k identifikaci *Hstx2* kandidátního genu přípravou nových subkonsomických kmenů, které zahrnují pouze minimální funkční oblast *Hstx2* z kmene PWD na genetickém pozadí kmene B6. Použili jsme klasické genetické zpětné křížení a cílený přístup k rekombinaci pomocí systému CRISPR-Cas9. Výsledný rekombinant zmenšil lokus $Hstx2^{PWD}$ na 2,70 Mb (chr X: 66,51 – 69,21 Mb). Nově definovaný lokus *Hstx2* stále funguje jako hlavní faktor hybridní sterility vázaný na chromozom X, který také kontroluje synapsi meiotických chromozomů a míru meiotické homologní rekombinace. Navzdory dalším rozsáhlým křížením jsme v intervalu 2,70 Mb $Hstx2^{PWD}$ neidentifikovali žádnou další homologní rekombinaci, oblast byla proto pojmenována „rekombinační chladné místo".

V této práci nově definovaný minimální lokus *Hstx2* byl následně studován se zaměřením na roli dvou kandidátních *Hstx2* genů *Fmr1nb* a *Fmr1*. Připravené KO a transgenní myší modely ukázaly důležitost *Fmr1nb* ve vývoji spermií, zvláště jako modifikátoru morfologie hlavičky spermií. V případě genu *Fmr1* jsme odhalili jeho klíčovou roli v regulaci meiotického crossing-overu. Pozoruhodné je, že ani *Fmr1* ani *Fmr1nb* nemění fenotyp samčí sterility spojený s meiotickou zástavou hybridů (PWD × B6)F1. Celkově naše nálezy, spolu s

profilováním exprese micro RNA genů, naznačují, že klastr *Mir-465* může být hlavním regulačním prvkem lokusu *Hstx2* odpovědným za hybridní sterilitu u samců (PWD × B6)F1.

Table of contents

Abstract 4
Abstrakt 5
Introduction 9
Species formation (speciation) 9
The Dobzhansky-Muller Incompatibility model 11
Sex chromosomes in speciation 11
Hybrid sterility and the house mouse model 13
Mammalian meiosis 17
Prophase I of meiosis 18
Sex chromosomes paring and silencing 22
Genetic architecture of hybrid sterility model 23
Material and methods 28
Mouse maintenance 28
DNA isolation, genotyping and sequencing 28
RNA isolation, reverse transcription, and quantitative real-time PCR 30
microRNA isolation and expression 32
Protein isolation and Western Blotting 34
Testis single-cell suspension, chromosome spreads and immunofluorescence microscopy 35
Histology: Hematoxylin and Eosin (H&E) staining, immunohistochemistry, and TUNEL assay of testes 36
Generation of new mouse lines 37
Construction of *Fmr1nb*-specific TALENs and generation of the *Fmr1nb*-KO mouse line .. 37
Design of *Fmr1*-specific CRISPR/Cas9 sgRNAs and generation of the *Fmr1*-KO mouse line 37
Generation of transgenic mouse lines B6-Tg(*Fmr1,Fmr1os,Fmr1nb*) and B6-Tg(XG20) with the BAC DNA clones 38
Hypothesis and aims of the thesis 40
Results 41
Hstx2 locus as a recombination cold spot 41
Targeting homologous recombination at *Hstx2* using CRISPR/Cas9 42
Phenotypes of newly defined *Hstx1*, *Hstx2* and *Meir1* loci 43
Hstx1 fertility phenotype 43
Hstx2 fertility and meiotic chromosome asynapsis phenotypes 45

Meir1 controls global meiotic recombination rate 48
Analysis of the candidate genes 50
Generation and confirmation of the *Fmr1nb* deletion line 53
Phenotypes of B6.DX.1s$^{Fmr1nb-}$ males 55
Generation and confirmation of the *Fmr1* null line 60
Phenotypes of B6.DX.1s^{Fmr1-} males 62
Tg(*Fmr1,Fmr1os,Fmr1nb)* transgenic lines phenotypes 65
MicroRNA expression profiling 70
Summary of hypotheses and objectives 73
Discussion 75
Interplay between PRDM9 and *Hstx2* in hybrid sterility 75
Hstx2 locus as a recombination cold spot 76
Role of candidates' gene *Fmr1nb* and *Fmr1* in male fertility 77
Mir465 cluster copy number variation within the *Hstx2* locus 78
Conclusions 78
Publications and author contributions 80
List of figures 81
List of tables 83
References 84

Introduction

Species formation (speciation)

The wide range of living organisms on Earth is the result of speciation, the process by which new species develop over time. For decades, speciation and its mechanisms have been a key focus for evolutionary biologists, including Charles Darwin who proposed the concept of natural selection as the main force in the evolution of species (Darwin, 1859). Speciation is an evolutionary process in which one population gives rise to two or more distinct populations through the accumulation of genetic differences, which eventually lead to reproductive isolation between these populations and the formation of new species. This process is essential for biodiversity, as it allows populations to evolve in separate ways in response to environmental changes or random genetic variations, leading to the vast variety of life forms we see today.

The most common form of speciation, allopatric speciation, occurs when a population is geographically split. During the independent evolution of the separated populations, genetic differences accumulate due to mutations, natural selection, and genetic drift. Over time, as the populations become more genetically distinct, they may evolve partial or complete reproductive isolation. If secondary contact between these isolated populations occurs and they are no longer able to produce fertile offspring, this reproductive barrier leads to the formation of new species (Dobzhansky, 1935). According to Ernst Mayr, a species is defined as a group of "actually or potentially interbreeding populations which are reproductively isolated from other such groups" (Mayr, 1963).

Genetic mechanisms play a crucial role in speciation. In isolated populations, random genetic mutations may lead to the formation of new traits that, in turn, may contribute to reproductive isolation. Natural selection may also favor traits that help populations adapt to different environments. Another genetic mechanism, genetic drift, leads to the fixation of one allele variant at the expense of other allele variants, which are gradually eliminated, further contributing to the genetic divergence of populations. The genetic loci that help the development of new species are often referred to as “speciation genes” (Gavrilets, 1997; Orr, 1995; Turelli and Orr, 2000).

The theory of speciation has been influenced by the concept of reproductive isolation, which refers to the reproductive barriers that prevent different populations from interbreeding.

These barriers can be either pre-zygotic, preventing mating and fertilization (e.g., differences in mating behaviors or physical incompatibility), or post-zygotic, which occur after mating and fertilization and result in hybrid inviability or sterility (Coyne and Orr, 2004; Orr and Presgraves, 2000). Postzygotic isolation mechanisms prevent or vastly diminish gene flow between populations even when mating occurs, ensuring that species remain distinct.

One well-known example of a postzygotic reproductive isolation mechanism is the infertility of interspecific hybrids, a phenomenon documented since Aristoteles. A classic example is a mule, a sterile hybrid of a horse and a donkey. According to Dobzhansky, hybrid sterility occurs when two fertile parental species, each of which is fertile, produce a progeny that is sterile (Dobzhansky, 1937). This mechanism results in viable hybrids that are unable to reproduce due to gene incompatibilities or chromosomal differences between the parental species.

According to the first hypothesis on genetic control of hybrid sterility, known as Dobzhansky–Muller incompatibility (Dobzhansky, 1936; Muller, 1942), two or more independently evolving genes may interact epistatically, resulting in a loss of cooperation when combined in a hybrid. The early works by Dobzhansky laid the foundation for modern evolutionary biology, helping us to understand how new species arise.

Since the pioneering work of Theodosius Dobzhansky's on speciation and reproductive isolation in the 1930s, many prominent evolutionary biologists and geneticists have contributed to our understanding of speciation. With the development of modern molecular biology methods and the genome sequencing of many organisms, evolutionary biologists have focused on the genetic and genomic aspects of reproductive isolation barriers, particularly hybrid sterility (Naveira, 1998; Orr and Presgraves, 2000; Coyne and Orr, 2004; Maheshwari and Barbash, 2011; Schilthuizen et al., 2011; Mack and Nachman, 2017). With the availability of genomic databases, scientists have studied the genetic basis of hybrid sterility in two classic model organisms, leading to the identification of the first hybrid sterility genes in *Drosophila* (Ting et al., 1998; Masly et al., 2006; Phadnis and Orr, 2009), and in the house mouse (Mihola et al., 2009).

Extensive genetic research on species like yeast, fruit fly, or house mouse has been conducted, yet the genetic basis and molecular mechanisms underlying hybrid sterility are still not well understood (Maheshwari and Barbash, 2011; Mack and Nachman, 2017).

The Dobzhansky-Muller Incompatibility model

The Dobzhansky–Muller incompatibility (DMI) is a genetic model proposed to explain how reproductive isolation evolves between two populations. It is based on epistatic interactions between at least two loci or genes. Specifically, the DMI model explains a situation where two populations diverge from a common ancestor with the genotype *AABB*. Mutations may arise in gene A, and the mutated *a* allele becomes fixed in one population, resulting in the genotype *aaBB*. In contrast, gene B mutates, and the allele *b* becomes fixed in the second population, resulting in the genotype *AAbb*. These mutations may function well within their respective parental genetic background, but it is uncertain whether the mutated alleles *AaBb* will interact properly in hybrid progeny (Figure 1) (Orr, 1995; Coyne and Orr, 1998; Presgraves, 2013).

The key feature of this model is that the newly established mutations are not harmful within the populations where they arise, but problems occur when these populations interbreed. The hybrid offspring may experience incompatibilities due to the failure of the mutated alleles to interact properly (Wu and Ting, 2004).

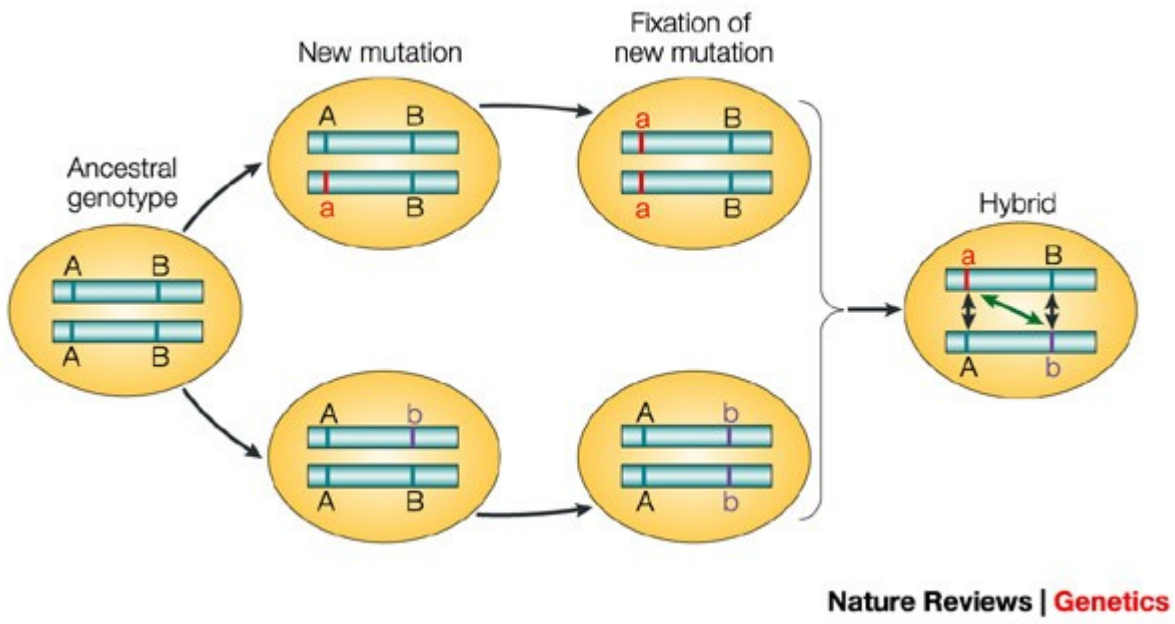

Figure 1. Dobzhansky-Muller model of hybrid incompatibility (Wu and Ting, 2004).

Sex chromosomes in speciation

Sex chromosomes play a significant role in speciation, particularly in hybrid sterility. This is more likely to occur in the heterogametic sex due to the presence of deleterious alleles

of X-linked genes (the large-X effect), and the rapid evolution of sex chromosomes. Observation of offspring from interspecific hybridizations has led to the formulation of the two rules of speciation.

The first rule observed at hybrid sterility, formulated by J. B. S. Haldane, states that in the hybrid offspring of two different animal species or subspecies, the sex that is absent, rare, or sterile, is the one with two different sex chromosomes (the heterogametic sex) (Haldane, 1922; Schilthuizen et al., 2011). In mammals and *Drosophila,* where males have XY chromosomes, hybrid male sterility is observed. In contrast, in birds, where females have ZW chromosomes, females tend to be sterile. This occurs because the heterogametic sex has only one copy of each sex chromosome and thus cannot "mask" the effects of deleterious alleles with a second, healthy copy. Haldane's rule is universal as it is observed across many taxa, such as insects, birds, fish, mammals, and plants, and often represents an intermediate stage before complete hybrid incompatibility (Coyne and Orr, 1998). This highlights the crucial role of sex chromosomes in speciation.

The other rule is known as the large X-effect (also known as Coyne's rule), which refers to the disproportionately large role of the X chromosome in reducing hybrids fitness (Presgraves, 2008; Charlesworth, 2015). In many species, genes on the X chromosomes are more often involved in incompatibility, leading to reproductive isolation. If the X-linked incompatibility is recessive, it tends to be more harmful to the heterogametic sex (Turelli and Orr, 1995; Laurie, 1997; McDonough et al., 2024). One explanation for this is that X chromosome accumulates mutations more rapidly than autosomes. The heterogametic sex (XY) has only one X chromosome and harmful alleles can be fixed faster in the absence of a second X chromosome. On the other hand, if the mutation is dominant, the homogametic sex (XX) will suffer more, as the dominant allele is always expressed (Orr, 1993). Additionally, the X chromosome is heavily involved in reproduction and fertility within species, and changes to its genes are a key to reproductive barriers (Charlesworth et al., 1987; Forejt, 1996; Coyne and Orr, 2004; Good et al., 2008; Presgraves, 2008).

To conclude, the study of the X chromosome has provided insights into the mechanisms of reproductive isolation and hybrid sterility. The unique characteristics of the X chromosome, including its rapid evolution and X-linked genes role in reproduction, make it a key player in the formation of new species.

Hybrid sterility and the house mouse model

Hybrid sterility is a form of postzygotic reproductive barrier that prevents gene flow between hybrids and their parental strains, as hybrids are unable to reproduce. This mechanism helps maintain species boundaries and contributes to speciation.

Most of our current knowledge about hybrid sterility in the animal kingdom has been gained from studies on *Drosophila* and house mouse. However, hybrid sterility has been observed in many other eukaryotic species, including yeast, plants and birds (Presgraves, 2003; Coyne and Orr, 2004; Maheshwari and Barbash, 2011; Forejt et al., 2021). Although hybrid sterility is generally a polygenic trait involving interactions between many genes, several key hybrid sterility genes have been identified in *Drosophila*, including *OdsH*, *Hmr*, *Nup96*, *JYAlpha*, *Ovd* (Ting et al., 1998; Barbash and Ashburner, 2003; Presgraves, 2003; Masly et al., 2006; Phadnis and Orr, 2009).

In mammals, the first hybrid sterility genetic locus, *Hst1*, was discovered and mapped in hybrids between the *Mus musculus musculus* and *Mus musculus domesticus* subspecies of the house mouse. This locus was later identified as the *Prdm9* gene (Forejt and Iványi, 1974; Mihola et al., 2009).

The hybrid sterility genes play crucial roles in reproductive processes such as sperm formation, meiosis, and nuclear transport. The discovery of these genes has helped our understanding of the molecular mechanisms underlying hybrid sterility. However, as more speciation genes are discovered, our understanding of the complex epistatic interactions involved in hybrid sterility will continue to improve.

Today, house mouse (*Mus musculus*) is widely used as a model system in many laboratories around the world in genetics and biomedical research. Due to their ease of maintenance, the availability of well-defined inbred strains and well-established genetic tools for manipulating the mouse genome, they serve as an ideal model organism for laboratory studies. Currently, three main lineages of *Mus musculus* are recognized: the Western house mouse (*Mus musculus domesticus)*, the Eastern house mouse (*Mus musculus musculus),* and the Southeast Asian house mouse (*Mus musculus castaneus).* These subspecies share a common ancestor and began diverging approximately 350 000 to 500 000 years ago (She et al., 1990; Boursot et al., 1996; Geraldes et al., 2008), evolving in response to different environmental and geographic pressures. As they spread and adapted to new habitats,

M.m.musculus and *M.m.domesticus* colonized Europe via distinct geographic pathways (Figure 2) (Didion and de Villena, 2013; Phifer-Rixey and Nachman, 2015).

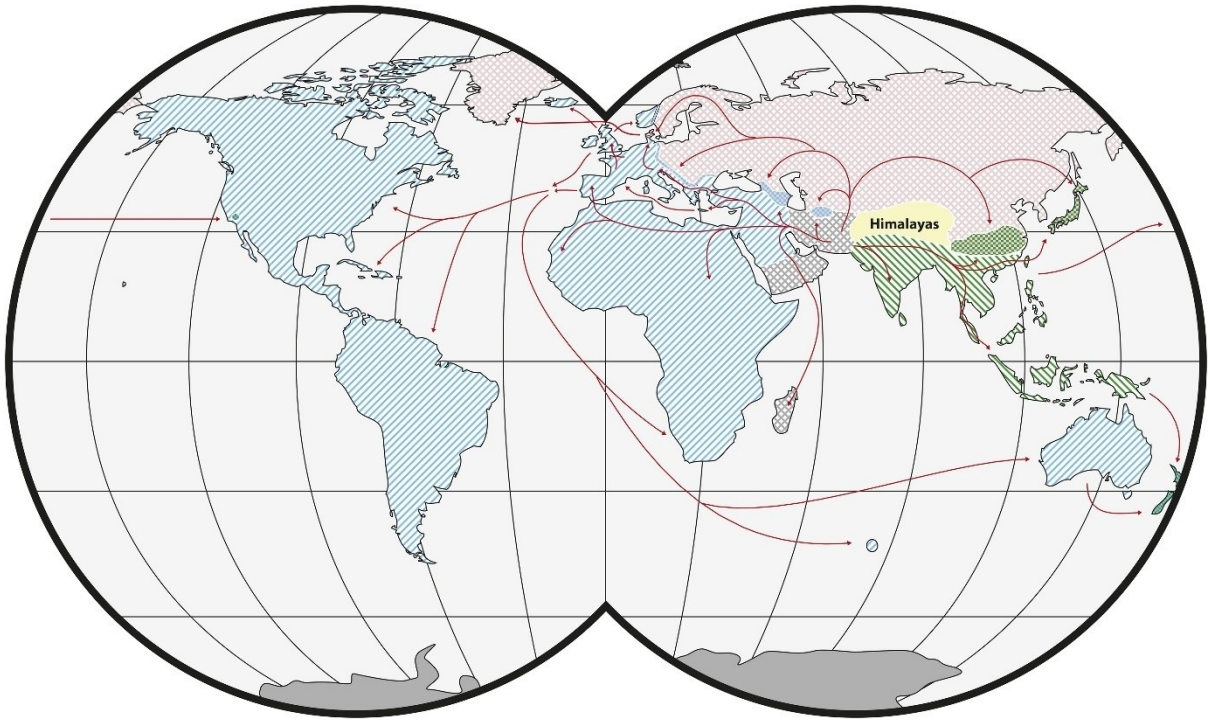

Figure 2. Worldwide distribution of *Mus musculus* subspecies (Phifer-Rixey and Nachman, 2015).

The distribution of *M. musculus* subspecies is represented using hatching patterns: green for *M.m.castaneus*, blue for *M.m.domesticus*, red for *M.m.musculus*, and grey for central populations and *M.m.gentilulus*. Areas with checkered patterns indicate regions of hybridization. Red arrows illustrate the inferred pathways of historical migrations as well as recent movements linked to human activity.

The two subspecies later made secondary contact in a narrow hybrid zone across central Europe, running northwest from Bulgaria to Denmark (Figure 3) (Baird and Macholán, 2012; Janoušek et al., 2012). Hybrid zones are key regions for studying the genetic basis of reproductive isolation in nature, as they allow us to observe the effects of interbreeding between subspecies. These two subspecies evolved independently, accumulating genetic mutations. After secondary contact, their interbreeding has resulted in reduced fertility in hybrid males. Reduced male fertility has been observed both in hybrid wild mice (Payseur et al., 2004; Vyskočilová et al., 2005; Macholán et al., 2007; Teeter et al., 2010) and in hybrids of wild-derived laboratory inbred strains (Forejt and Iványi, 1974; Forejt, 1996; Gregorová and Forejt, 2000; Vyskočilová et al., 2005; Forejt et al., 2021). Genome-wide research in mice from the hybrid zone reveled that male fertility is controlled by many genes, with the X chromosome having bigger effect than others (Janoušek et al., 2012; Turner, 2015).

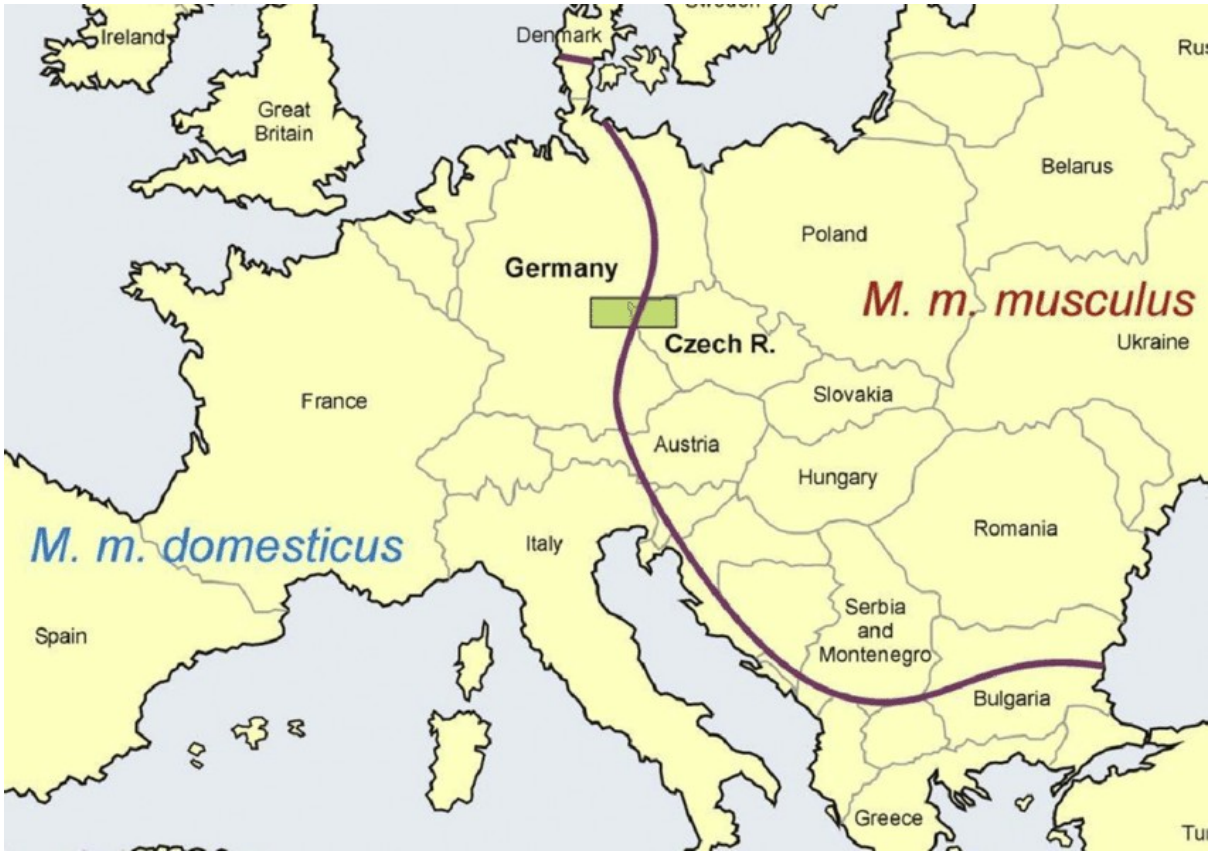

Figure 3. A map of *Mus musculus* subspecies hybrid zone across Europe (Macholán et al., 2008)

Both classical laboratory strains and wild-derived laboratory strains serve as a model for hybrid sterility in wild mice. In our laboratory, we have been using the C57BL/6 laboratory strain (hereafter B6), representing 90% of the *M.m.domesticus* genome, and the PWD/PhJ wild-derived strain (hereafter PWD), representing the *M.m.musculus* genome, as a model system to study mammalian hybrid sterility (Forejt, 1996; Gregorová and Forejt, 2000). Genetic studies using these two strains are more manageable due to their controlled, homozygous genetic backgrounds, which eliminate variability and allow us to focus on investigating specific genetic interactions responsible for hybrid sterility. This laboratory model enables us to generate identical hybrid crosses multiple times, ensuring consistent and reproducible results. Furthermore, the genomes of laboratory strains have been sequenced and are well-characterized (Waterston et al., 2002; Keane et al., 2011; Skarnes et al., 2011), which helps us to compare the genomes of both subspecies to better understand the development of reproductive barriers.

Hybrid sterility between the subspecies *Mus musculus musculus (Mmm)* and *Mus mus domesticus (Mmd)* was first documented by Forejt and Ivanyi (1974) who observed male sterility traits in hybrids between the *Mmd* laboratory strain (C57BL/10) and wild-caught *Mmm*

individuals. This initial discovery laid the foundation for the subsequent genetic research on hybrid sterility in mice.

Hybrids between the PWD wild-derived inbred strain (representing *Mmm*) and B6 laboratory inbred strain (representing *Mmd*) serve as a reliable, reproducible, and genetically well-characterized model for studying hybrid sterility. One of the key features of this model is the contrasting outcomes of male sterility depending on the direction of the cross. In the (B6 × PWD)F1 hybrids (the first parent in the cross is female), spermatogenesis shows an incomplete arrest where reproductive processes are disrupted, but those males are not entirely sterile. In contrast, the reciprocal (PWD × B6)F1 hybrid males are completely sterile (Figure 4) (Storchová et al., 2004; Forejt et al., 2012). This difference suggests that certain genetic factors linked to chromosome X play a key role in the process of hybrid sterility.

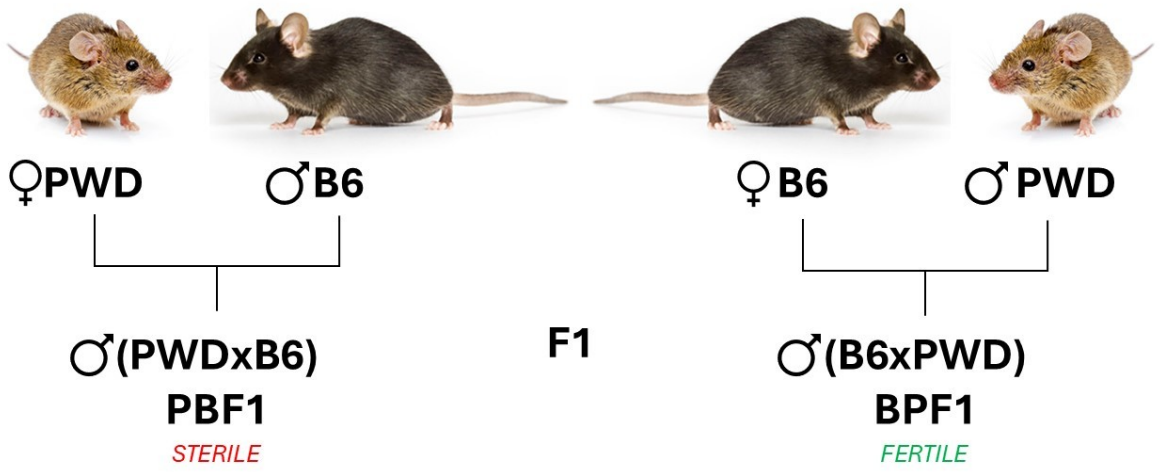

Figure 4. Mouse crossing diagram for hybrid sterility between PWD and B6 strains.

The (PWD x B6)F1 hybrid males are completely sterile, exhibiting smaller testes and no sperm in the epididymis. Therefore, they are unable to produce any offspring. Examination of their seminiferous tubules revealed pachytene meiotic arrest, with no cells present beyond the prophase I meiotic stage and an absence of sperm, as previously described (Forejt and Iványi, 1974; Gregorová and Forejt, 2000; Storchová et al., 2004). The observed meiotic pachytene arrest in (PWD x B6)F1 hybrids males highlights the essential role of proper meiotic progression for fertility. Dissecting the genetic basis of hybrid sterility should reveal critical

molecular mechanisms of meiotic progression, failure of which leads to reproductive isolation and speciation.

Mammalian meiosis

In sexually reproducing organisms, meiosis plays a critical role in providing offspring with a unique mix of genetic material inherited from each parent. The unique genetic variations transmitted into individual progeny are fundamental for both genetic diversity inside a population and for the process of evolution. Two meiotic processes are essential for this: homologous recombination and independent assortment of chromosomes. Crossing over between homologous chromosomes ensures the exchange of genetic material, resulting in novel allele combinations. At the same time, independent assortment ensures that individual chromosomes are randomly distributed into gametes. Without recombination , all organisms would be genetically identical. The evolutionary significance of meiosis extends beyond individual populations and has contributed to the biodiversity seen on Earth today.

Meiosis is a specialized two-phase cell division that halves the number of chromosomes in each cell. Through one round of DNA replication followed by two rounds of cell division and chromosome segregation, it creates four genetically unique haploid cells from one diploid cell. Two haploid (1N) gametes (sperm and egg in mammals) – create a diploid (2N) zygote during fertilization, making the earliest stage of embryogenesis (Bolcun-Filas and Schimenti, 2012; Zickler and Kleckner, 2015; Bolcun-Filas and Handel, 2018).

Meiosis consists of two distinct cell divisions, meiosis I and meiosis II, each with specific roles. Meiosis I is a reductional phase, where the chromosome number is reduced by half, while meiosis II is an equational phase, similar to mitosis, where sister chromatids are separated. After premeiotic DNA replication in S phase, germ cells enter a prolonged prophase I, which is the most complex stage, where homologous chromosomes pair with each other, synapse and exchange segments of DNA by homologous recombination. In metaphase I, homologous chromosomes align randomly along the metaphase plate, and in anaphase I, they are pulled apart. Telophase I and cytokinesis follow, resulting in two haploid cells, each containing one chromosome from each homologous pair. Later, these haploid cells enter meiosis II, which like mitosis, involves separation of sister chromatids. This process produces four haploid daughter cells, each with a unique combination of genetic material (Figure 5) (Handel and Schimenti, 2010; Bolcun-Filas and Handel, 2018; Zickler and Kleckner, 2023).

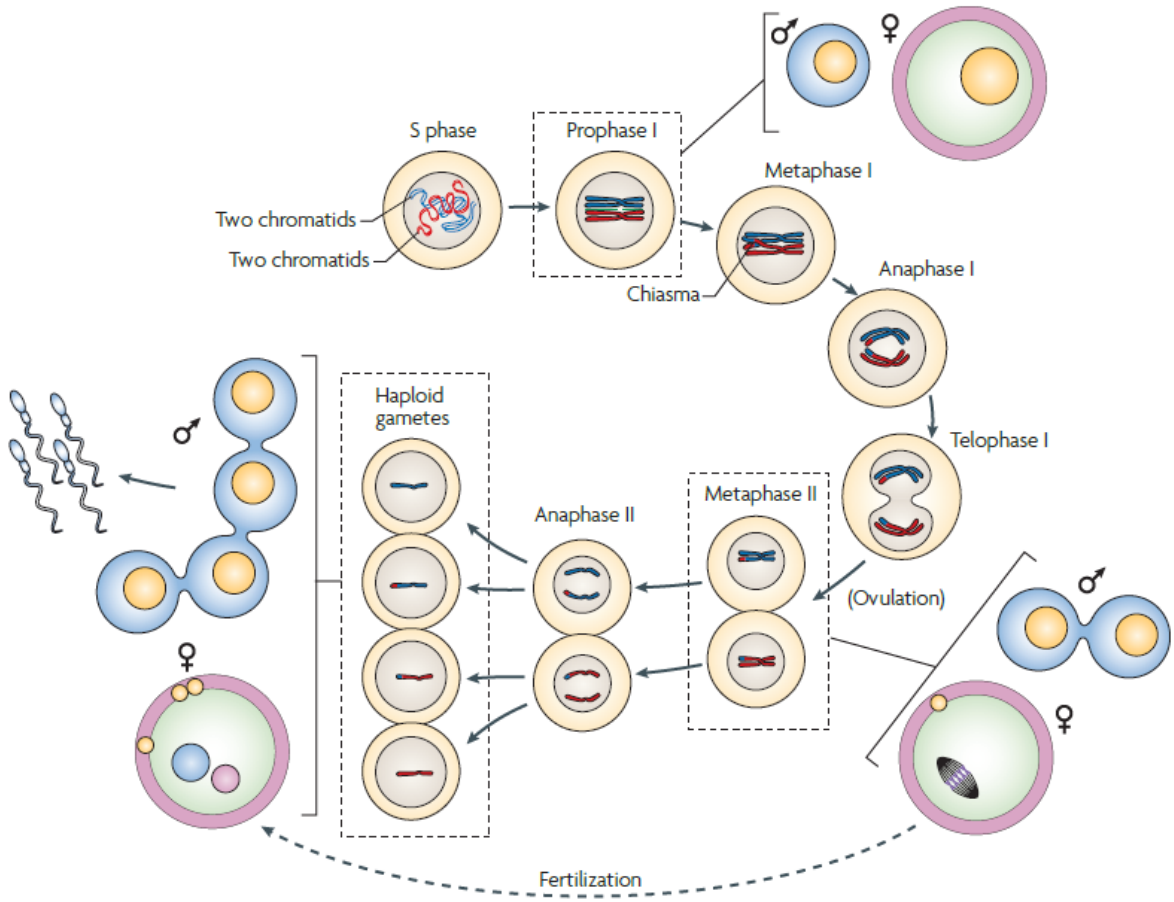

Figure 5. Mammalian meiosis and gametogenesis (Handel and Schimenti, 2010).

An overview of the gametogenesis process with all its stages, which result in the production of four haploid gametes from one diploid cell.

Prophase I of meiosis

Prophase I of meiosis is a crucial stage in the entire process, where meiotic recombination occurs. This recombination involves the exchange of genetic material between homologous chromosomes, leading to the creation of new allele combinations. Since each homologous chromosome is inherited from a different parent, they must first locate and synapse with their homologous partner. As mature spermatogonia enters prophase I, the nuclear DNA is replicated, and instantly double-strand breaks (DSBs) are formed in the DNA of homologous chromosomes. After this, the search for the homologous partner begins, followed by the formation of a Holliday junction. This junction can be resolved either through crossover (CO) or non-crossover (NCO) formation (Handel and Schimenti, 2010; Hunter, 2015; Gray and Cohen, 2016; Zickler and Kleckner, 2023).

In male mice, the first wave of spermatogonia enters a prolonged prophase I of meiosis at pre-leptotene stage around day 10 postpartum, and the complete prophase I takes more than 12 days. Cells progress through the leptotene and zygotene stages, reaching pachytene by approximately day 12. The pachytene stage takes about 10 days of prophase I. By days 22-23, cells advance to metaphase I, and the first mature spermatozoa appear around day 27. From this point, new cohorts of spermatogenic cells initiate prophase I in a wave-like pattern, ensuring continued progression through spermatogenesis (Cohen et al., 2006).

Meiotic recombination starts with the selection and activation of specific DNA recombination sites, known as hotspots. These hotspots are bound by the protein PRDM9, which trimethylates histone H3 on lysine 4 (H3K4me3) during the leptotene stage and guides the initiation of programmed DSBs formation (Buard et al., 2009; Parvanov et al., 2010; Smagulova et al., 2011). One of the earliest markers of DSBs formation is the appearance of phosphorylated histone H2AX (γH2AX), a process initiated by ATM kinase. This phosphorylation acts as a key signal, recruiting proteins responsible for DSBs repair (Mahadevaiah et al., 2001).

Meiotic DSBs are catalyzed by evolutionary conserved Spo11 protein (Keeney et al., 1997; Baudat et al., 2013). SPO11, a type II topoisomerase, introduces DSBs with characteristic 3′ single-stranded overhangs on both sides of the break (Neale et al., 2005). These DNA ends must be processed, allowing the recombinases RAD51 and DMC1 to bind (Figure 6) (Tarsounas et al., 1999). These recombinases promote the interaction and pairing of homologous chromosomes. Once paired, structural proteins stabilize these interactions by forming the synaptonemal complex (Zickler and Kleckner, 1999; Yang and Wang, 2009; Zickler and Kleckner, 2023). This process occurs during the transition from leptotene to zygotene stage of prophase I.

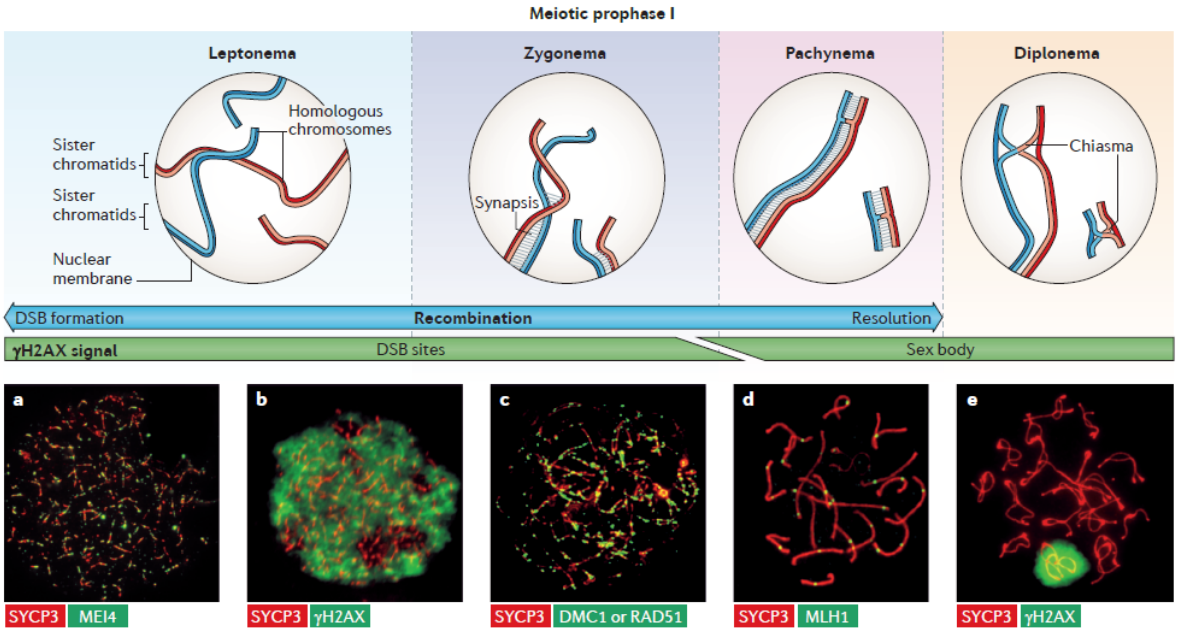

Figure 6. Chromosome organization during meiotic prophase I (Baudat et al., 2013).

The synaptonemal complex (SC) is a protein structure that is formed during prophase I and functions as a scaffold, holding homologous chromosomes together (Zickler and Kleckner, 1999; Yang and Wang, 2009). The SC has three main components: two lateral elements (LEs), which run along each homologous chromosome, a central element (CE), which acts like a zipper, connecting the lateral elements, and multiple transverse filaments (TFs), which bridge the gap between the homologous chromosomes (Schmekel and Daneholt, 1995; Bolcun-Filas and Handel, 2018). Key SC proteins include SYCP1, which forms the transverse filaments, and SYCP2 and SYCP3 and HORMAD2, which form the axial elements (AEs) and later lateral elements of SC, and TEX 12, which forms the central elements (Figure 7) (Hamer et al., 2006; Yang and Wang, 2009; Handel and Schimenti, 2010; Bolcun-Filas and Schimenti, 2012; Wojtasz et al., 2012).

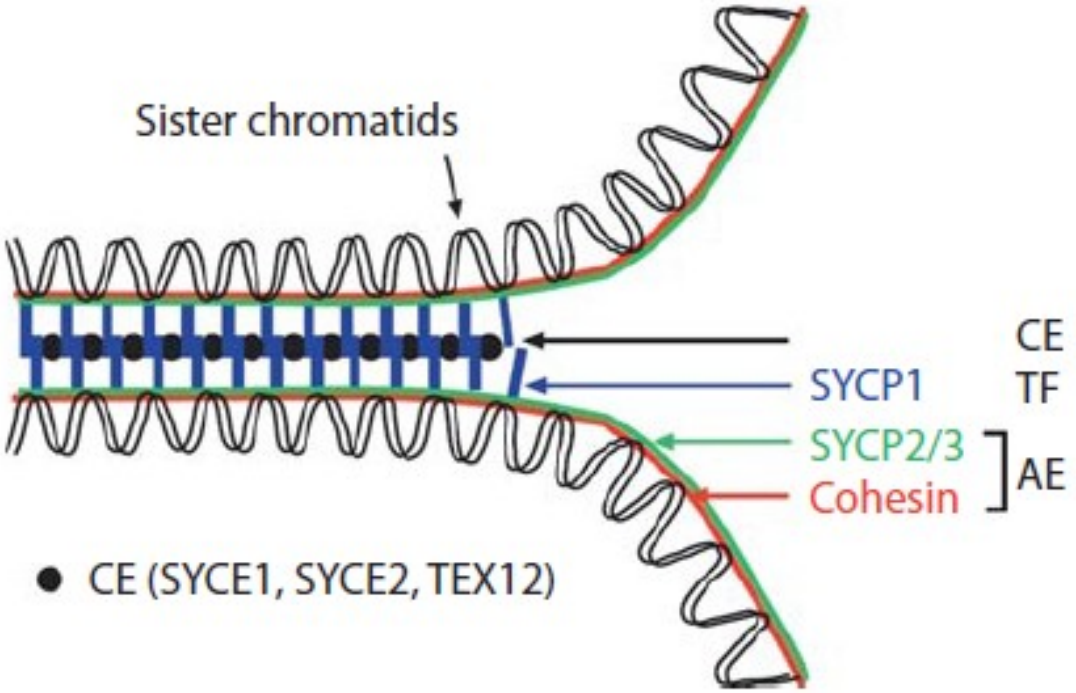

Figure 7. Schematic synaptonemal complex (Yang and Wang, 2009).

During the zygotene stage, the formation of synaptonemal complex continues as homologous chromosomes begin to pair up in a process known as synapsis. The axial elements align and come together to form the lateral elements, which are connected by transverse filament. These, along with proteins from the central elements, form the central region of the SC. The complex is fully formed during the following pachytene stage, when synapsis is complete, allowing for the homologous recombination to be finished (Handel and Schimenti, 2010; Zickler and Kleckner, 2023).

Programmed meiotic DSBs (200-300 DSBs per cell), which are formed during the leptotene stage, must be repaired by DNA-repair protein machinery by the end of pachytene stage. If any DSB remains unrepaired, the cell is arrested in prophase I and is not allowed to proceed to the first meiotic division. During pachytene stage, most DSBs are repaired by homologous recombination. The majority of DSBs are repaired as non-crossover (NCO) events, while about 10% are resolved as reciprocal crossover (CO) events. The repair of meiotic DSBs is tightly regulated to ensure the formation of at least one crossover between each homologous chromosome pair, known as the obligatory crossover rule. This process is controlled by the MutS and MutL protein homologue heterodimers, MSH4-MSH5 and MLH1-MLH3 (Figure 6). The regulation of this repair process ensures accurate segregation of

chromosomes during meiosis (Handel and Schimenti, 2010; Bolcun-Filas and Schimenti, 2012; Gray and Cohen, 2016).

Once recombination is completed, the chromosomes enter the diplotene stage, where they desynapse and condense. During this phase, the homologous chromosomes remain connected only at crossovers sites. These crossover points, observable as chiasmata, represent regions where genetic material was exchanged (Figure 6). The chiasmata ensure the proper alignment and separation of homologous chromosomes as meiosis progresses (Handel and Schimenti, 2010; Bolcun-Filas and Schimenti, 2012).

Sex chromosomes paring and silencing

The X and Y sex chromosomes present unique challenges during meiosis due to their limited homology, restricted to a small region called the pseudo-autosomal region (PAR) in mammals. This PAR is critical for ensuring that at least one crossover occurs between the X and Y chromosomes during meiosis, which is essential for their proper segregation. Crossovers in this region are highly regulated because of the limited homology between X and Y compared to autosomes.

While DSBs on autosomes are typically repaired using their homologous chromosome, the X and Y chromosomes often rely on their sister chromatids for DSBs repair outside of the PAR. The formation of DSBs and the pairing of the PAR occur later in prophase I than for autosomes, resulting in the formation of a structure known as the sex body. The sex body is a specialized chromatin domain that forms around the unsynapsed, non-PAR regions, of the X and Y chromosomes and is marked by phosphorylated histone H2AX (γH2AX) (Figure 6) (Bolcun-Filas and Schimenti, 2012; Baudat et al., 2013).

A key feature of the sex body is transcriptional silencing of the unsynapsed chromatin, non-PAR regions, during meiotic prophase I, a process known as meiotic sex chromosomes inactivation (MSCI). MSCI is triggered by the presence of unsynapsed axes of the sex chromosomes and is crucial for proper meiotic progression. Failure to silence these regions can lead to meiotic arrest, thereby disrupting gamete formation and leading to infertility (Forejt and Gregorová, 1977; Homolka et al., 2007; Turner, 2007, 2015).

Genetic architecture of hybrid sterility model

Several studies have explored the genetic mechanisms contributing to the sterility between *Mmd* and *Mmm* subspecies. The first hybrid sterility locus in vertebrates was mapped to chromosome 17 and named *Hybrid sterility 1 (Hst1)* (Forejt and Iványi, 1974). Later, through high-resolution genetic and physical mapping, as well as transgenesis, this gene was identified as *Prdm9* (encoding PR/SET domain-containing protein 9) (Mihola et al., 2009; Forejt et al., 2021), which plays a crucial role in meiotic recombination (Baudat et al., 2010; Myers et al., 2010; Parvanov et al., 2010).

The PRDM9 protein binds to genomic DNA at allele-specific sites via a zinc finger domain and modifies histone 3 proteins by trimethylating lysine 4 and lysine 36. In mice, humans, and other mammals, PRDM9 directs meiotic recombination by activating the recombination hotspots (Baudat et al., 2010; Myers et al., 2010; Parvanov et al., 2010).

The $Prdm9^{dom2}$ allele from the *domesticus* B6 strain and $Prdm9^{msc1}$ from *musculus* PWD strain exhibit significant evolutionary erosion in their recombination hotspots. Erosion is explained by biased gene conversion at non-crossover sites, favoring repair using templates with lower PRDM9 affinity (more degraded PRDM9-binding sites). This bias occurs because PRDM9 binding is more likely at sites with higher affinity (better-preserved PRDM9-binding sites). As a result, over evolutionary time, PRDM9-binding sites with lower affinity gradually accumulate in the genome, while the number of high-affinity sites declines (Figure 8) (Baker et al., 2015; Forejt and Jansa, 2023). This erosion means that these genetic hotspots, which are normally active in promoting recombination during meiosis, have disappeared or become inactive over time in these subspecies (Baker et al., 2015; Davies et al., 2016; Smagulova et al., 2016). In (PWD x B6)F1 hybrids, the recombination process becomes imbalanced due to the asymmetric formation of DSBs, which disrupts homologous chromosome synapsis and recombination. This process is crucial for successful meiotic division, and the failure to achieve proper synapsis results in male sterility (Figure 8) (Forejt and Jansa, 2023).

Theory about asymmetric DSBs and its role in hybrid sterility was supported by experiments in which increasing the number of the symmetric DSBs enhanced the synapsis of homologous chromosomes and partially reversed male infertility. The symmetric DSBs were introduced by random insertion of the PWD/PWD sequence into the smallest four autosomes of the (PWD x B6)F1 hybrids (Gregorova et al., 2018). Further improvement in the synapsis

of pachytene chromosomes was observed when exogenous DSBs were induced through the administration of a single dose of cisplatin (Wang et al., 2018).

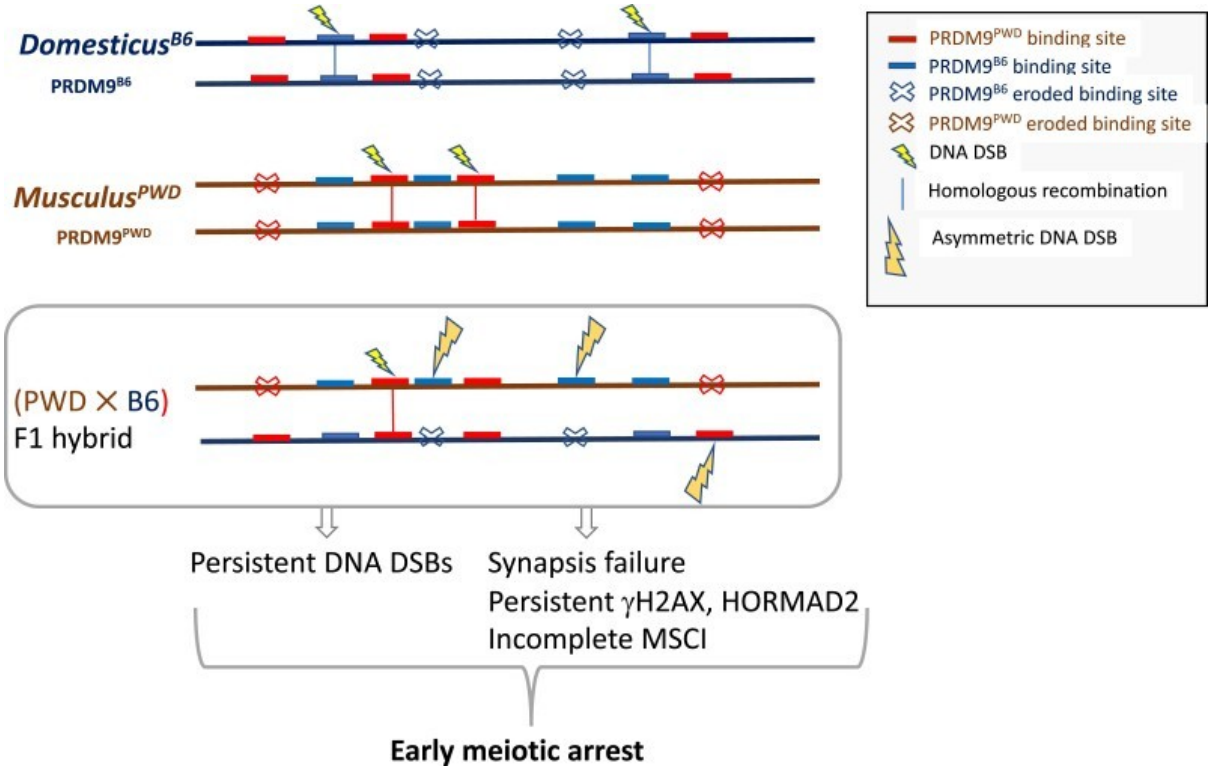

Figure 8. Model of molecular mechanism of the asymmetric formation of DSBs (Forejt and Jansa, 2023).

In our model of hybrid sterility, *Prdm9* causes early meiotic arrest and complete male sterility through its interaction with an X-linked locus. The study initially begun using chromosome substitution strains (intersubspecific consomic), each carrying a single PWD chromosome substituted into the B6 genetic background (Gregorová et al., 2008). The X chromosome substitution strains have been particularly useful in accelerating the discovery of X-linked hybrid sterility loci (Storchová et al., 2004; Dzur-Gejdosova et al., 2012; Bhattacharyya et al., 2013, 2014; Lustyk et al., 2019).

The *Hstx1* (hybrid sterility locus) was first identified in the central region of the Chr X^{PWD} as a quantitative trait locus (QTL) associated with various X-linked male fertility phenotypes. The same study observed suppression of recombination within the Chr X: 59.65–72.41 Mb interval, where QTLs linked to offspring number, testes weight, and sperm morphology were also mapped (Storchová et al., 2004).

The analysis of male hybrids between females of B6.PWD-Chr X.1, X.2, or X.3 consomic strains and PWD males provided direct evidence that male infertility is controlled by the central region of Chr X^{PWD}. Genome-wide mapping of hybrid sterility genes revealed strong

QTLs for testes weight and sperm count spanning *Hstx1* region on X chromosome (Dzur-Gejdosova et al., 2012). Later, the X-linked *Hstx2* locus, which regulates early meiotic arrest in (PWD x B6)F1 hybrids, was mapped to the same region (Bhattacharyya et al., 2014).

Asynapsis during the pachytene stage was the first meiotic phenotype identified in sterile (PWD x B6)F1 males, along with the absence of the typical sex body. Histological cross-sections revealed that spermatogenesis does not progress beyond epithelial stage IV, with a lack of postmeiotic cells and high apoptosis rates in primary spermatocytes at the pachytene stage. Although the induction of DSBs during meiosis was not affected, most homologous chromosomes failed to synapse. However, crossover formation on the synapsed chromosomes was unaffected. On the unsynapsed chromosomes, DSB repair proteins remained persistent, suggesting issues with repairing these breaks. Furthermore, misexpression of X chromosome genes during the pachytene stage was detected, even though these genes should be silenced. Based on these findings, it was concluded that genetically controlled meiotic asynapsis of heterospecific chromosomes represents a key pathway leading to sterility in (PWD x B6)F1 hybrids (Bhattacharyya et al., 2013).

Later, using chromosome substitution strains, the hybrid sterility locus on chromosome X was mapped to a 4.7Mb critical region, named the *Hstx2* locus (hybrid sterility chromosome X 2). The position of the *Hstx2* region was mapped to Chr X:64.88–69.58 Mb (GRCm38). Hybrids between partially consomic B6.PWD-Chr X.# females crossed with PWD males exhibited a complete sterility phenotype, characterized by low testes weight and no sperm count. The pachytene chromosome asynapsis phenotype was confirmed in these hybrids containing the *Hstx2* locus. Candidate genes were selected based to their expression during meiosis, however none showed misexpression between reciprocal hybrid males (Bhattacharyya et al., 2014).

Among the candidate genes in the *Hstx2* region, *Fmr1nb* showed expression during early meiotic prophase I (Margolin et al., 2014; Ball et al., 2016; Jung et al., 2019; Ernst et al., 2019) and has two nonsynonymous single nucleotide polymorphisms between the PWD and B6 parental strains (Bhattacharyya et al., 2014; Lustyk et al., 2019). Moreover, the *Fmr1nb* gene was among nine predicted candidate genes for X-linked hybrid sterility in other studies (Good et al., 2008).

Fmr1, another possible candidate, shows expression during early prophase I (Margolin et al., 2014) and its protein (FMRP) is involved in DNA damage response (DDR) and repair

complexes, e.g., with BRCA1 (Cabart et al., 2004), PARP complexes (Isabelle et al., 2010) and DNA topoisomerase TOP3b (Kwan et al., 2003). Additionally, it has been shown that FMRP is present on meiotic chromosomes and regulates the resolution of single-strand repair intermediates during meiosis. *Fmr1* knockout mutant mice exhibit delayed repair of these intermediates, leading to impaired crossover formation. Moreover, spermatocytes lacking FMRP show defects in homologous chromosomes synapsis during meiotic prophase I (Alpatov et al., 2014). Malformed spermatids have also been observed in *Fmr1* knockout mice, suggesting a defect in sperm development (Slegtenhorst-Eegdeman et al., 1998).

Furthermore, *Meir1* (meiotic recombination 1) genetic factor was mapped to the *Hstx2* locus. *Meir1* is a modifier of meiotic recombination rate in B6.DX.1s males. The $Meir1^{PWD}$ allele from the high recombination rate PWD parent causes downregulation of the crossover rate after introgression into the low recombination rate B6 strain. Thus, the localization of *Meir1* within the *Hstx2* locus indicates a link between meiotic recombination and hybrid sterility (Balcova et al., 2016). Additionally, Alpatov (2014) demonstrated that lack of FMRP protein led to impaired crossover formation, suggesting its role as the MEIR1 putative protein.

The *Hsxt2* locus also contains miRNA clusters that are important for testicular function. These clusters are located between the *Slitrk2* and *Fmr1* protein-coding genes and are conserved to different degree across 12 mammalian species (Zhang et al., 2019). Specifically, these miRNA clusters are actively transcribed in spermatogonia and are silenced by meiotic sex chromosome inactivation (MSCI) during the pachytene stage of meiosis (Royo et al., 2010). In sterile hybrids, where MSCI is disrupted, these miRNAs could misregulate genes necessary for meiosis and contribute to meiotic arrest.

Notably, overexpression of the *Mir-465* cluster microRNAs was observed in sterile (PWD x B6)F1 hybrids compared to reciprocal hybrids (Bhattacharyya et al., 2013). Moreover, this cluster is subject to copy number variation between PWD and B6 strains, as shown by optical mapping of these mouse genomes (Lustyk et al., 2019). Given that miRNAs can influence gene expression post-transcriptionally, variations in the *Mir-465* cluster may contribute to the hybrid sterility phenotype. Curiously, using the reverse genetic approach Morimoto et al. (2020) showed that the loss of function of *Mir-465* cluster did not affect the meiotic progression on the B6 genetic background, suggesting that it does not have a role during meiosis in contrast to first hybrid sterility gene, *Prdm9*, whose knockout results in complete male sterility (Mihola et al., 2009).

Specific allelic combinations of the *Prdm9* gene (*Prdm9*$^{PWD/B6}$) and *Hstx2* locus (*Hstx2*^{PWD}) were shown to be necessary, but not sufficient, to fully explain the meiotic arrest in hybrids. This was demonstrated by reconstructing the F1 sterile genotype using consomic B6.PWD-ChrX and B6.PWD-Chr17 strains. Three or more additional hybrid sterility genes with small effects have been suggested (Dzur-Gejdosova et al., 2012). However, an alternative, non-genic explanation has emerged from studying the meiotic characteristics of sterile hybrids. Based on the observation of multiple asynapsis of autosomal pairs, it was suggested that the rapid evolution of non-genic DNA sequences might be contributing to sterility (Bhattacharyya et al., 2013, 2014).

Later, it was found that by introducing long segments of PWD DNA into the shortest of PWD/B6 hybrid chromosomes, these chromosomes could fully synapse during meiosis in hybrid males. This suggests that adding sufficient lengths of homologous DNA, specifically 27 megabases (Mb) or more, enabled proper chromosome alignment. By deliberately manipulating the pairing of homologous chromosomes, it was possible to predictably adjust the extent of meiotic arrest in (PWD x B6)F1 hybrids (Gregorova et al., 2018).

Today we know that the genetic basis of *Prdm9*-driven hybrid male sterility (HMS) in our model involves the epistatic interaction of *Prdm9* gene, X-linked *Hstx2* locus, and the autosomal heterozygosity found in F1 hybrids (Bhattacharyya et al., 2013, 2014; Lustyk et al., 2019; Mukaj et al., 2020; Forejt et al., 2021; Valiskova et al., 2022).

The study of the *Hstx2* locus is essential for understanding the complex genetic interactions that drive hybrid male sterility, particularly in relation to recombination, meiotic arrest and homologous chromosome synapsis. It may also shed light on the mechanisms of reproductive isolation between mouse subspecies and uncover the genetic principles of speciation.

Material and methods

Mouse maintenance

The mice were maintained in the Pathogen-Free Facility at the Institute of Molecular Genetics, Czech Academy of Sciences, in accordance with animal care protocols approved by the Institute's Committee on the Ethics of Animal Experiments (No. 45/2020). Transgenic mouse lines were generated at the Transgenic Unit of the Czech Centre for Phenogenomics (CCP) - Institute of Molecular Genetics, Czech Academy of Sciences, BIOCEV division, in Vestec. Animal care adhered to the Czech Republic Act for Experimental Work with Animals (Decree No. 207/2004 Sb and Acts Nos. 246/92 Sb and 77/ 2004 Sb), fully compatible with the corresponding European Union regulations and standards (Council Directive 86/609/ EEC and Appendix A of the Council of Europe Convention ETS123).

DNA isolation, genotyping and sequencing

Genomic DNA was isolated from tail or ear biopsies, or from dissected spleen tissue, using either the NaOH method (Truett et al., 2000) or the Puregene Core Kit A (QIAGEN). For the NaOH method, the tissue was fragmented with scissors in 0.6 ml of 50mM NaOH and incubated for 1.5 hours at 95°C. The sample was then cooled on ice and neutralized with 50 µl of 1M TRIS. For the QIAGEN kit, the tissue was incubated with Cell Lysis Solution and Proteinase K overnight at 55°C. The following day, Protein Precipitation Solution was added, and the sample was centrifuged. The supernatant was transferred to a clean tube, and DNA was purified by isopropanol precipitation, washed with 70% ethanol, and the air dried-DNA pellet was dissolved in 50 µl water. The purified DNA samples were stored at 4°C for further analysis.

To determine the PWD or B6 origin of the X chromosome regions in the backcross (BC1) population, allele-specific microsatellite markers, both published (Marker Query Summary at jax.org) and newly designed (listed in the table of primers) were employed in a simple sequence length polymorphism (SSLP) PCR assay. Transgenic and deletion mutant lines were genotyped by gene- or transgene-specific markers in PCR assay. Primer sequences were either commercially available or designed using Primer-3 (http://bioinfo.ut.ee/primer3-0.4.0/) and are listed in Table 1.

Recombination breakpoints in the recombinant congenic lines derived from BC1 population were accurately mapped by Sanger DNA sequencing of PCR amplicons containing informative

PWD/B6 SNP polymorphisms. Deletion/insertion mutant lines were confirmed by primer-specific PCR assays and, alternatively, by Sanger DNA sequencing.

Primers pair	**Gene/transgene**	**GRCm38/mm10 position**	**Sequence (5`-3`)**
DXMit55 F	--	X:7360056-7360192	CTGCTTCCAGAATATTATCACTACTCC
DXMit55 R			AAAACATCCATTTATGTTAACACACA
DXMit81 F	--	X:36201307-36201506	GAGGAGCATCAACCTTCTCG
DXMit81 R			GAGGTGGGGAGAAACAGAGG
DXMit73 F	--	X:59656746-59656858	ACATGAAAGTTAGAAAGAGACCCG
DXMit73 R			GTGCACATTTGTGTGTGTATGC
DX64843 F	--	X:64843450-64843713	ACTGTCAACTCCCCAATTCA
DX64843 R			ATGAGGAGGTGCAGTTGCTT
DX65100 F	--	X:65100392-65100563	AAAAAGGCTGCTGGAAGTCA
DX65100 R			ATGAGGCTGGGATTCTTCCT
DX66265 F	--	X:66265169-66265383	TCCTTGACTTCAAGCTGCAC
DX66265 R			TTGAAGATGCTCTGCCCTTT
DX66532 F	--	X:66532235-66532429	CCCACTGCCAGCTTTTCTTA
DX66532 R			ATATCCCCTGGTGGTGTCTG
SR51 F	--	X:67841601-67841743	CAGGAGAAGATGGCACAATA
SR51 R			TAACCCTTTCACCATGTTTC
DX68233 F	--	X:68233480-68233728	TGTGAAGTGAGGGCAGTTTG
DX68233 R			GCTCTCCCTTTCATCGTCAA
DX69084 F	--	X:69084174-69084417	AGGCCTTCTGGGCTTATCTC
DX69084 R			AAAGCTCATGGATGAGAAAACA
BCe36 F2	Tg(*Fmr1, Fmr1os, Fmr1nb*)	--	GGCCGCTAATACGACTCACT
XC7-3` R			CCATTTCTTCCTTGCTCAACA
XC7-5` F		--	GGTCACTTTCTTTTTCATCTGTG

BCe36 R3	Tg(*Fmr1, Fmr1os, Fmr1nb*)		CGTCGACATTTAGGTGACA
Fmr1nb F2	*Fmr1nb*	X:68761860-68762131	CAGGAGGTTCTGGACTGCTC
Fmr1nb R2			TGAAGTCCAGAAGCCAAACC
Fmr1T500 F	*Fmr1*	X:68678600-68679183	GAGCGTTTCGGTTTCACTTC
Fmr1T500 R			TTGGGAAAGCTGGACTAAGC
BCE36 F1	Tg(XG20)	--	ACGACTCACTATAGGGAGAGGA
XG20-5` R1			TCTGCAATGTCGCCTGAGTA

Table 1. List of primers

RNA isolation, reverse transcription, and quantitative real-time PCR

Mice were euthanized by cervical dislocation, testes were dissected, and the *tunica albuginea* was removed. Total RNA was extracted using 0.5 ml of TRI Reagent (Sigma-Aldrich, #T3934) from 25 mg of testicular tissue in a 2ml tube with stainless steel bead. Samples were vigorously shaken for 2 minutes (QIAGEN, TissueLyser II) and incubated for 5 minutes at room temperature. The mixture was centrifuged at 9800 rpm for 15 minutes at 4ºC, and the supernatant was transferred to a new tube with 0.125 ml of chloroform. Samples were vortexed, incubated for 3 minutes, and centrifuged at 12000g for 15 minutes at 4ºC. The upper aqueous phase was transferred to a new tube, and 0.6 volumes of isopropanol were added, followed by a 10-minute incubation at room temperature. Tubes were then centrifuged at 12000g for 10 minutes at 4ºC. The supernatant was discarded, and the RNA pellet was washed twice with 75% ethanol, air-dried for 5 minutes, and dissolved in RNase-free water. RNA concentration was measured using a NanoDrop 2000 Spectrophotometer (Thermo Scientific).

RNA was reverse transcribed into the first strand of complementary DNA (cDNA) using M-MLV RT (Moloney Murine Leukemia Virus Reverse Transcriptase, Invitrogen #18057-018). RNA was combined with random hexamer primers, denatured at 70ºC for 5 minutes, and then quickly cooled on ice. A reaction mixture containing 5x M-MLV RT Buffer, 0.1M DTT and RNAsin (40 units/µl) was added, followed by a 2-minute incubation at 37ºC. M-MLV Reverse Transcriptase (200 units, Invitrogen, #28025-013) was added, and the reaction was incubated as follows: 25ºC for 10 minutes, 37ºC for 50 minutes, 42ºC for 5 minutes, 55ºC for

5 minutes, and enzyme inactivation at 70ºC for 15 minutes. Finally, 5 µl of 5 mM TRIS (pH 6,8) was added, and cDNA was stored at -80ºC for further analysis.

Quantitative real-time PCR was performed with cDNA samples using the LightCycler 480 SYBR Green I Master Mix (Roche, #04887352001) on a LightCycler 480 Instrument II, following the conditions described in Table 2. Primers for quantitative real-time PCR were designed using the Universal Probe Library tool (https://lifescience.roche.com/en_cz/articles/Universal-ProbeLibrary-System-Assay-Design.html) and are listed in Table 3.

Relative quantification of gene expression was calculated using ΔΔCp method. The expression of the target gene was normalized to the endogenous reference gene (β actin, housekeeping gene) according to equation: $\Delta Cp = Cp_{target} - Cp_{reference}$. Normalized ΔCp values were calculated for three biological replicates of each examined strain/line and the control B6 strain. Relative gene-specific expression profiles were calculated using the equation $R = 2^{-\Delta\Delta Cp}$. Statistical significance between relative gene expression levels of different mouse strains was determined using Student's t-test.

Procedure	**Temp. [ºC]**	**Time**	**Ramp rate**	
Pre-Incubation	95	5 min	4.8	
Amplification	95	10 sec	4.80	45 CYCLES
	60	15 sec	2.50	
	72	15 sec	4.80	
Melting Curve	95	5 sec	4.80	
	65	1 min	2.50	
	97	continuous	-	
Cooling	40	10 sec	2.00	

Table 2. Conditions for quantitative real-time PCR for gene expression

Primers pair	**Gene**	**Sequence (5`-3`)**
Fmr1nb_UPL#25_F	*Fmr1nb*	TCCTGGGATTTCTGCCTATG
Fmr1nb_UPL#25_R		CCTTCAACATCCTGTTCATCC

FMR1_UPL#25_F	*Fmr1*	TTCCTGCGCAGAGGAGAC
FMR1_UPL#25_R		TTCGGGAATGATCGTCGT
Gm10474_UPL#83_F	*Fmr1os*	GCCAATGTTTAGGTTGTTTATGAG
Gm10474_UPL#83_R		CACTCCAAAATCCCGGAAA
Aff2_UPL#34_F	*Aff2*	TCTGTGCTACTTTCAAGGGGATA
Aff2_UPL#34_R		AGCCATATTGGCGACAGTAAC
Actb_UPL#64_F	*β actin*	CTAAGGCCAACCGTGAAAAG
Actb_UPL#64_R		ACCAGAGGCATACAGGGACA

Table 3. List of qPCR primers – design Universal Probe Library (Roche)

microRNA isolation and expression

MicroRNAs were isolated using the miRNeasy Mini Kit (QIAGEN, #217004). Firstly, total RNA was extracted from the testes. Testes were dissected from juvenile (12dpp and 18dpp) and adult males from different wild and transgenic strains. 0.7 ml of QIAzol Lysis Reagent (QIAGEN) was added per both testes of juvenile and one testis of adult males. Tissue was homogenized (QIAGEN, TissueLyser II) for 2 min followed by 5 min incubation at room temperature. 0.140 ml of chloroform was added to the sample, vigorously vortexed and incubated for 3 min, followed by centrifugation at 12000g for 15 min at 4ºC. The upper aqueous phase was transferred to the new tube and 1.5 volume of 100% ethanol was added. The mixture was transferred to the RNeasy Mini column, washed once with RWT buffer and twice with RPE buffer. Finally, RNA was dissolved in RNase free water. The RNA concentrations were measured by spectrophotometric analysis on NanoDrop 2000 Spectrophotometer (Thermo Scientific).

The universal reverse transcription reaction was performed with adjusted amount of sample RNA using miRCURY LNA miRNA PCR Assay (QIAGEN, #339306). 5 ng/ul of RNA was mixed with miRCURY RT Buffer and miRCURY RT Enzyme Mix and incubated for 1h at 42ºC followed by inactivation of reverse transcriptase for 5 min at 95ºC.

Quantitative real-time PCR was performed with the miRCURY LNA SYBR Green PCR Kit (QIAGEN, #339345) at LightCycler® 480 Instrument II in conditions as shown in Table 4. The specific microRNA LNA primers for the qRT-PCR analysis were chosen and ordered from QIAGEN and are listed in Table 5. Target miRNA transcripts and the *let-7a* transcript

(housekeeping miRNA used for normalization) were measured from the cDNA samples from three different mice of the same strain/line. The crossing point (Cp) values for specific target miRNA transcripts were normalized to *let-7a* miRNA Cp value (ΔCp). Differences between specific miRNA expression levels of different mouse strains were evaluated by Student's t-test.

Procedure	**Temp. [ºC]**	**Time**	**Ramp rate**	
PCR initial heat activation	95	2 min	Maximal/fast mode	
2-step cycling:				45 CYCLES
Denaturation	95	10 sec	Maximal/fast mode	
Combined annealing/ extension	56	60 sec	Maximal/fast mode	
Melting Curve	95	5 sec	4.80	
	65	1 min	2.00	
	95	continuous	--	
Cooling	40	10 sec	2.00	

Table 4. Conditions for quantitative real-time PCR for microRNA expression

	Primers	**Target**	**Cat. Nr.**
1	mmu-miR-743a-3p	miR-743a-3p	YP00205472
2	mmu-miR-743a-5p	miR-743b-5p	YP02113496
3	mmu-miR-743b-3p	miR-743b-3p	YP00205617
4	mmu-miR-743b-5p	miR-743b-5p	YP00205240
5	mmu-miR-465a-3p	miR-465a-3p, miR-465b-3p, miR-465c-3p	YP00205023
6	mmu-miR-465a-5p	miR-465a-5p	YP00205024
7	mmu-miR-465b-5p	miR-465b-5p	YP00205668
8	mmu-miR-465c-5p	miR-465c-5p	YP00205026
9	mmu-miR-465d-3p	miR-465d-3p	YP02108068
10	mmu-miR-465d-5p	miR-465d-5p	YP02100902

11	mmu-let-7a-5p	let-7a-5p	YP00205727

Table 5. List of microRNA specific LNA primers

Protein isolation and Western Blotting

The whole testes were dissected, the *tunica albuginea* removed, and the tissue was snap-frozen in liquid nitrogen. Lysis buffer, supplemented with 1x protease inhibitor cocktail (MedChemExpress, HY-K0010), 1x phosphatase inhibitor cocktail I (MedChemExpress, HY-K0021), and benzonase (Merck, 1.01654.0001), was used to homogenize the tissue (QIAGEN, TissueLyser II). After 5 minutes of incubation, 2% SDS was added, and the mixture was heated at 95ºC for 15 minutes. The sample was then cooled and centrifuged at >13000 rpm, and the supernatant was transferred to a new tube. Total protein concentration was measured using the Pierce BCA Protein Assay Kit (Thermo Scientific, #23225).

Protein samples were separated by SDS-PAGE electrophoresis on a Bolt 4-12% Bis-Tris Plus gradient gel (Invitrogen, NW04120BOX) and transferred onto a polyvinylidene difluoride (PVDF) membrane (Amersham Hybond, #GE10600069) for 1 hour in 65V. The membrane was blocked with 5% milk (Santa Cruz, #2324) in 1x TBS buffer with Tween-20 (TBS-T, 50 mM TRIS, 150 mM NaCl, 0.01% Tween-20) for 20 minutes. Primary antibodies (Table 6) were diluted in 3% BSA in 1x TBS-T and incubated overnight in 4ºC. Secondary antibodies (donkey anti-goat IgG-HRP antibody, Santa Cruz Biotechnology, sc-2020; horse anti-mouse IgG-HRP antibody, Cell Signaling Technology, #7076S; goat anti-rabbit IgG-HRP antibody, Cell Signaling Technology, #7074S) conjugated to horseradish peroxidase (HRP) were used at a 1:10000 dilution in 5% milk in 1x TBS-T for 30 minutes at room temperature. Different chemiluminescent substrates, depending on the abundance of the target protein, were used to detect the bound secondary HRP antibodies (SuperSignal West Femto, Thermo Fisher, #34095; WesternBright ECL, Advansta, #K-12045-D).

Images were captured using the BioRad *ChemiDoc MP Imaging* System and processed with ImageLab software (Bio-Rad).

Antigen	**Host species**	**Source**	**Cat. Nr**	**IF dilution**	**WB dilution**
SYCP1	Rabbit	Abcam	ab15087	1:500	
SYCP3	Mouse	Santa Cruz	sc-74596	1:100	
MLH1	Mouse	Abcam	ab14206	1:30	
Centromere	Human	Antibodies Incorporated	15-234	1:200	

HORMAD2	Rabbit	gift from Attila Toth	TU Dresden, Germany	1:700	
DMC1	Rabbit	Santa Cruz	sc-22768	1:200	
H1t	Guinea Pig	gift from Mary-Ann Handel	The JAX, USA	1:700	
HORMAD2	Guinea Pig	gift from Attila Toth	TU Dresden, Germany	1:1000	
γH2AX	Rabbit	Abcam	ab2893	1:1000	
Fmr1nb	Goat	Santa Cruz	sc-246953	1:50	1:500
Fmr1 N-term	Rabbit	OriGene	TA324874	1:50	1:1000
Fmr1 C-term	Rabbit	Abcam	ab17722	1:50	1:0000
β actin	Rabbit	Santa Cruz	sc-69879		1:1000
α tubulin	Mouse	Proteintech	66031-1-IG		1:2000

Table 6. List of primary antibodies for western blot and immunocytochemistry

Testis single-cell suspension, chromosome spreads and immunofluorescence microscopy

Meiotic chromosome spreads were performed as previously described (Anderson et al., 1999) with minor modifications. Testes were dissected and transferred to 1ml of RPMI (Sigma, #R8758). The tubules were disintegrated and macerated with scissors. The cell clumps were filtered through a Falcon 40 µm dense cell strainer (Corning, #352340) into a new tube. The number of cells was counted using Burker's chamber, and approximately 300,000 cells were transferred to a fresh tube to prepare a single microscopy slide. The aliquot was centrifuged for 3 minutes at 1500 rpm, and the cells were resuspended in 100 µl of RPMI. Next, 150 µl of 0.1M sucrose was added as a hypotonic solution for 13 minutes, and then the cells were dropped onto a slide with 1% paraformaldehyde in 50mM NaBorate (pH 9,0) containing 0.15% Triton X-100 and 1x protease inhibitors (Roche, #1836153). After 3 hours at 4ºC, the slides were washed three times in 1x PBS, air-dried, and blocked with 0.5x blocking buffer (1.5% BSA, 5% goat serum, 0.05% Triton X-100 or 3% BSA, 0.05% Triton X-100) containing 1x protease inhibitors (Roche, #1836153) for 1 hour at 4ºC.

Primary antibodies (Table 6) were added, and the slides were incubated overnight in a humid chamber at 4ºC. After washing three times in 1x PBS, the slides were incubated with secondary antibodies conjugated to fluorophores (Table 7) for 2 hours at 4ºC. The slides were mounted with Vectashield mounting medium containing DAPI (Vector Laboratories, H1200-10).

Immunofluorescence images were captured using a Nikon Eclipse 400 epifluorescence microscope with single bandpass filters for infrared, red, blue and green fluorescence (Chroma Technologies) and a 60x Plan Fluor objective (Nikon, MRH00601). Images were acuired using a DS-QiMc monochrome CCD camera (Nikon) and processed using NIS Elements software (NIS-Elements Microscope Imaging Software). Image adjustments were made using Adobe Photoshop (Adobe Systems) and ImageJ (Image Processing and Analysis in Java).

	Host	Dilution	Source, Cat. Nr
anti-Rabbit IgG-AlexaFluor568	Goat	1:400	MolecularProbes, A-11036
anti-Rabbit IgG-AlexaFluor488	Goat	1:400	MolecularProbes, A-11034
anti-Mouse IgG-AlexaFluor568	Goat	1:400	MolecularProbes, A-11031
anti-Mouse IgG-AlexaFluor488	Goat	1:400	MolecularProbes, A-11001
anti-Human IgG-AlexaFluor647	Goat	1:400	MolecularProbes, A-21445
anti-Rabbit IgG-AlexaFluor488	Goat	1:400	MolecularProbes, A-11005
anti-Goat IgG-AlexaFluor594	Donkey	1:400	MolecularProbes, A-11058
anti-Guinea pig IgG-FITC	Goat	1:400	Sigma F6261
anti-Guinea pig IgG-Cy3	Goat	1:400	JacksonImmuno, 106-165-003

Table 7. List of secondary antibodies for immunocytochemistry

Histology: Hematoxylin and Eosin (H&E) staining, immunohistochemistry, and TUNEL assay of testes

Males were euthanized, and the testes were dissected and fixed in 4% PFA overnight at 4°C. The testes were then dehydrated and embedded in paraffin. Paraffin blocks were sectioned into 3 um thick slices and mounted on microscope slides. The histological sections were deparaffinized by incubation in xylene, followed by rehydration in graded ethanol series (100%, 75%, 50% and 25%) and ddH_2O. The slides were stained with hematoxylin for 5 minutes, followed by staining with 0.5% eosin for 3 minutes at room temperature. Finally, the sections were dehydrated through an ethanol series (25%, 50%, 75% and 100%), incubated in xylene, and mounted using a xylene-based mounting medium.

For immunohistochemistry, 5 um thick sections of testes were subjected to antigen retrieval by incubating in citrate antigen retrieval solution for 15 minutes at pH 6,0. The slides were then processed following the same procedure as for immunofluorescence microscopy.

Apoptotic cells in the tissue sections were identified using terminal deoxynucleotidyl transferase-mediated dUTP nick-end labelling (TUNEL) with the in situ DeadEnd Fluorometric Detection Kit (PROMEGA, #G3250), according to the manufacturer's protocol (#TB235). TUNEL-treated sections were mounted in Vectashield with DAPI to visualize nuclei. Images were captured using a DS-QiMc monochrome CCD camera (Nikon) and processed with NIS Elements software (NIS-Elements Microscope Imaging Software). The captured images were analyzed for TUNEL-positive cells using the NIS Elements image analyzer and further processed with Adobe Photoshop (Adobe Systems).

Generation of new mouse lines

Construction of *Fmr1nb*-specific TALENs and generation of the *Fmr1nb*-KO mouse line

TALEN nucleases were designed using TAL Effector Nucleotide Targeter 2.0 (https://tale-nt.cac.cornell.edu/), and assembled using the Golden Gate Cloning system (https://international.neb.com/applications/cloning-and-synthetic-biology/dna-assembly-and-cloning/golden-gate-assembly). The assembled TALENs were cloned into the ELD-KKR backbone plasmid. The TALENs were designed to target a locus close to the ATG start codon of *Fmr1nb*. Each TALENs plasmid was linearized with *NotI* and transcribed using the mMESSAGE mMACHINE T7 Kit (Ambion). Polyadenylation of the resulting mRNAs was performed using the Poly(A) Tailing Kit (Ambion), and the mRNA was purified using RNeasy Mini columns (Qiagen). TALEN mRNAs were diluted in nuclease-free water and stored at −80°C. Transgenic mice were generated by injecting the purified mRNA of *Fmr1nb*-specific TALENs into the male pronuclei of 1-cell embryos from the B6.DX.1s strain. Mice positive for mutations were identified by PCR, followed by sequencing of the PCR fragment. The B6.DX.1s.*Fmr1nb*^{em1ForeJ} line (hereafter B6.DX.1s$^{Fmr1nb-}$), carrying 19 base-pair deletion over the ATG start codon creating a frameshift in the *Fmr1nb*^{PWD} allele, was established.

Design of *Fmr1*-specific CRISPR/Cas9 sgRNAs and generation of the *Fmr1*-KO mouse line

Single guide RNAs (sgRNAs) for the CRISPR/Cas9 experiment were designed using CRISPR/Cas9 target online predictor (https://crispr.cos.uni-heidelberg.de/). Three candidate sgRNA were selected, and the corresponding oligonucleotides were synthesized, annealed for 5 minutes at 95°C, and cooled. The pX335X6SN plasmid was digested with *BbsI* restriction enzyme and ligated with the diluted oligonucleotides using T4 DNA ligase at room temperature

for 1 hour. Competent DH5α cells (Invitrogen, #18265-017) were transformed with the ligation mixture, incubated in LB medium for 1 hour at 37ºC while shaking at 225 rpm. The cells were centrifuged, plated on agar plates with ampicillin, and incubated overnight at 37ºC. A single colony was selected, grown in LB medium with ampicillin for 16 hours at 37ºC with shaking at 250 rpm, and the plasmid was purified using the GeneJET Plasmid Miniprep Kit (Thermo Fisher, #K0503). Plasmid concentration was measured, and successful ligation was confirmed via 1% agarose gel. The plasmid was sequenced using the U6 forward primer 5'-ACTATCATATGCTTACCGTA-3'.

The efficiency of the sgRNA was validated in vitro. The template for in vitro transcription was synthesized by PCR from the CRISPR pX335X6SN plasmid using primers overlapping the sgRNA sequence and introducing T7 promoter. T7 RNA polymerase (Ambion) was used to produce sgRNA by in vitro transcription. The sgRNA were incubated with Cas9 nuclease and a PCR amplicon (approximately 500 bp) covering the target sequence. The efficiency of the CRISPR/Cas9 cleavage was validated by separating the digest products using agarose gel electrophoresis.

Synthetic sgRNAs were further validated using SYNTHEGO (https://www.synthego.com/cart?from_design_tool=1) and ordered from KRD company. CRISPR/Cas9 mutations were introduced at the fertilized oocyte stage of B6.DX.1s mice. Positive mutations were confirmed by PCR, followed by sequencing of the PCR fragment. A 2 bp insertion was detected at the expected Cas9 nuclease cut site. The B6.DX.1s.*Fmr1*^{em1ForeJ} mouse line (hereafter B6.DX.1s^{Fmr1-}) was established.

Generation of transgenic mouse lines B6-Tg(*Fmr1,Fmr1os,Fmr1nb*) and B6-Tg(XG20) with the BAC DNA clones

The transgenic lines were created by random insertion of C57BL/6J BAC clones into genomic DNA. BAC clones were selected from the RPCI-23 (RP23) BAC library (https://www.sourcebioscience.com/life-science-research/clones/genomic-clones/mouse-genomic-clone-collections/mouse-bac-rpci-23/). The RP23-149C7 BAC clone was selected for C57BL/6J-Tg(RP23-149C7)^{1ForeJ} (hereafter B6-Tg(*Fmr1,Fmr1os,Fmr1nb*); B6.XC7), and the RP23-152G20 BAC clone was selected for C57BL/6J-Tg(RP23-152G20)^{1ForeJ} (here B6-Tg(XG20)).

BAC DNA was prepared using the Sepharose 4B-CL Chromatography BAC DNA Purification protocol (Osoegawa et al., 2000). BAC clones were grown in LB media containing

chloramphenicol at 37ºC with vigorous shaking overnight, and the cells were harvested by centrifugation at 4000 for 20 minutes at 4ºC. Lysis of the bacterial cells was performed with 0.2 M sodium hydroxide, 1% SDS, and 3 M potassium acetate (pH 5,5). The genomic DNA-SDS-protein precipitate was removed by centrifugation, and the supernatant was transferred to a fresh tube. DNA was precipitated with 100% isopropanol and washed with 70% ethanol. The BAC DNA was dissolved in 10 mM NaCl and stored in -80ºC.

BAC DNA was linearized using *NotI-HF* restriction endonuclease (NEB, R3189S) at 37ºC for 4 hours and separated by pulsed-field gel electrophoresis (PFGE) for 12 hours. The digestion products were purified using a Sepharose 4B-CL column, eluted in 0.1 M NaCl, 10 mM TRIS (pH 7,5), and 0.25 mM EDTA after 2 hours. Positive fractions fractions were validated by PFGE and stored at 4ºC. Transgenic mice were generated by pronuclear injection of purified linearized BAC DNA into 1-cell embryos from C57BL/NCrl mice, which were then transferred into the oviducts of pseudopregnant females. Potential transgenic founders were genotyped by PCR, followed by sequencing of the PCR fragment. The transgenic founders were backcrossed to C57BL/6J, and the offspring were genotyped by PCR. This resulted in the establishment of the B6-Tg(*Fmr1,Fmr1os,Fmr1nb*) and B6-Tg(XG20) transgenic lines.

Hypothesis and aims of the thesis

The sterility of hybrids between different species or subspecies is a well-known form of reproductive isolation that plays a crucial role in speciation. In the case of hybrid sterility (HS) between the house mouse subspecies *Mus musculus domesticus* and *Mus musculus musculus*, our laboratory introduced a model involving sterile male hybrids of PWD and B6 inbred strains.

Male sterility of (PWD x B6)F1 hybrid mice is well-documented, with phenotypes such as reduced testis weight, lower sperm count, and autosomal asynapsis. Previous studies mapped the *Hstx2* locus using females B6.DX.1 and B6.DX.1s subconsomic strains, crossed with PWD males, which reconstituted autosomal heterozygosity and a shortened proximal segment of the PWD X chromosome. While the proximal part of the X chromosome could not be fully excluded, the *Hstx2* was shown to contribute to hybrid sterility.

To better characterize the *Hstx2* locus, we aimed to develop new subconsomic strains that would minimize the size of the *Hstx2* region from the PWD strain. This would be achieved through two approaches: classical genetic backcrossing of B6.DX.1s females with B6 males and a targeted recombination approach using the CRISPR-Cas9 system, both aimed at refining the *Hstx2* locus.

Recently, we identified two *Hstx2* candidate genes, *Fmr1nb* and *Fmr1*, based on their expression profiles during meiosis and single nucleotide polymorphisms (SNPs) between PWD and B6 alleles. To investigate the role of these genes in hybrid sterility, we decided to generate knockout models for the PWD sterile allele and develop transgenic lines containing the B6 alleles. This could allow us to determine whether the absence of the PWD allele in these candidate genes can rescue hybrid sterility. Additionally, we will evaluate whether introducing extra copies of these genes on autosomes could further alleviate sterility. Furthermore, we will conduct expression profiling of the *Mir-465* family cluster to examine differences between B6 and PWD alleles in juvenile and adult males in both parental strains and hybrid mice.

In parallel, we will examine the involvement of the *Hstx1* and *Meir1* loci by assessing meiosis progression, crossover formation, and sperm morphology in subconsomic strains, as well as in newly developed knockout and transgenic mouse models.

Results

Hstx2 locus as a recombination cold spot

Firstly, we defined the PWD/B6 distal boundary of the B6.PWD-ChrX.1s consomic strain at Chr X: 69.21 Mb, narrowing the *Hstx2* locus to a 4.3 Mb region of the PWD sequence (Figure 9). To further reduce the size of the *Hstx2* locus and investigate the potential role of the proximal region of the X^{PWD} sequence, we backcrossed females of two subconsomic strains, DX.1s and DX.51-69, with B6 male generating BC1 progeny (Table 8). Genotyping of 168 (B6.DX.1s x B6) x B6 BC1 mice showed 51 recombinants with crossovers in the proximal region of chromosome X. From this backcross, we derived a new congenic strain C57BL/6J-ChrX.64-$69^{PWD/Ph}$ (abbreviated B6.DX.64-69) which kept only a 4.34 Mb segment of the PWD sequence (Chr X: 64.87-69.21 Mb; mouse genome assembly GRCm38.p6) (Figure 9).

However, no recombination was observed within the *Hstx2* locus, as indicated by markers at Chr X: 65.10 and 69.08 Mb (Table 8). In the second backcross experiment, using the B6.DX.51-69 subconsomic strain (which carries PWD sequence between 51 – 69 Mb), none of the 111 BC1 animals showed recombination within the *Hstx2* locus.

In total, across both backcross experiments involving 279 BC1 mice, no recombination events were detected in the 65.10 Mb - 69.08 Mb *Hstx2* region, suggesting that this locus is a recombination cold spot.

		Number of recombination events (N) in the specific X chromosome intervals / recombination rate (cM/Mb)				
Backcross (BC1)	Number of BC1 (n)	X:7.36-65.10 Mb	X:7.36-36.20 Mb	X:36.20-59.66 Mb	X:59.66-65.10 Mb	X:65.10-69.08 Mb
(DX.1s x B6) x B6	168	51 / 0.526	17 / 0.351	30 / 0.761	4 / 0.438	0
(DX.51-69 x B6) x B6	111	N.D.	N.D.	N.D.	1 / 0.166	0

Table 8. Distribution of PWD/B6 recombination events along the X chromosome.

The recombination rate (cM/Mb) was calculated from the number of recombination events (N) and the number of BC1 animals tested (n) using the length (L) of a specific region on the X chromosome.

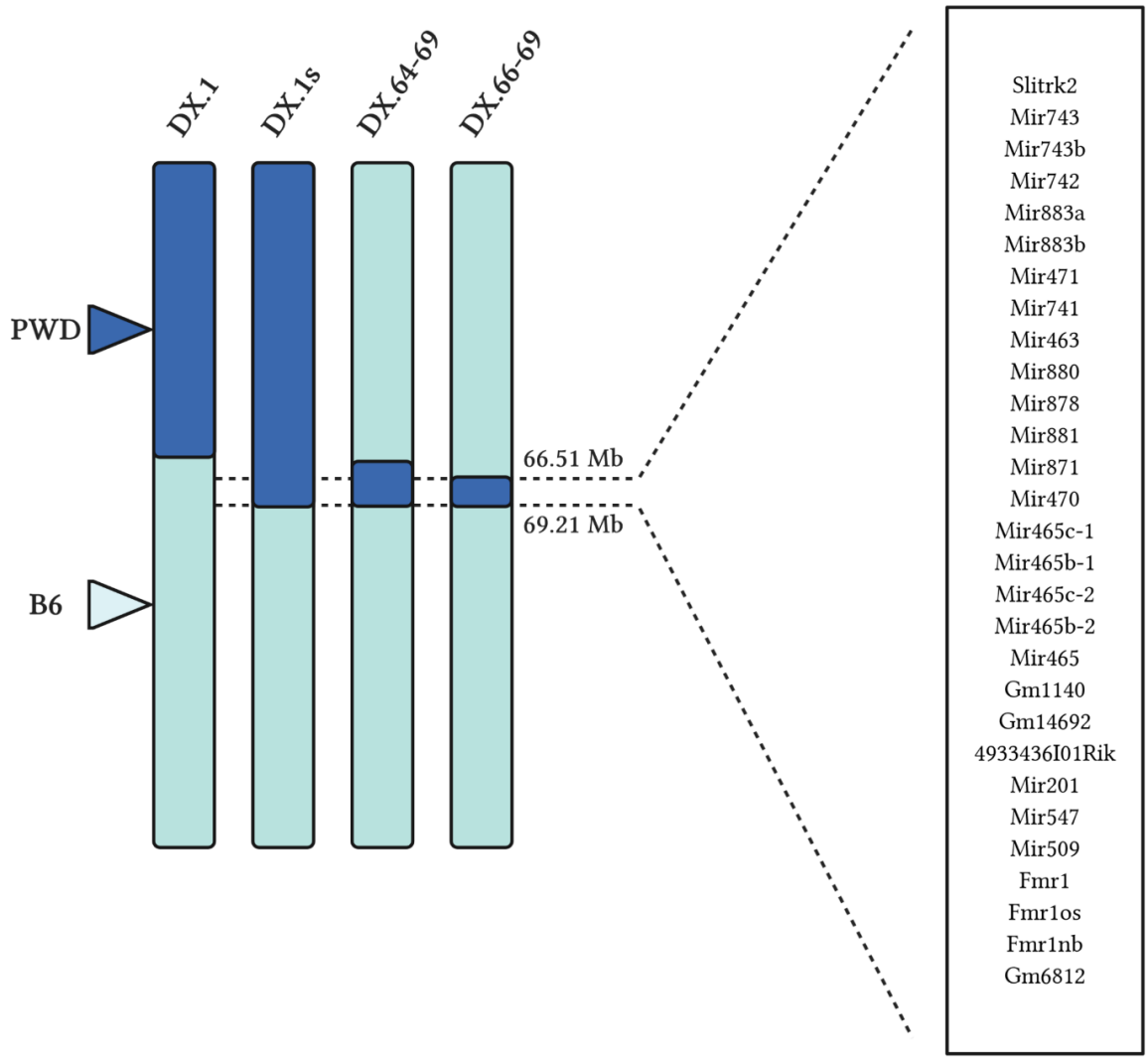

Figure 9. Mapping of hybrid male sterility at the *Hstx1* and *Hstx2* loci in subconsomic and congenic strains.

A schematic representation of the chromosome X architecture in subconsomic and congenic strains B6.DX.1, B6.DX.1s, B6.DX.64-69, and B6.DX.66-69 is provided. Chromosomal intervals of PWD and B6 origin are depicted in dark and light blue, respectively. The list includes protein-coding genes, noncoding RNAs, and microRNAs within the newly defined *Hstx1/2* locus (66.51– 69.21 Mb).

Targeting homologous recombination at *Hstx2* using CRISPR/Cas9

Since the *Hstx2* locus behaves as a recombination cold spot, we tried to recruit the recombination machinery to this region by inducing double-strand breaks (DSBs) with Cas9

endonuclease. For this purpose, two transgenic lines were created (the transgenic constructs were prepared in the collaborating laboratory of Dr. Frank Chen by Michelle Yancoskie, Tubingen University). The first line carried Cas9 endonuclease under the control of *SPO11* genomic region, ensuring its expression exclusively during early prophase I of meiosis. The second transgenic line carried a U6-promoter-driven CRISPR cassette targeting three sites within the *Hstx2* locus.

Double-transgenic females (B6.DX.1s.TgSPO11-Cas9 x B6.TgCRISPR-*Hstx2*)F1 were then mated with B6 males to generate the BC1 population. This approach enabled the generation of targeted DSBs within the *Hstx2* locus. We observed that these double-transgenic F1 females produced a 15-fold increase in recombination frequency in the 64.8 - 65.1 Mb interval, immediately adjacent to the *Hstx2* locus (10 recombinants in 181 BC1 offspring, 18.42 cM/Mb) compared to previous classical backcrosses (with only one recombination event in 279 BC1 offspring, 1.19 cM/Mb).

However, only one homologous recombination event was detected within the *Hstx2* locus itself, resulting in the generation of the congenic strain B6.PWD-ChrX.66-69 (abbreviated as B6.DX.66-69). This new congenic line restricts the PWD sequence on Chr X to 2.70 Mb interval (66.51 - 69.21 Mb) (Figure 9). Notably, all recombination events occurred within the region flanked by the gRNAs, but at some distance from the exact target sites. The cause of the increased recombination rate near, but not at, the targeted sites have not yet been determined.

Phenotypes of newly defined *Hstx1*, *Hstx2* and *Meir1* loci

Hstx1 fertility phenotype

To investigate the *Hstx1* phenotype controlled by the newly reduced PWD intervals, we compared the fertility parameters of B6.DX.64-69 and B6.DX.66-69 congenic males, which carry shortened 4.34 Mb (Chr X: 64.87 - 69.21) and 2.70 Mb (Chr X: 66.51 - 69.21) regions of the PWD sequence, respectively, to those of B6.DX.1 and B6.DX.1s males, which carry larger proximal PWD intervals of 64.9 Mb and 69.2 Mb. We assessed testes weight, sperm count, and the percentage of sperm head malformations.

Both shortened PWD intervals significantly reduced testes weight compared to B6.DX.1 ($P<0.001$, t-test) and to B6.DX.1s ($P<0.05$, t-test) (Table 10, Figure 10). Similarly, B6.DX.66-69 and B6.DX.64-69 males showed lower sperm counts compared to B6.DX.1 and B6.DX.1s

(P<0.05, t-test) (Table 10, Figure 10). As expected, both B6.DX.64-69 and B6.DX.66-69 showed a higher frequency of morphologically malformed sperm heads compared to B6.DX.1 (P<0.01, t-test) (Table 10, Figure 10). However, compared to B6.DX.1s, the level of malformed sperm heads in males carrying the 4.34 Mb and 2.70 Mb PWD regions was significantly lower (40.8 % and 40.3 % vs. 69 %, P<0.01, t-test) (Table 10). This suggests that additional genetic factors located proximally to the Chr X: 64.87 - 69.21 interval are required to fully manifest the *Hstx1* phenotype.

Strain	**n**	**Testes weight [mg]**	**Sperm count [x10^6]**	**Sperm head malformation rate [%]**
PWD	10	112.0 ± 7.2	27.1 ± 10.6	N/A
B6	19	176.9 ± 15.0	58.2 ± 14.8	N/A
DX.1	9	187.4 ± 12.2	50.4 ± 12.5	24.8 ± 2.2
DX.1s	26	167.8 ± 9.5	48.0 ± 12.7	69.0 ± 7.2
DX.64-69	14	158.2 ± 14.0	38.8 ± 11.5	40.8 ± 2.8
DX.66-69	12	152.3 ± 6.1	31.9 ± 7.9	40.3 ± 4.9

Table 9. *Hstx1* locus mapping.

Fertility parameters of subconsomic and congenic males, including testes weight (in milligrams), sperm count (millions of sperm per pair of epididymis), and the frequency of malformed sperm heads (in percent). n refers to the number of males analyzed; N/A indicates data not analyzed.

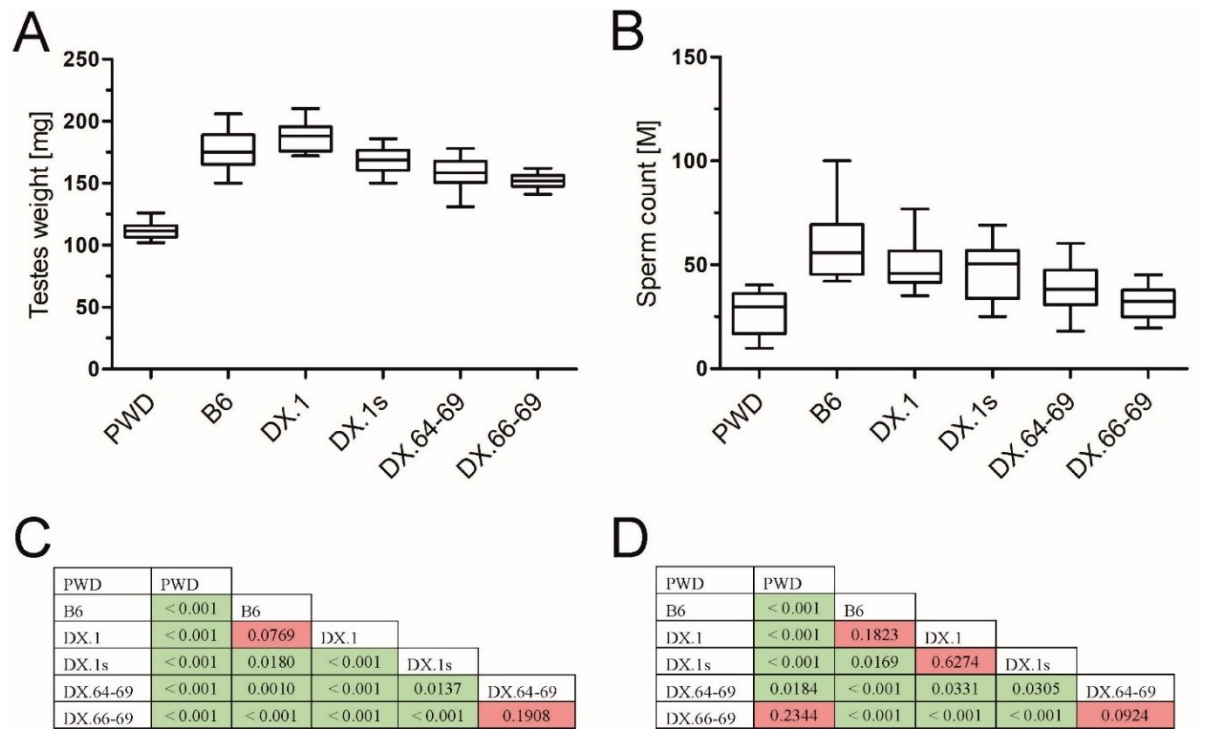

C

PWD	PWD				
B6	< 0.001	B6			
DX.1	< 0.001	0.0769	DX.1		
DX.1s	< 0.001	0.0180	< 0.001	DX.1s	
DX.64-69	< 0.001	0.0010	< 0.001	0.0137	DX.64-69
DX.66-69	< 0.001	< 0.001	< 0.001	< 0.001	0.1908

D

PWD	PWD				
B6	< 0.001	B6			
DX.1	< 0.001	0.1823	DX.1		
DX.1s	< 0.001	0.0169	0.6274	DX.1s	
DX.64-69	0.0184	< 0.001	0.0331	0.0305	DX.64-69
DX.66-69	0.2344	< 0.001	< 0.001	< 0.001	0.0924

Figure 10. Fertility parameters of subconsomic and congenic males.

(A) Mean testes weight (in milligrams ± SD). (B) Mean sperm count (in millions per pair of epididymis ± SD). Comparisons of testes weight (C) and sperm count (D) between individual animal groups were performed using a two-tailed t-test, with P-values shown in the tables.

Hstx2 fertility and meiotic chromosome asynapsis phenotypes

To verify the presence of *Hstx2* in the newly derived congenic strains, testes weight and sperm count were compared in F1 hybrid males from crosses of PWD males and B6.DX.1, B6.DX.1s, B6.DX.64-69 and B6.DX.66-69 females. The semi-fertile phenotype of (B6.DX.1 x PWD)F1 hybrids contrasted with the complete sterility of the remaining three types of hybrids, as indicated by significantly lower testes weight ($P<0.001$, t-test) (Table 11, Figure 11) and almost no sperm count ($P<0.001$, t-test) (Table 11). Surprisingly, both (B6.DX.64-69 x PWD)F1 and (B6.DX.66-69 x PWD)F1 hybrids showed significantly lower testes weight compared to (B6.DX.1s x PWD)F1 and (PWD x B6)F1 hybrids ($P<0.001$, t-test) (Table 11, Figure 11).

To evaluate meiotic chromosome synapsis in prophase I of meiosis we visualized the axial elements of partially or fully asynapsed chromosomes. This was achieved through co-immunostaining of HORMA domain-containing protein-2 (HORMAD2) (Wojtasz et al., 2012) and synaptonemal complex protein 3 (SYCP3) in pachytene cells of F1 hybrids carrying different intervals of X^{PWD} (Figure 12B).

The highest proportion, 85.3 ± 1.3 % of pachytene cells affected by asynapsis, was observed in the (PWD x B6)F1 hybrid males with an intact X^{PWD} chromosome. The asynapsis rates in two subconsomic F1 hybrids, (B6.DX.64-69 x PWD)F1 and (B6.DX.66-69 x PWD)F1, were 70.5 ± 8.6 % and 70.4 ± 9.0 %, respectively. These values did not differ significantly from each other but were notably lower than those in (PWD x B6)F1 hybrids ($P < 0.05$, t-test) (Table 11, Figure 12). Both (B6.DX.64-69 x PWD)F1 and (B6.DX.66-69 x PWD)F1 hybrids had significantly lower rates of autosomal asynapsis compared to (B6.DX.1s x PWD)F1 hybrids ($P<0.05$, t-test) (Table 11, Figure 12). Nevertheless, we conclude that the asynapsis levels in these strains are sufficient to cause sterility in the hybrids. Importantly, the X^{B6} chromosome in (B6 x PWD)F1 did not completely eliminate the asynapsis, as the rate remained at 38.9 ± 5.2 % in these males (Table 11, Figure 12).

In contrast to the *Hstx1* locus, the shortest version of *Hstx2* (Chr X: 66.51 - 69.21 Mb) was both necessary and sufficient to fully recreate the sterility phenotype of (PWD x B6)F1 male hybrids. In conclusion, approximately three-quarters of the *Hstx2* effect on asynapsis rate is preserved in the newly reduced 2.70 Mb version of the PWD sequence (Chr X: 66.51 - 69.21 Mb). However, the proximal part of the X chromosome is still required to fully reconstruct the (PWD x B6)F1 asynapsis rate.

Strain	**n**	**Testes weight [mg]**	**Sperm count [x10^6]**	**Autosomal asynapsis [%]**
(B6 x PWD)F1	64	99.7 ± 12.0	6.1 ± 4.2	38.9 ± 5.2
(PWD x B6)F1	19	65.8 ± 4.3	0.002 ± 0.01	85.3 ± 1.3
(DX.1 x PWD)F1	3	106.0 ± 7.5	7.4 ± 4.6	N/A
(DX.1s x PWD)F1	20	62.9 ± 2.9	0.01 ± 0.02	79.8 ± 2.6
(DX.64-69 x PWD)F1	25	54.7 ± 6.4	0.004 ± 0.01	70.4 ± 8.6
(DX.66-69 x PWD)F1	20	56.1 ± 5.7	0.01 ± 0.04	70.4 ± 9.0

Table 10. *Hstx2* locus mapping.

The fertility parameters of (B6 x PWD)F1 and the reciprocal (PWD x B6)F1 hybrid males, as well as F1 male progeny from crosses of B6.DX.1, B6.DX.1s, B6.DX.64-69, and B6.DX.66-69 congenic females with PWD males, are presented as mean ± SD. These parameters include testes weight (in milligrams), sperm count (in

millions per pair of epididymis), and the frequency of asynapsed autosomes (in percent). The number of analyzed males is denoted as "n," and "N/A" indicates parameters that were not analyzed.

A

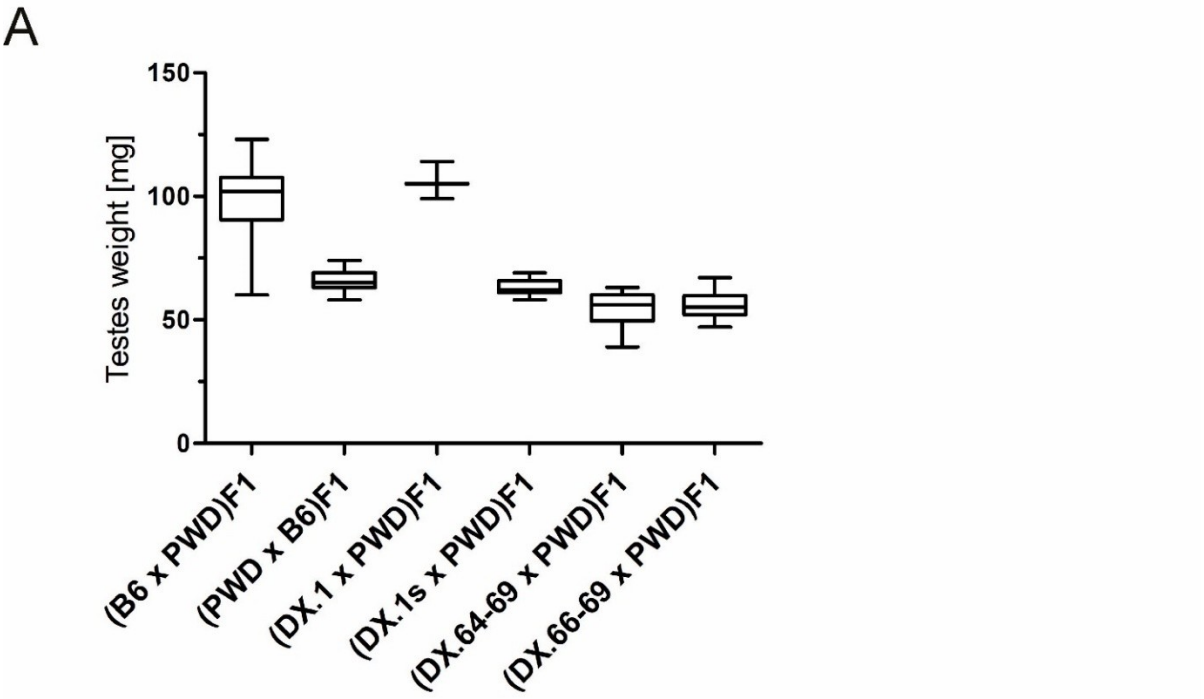

B

(B6 x PWD)F1	(B6 x PWD)F1				
(PWD x B6)F1	< 0.001	(PWD x B6)F1			
(DX.1 x PWD)F1	0.3757	< 0.001	(DX.1 x PWD)F1		
(DX.1s x PWD)F1	< 0.001	0.0149	< 0.001	(DX.1s x PWD)F1	
(DX.64-69 x PWD)F1	< 0.001	< 0.001	< 0.001	< 0.001	(DX.64-69 x PWD)F1
(DX.66-69 x PWD)F1	< 0.001	< 0.001	< 0.001	< 0.001	0.4582

Figure 11. Fertility parameters of hybrid males.

(A) Testes weight of (B6 x PWD)F1, reciprocal (PWD x B6)F1 hybrid males, and F1 male progeny from crosses of B6.DX.1, B6.DX.1s, B6.DX.64-69, and B6.DX.66-69 congenic females with PWD males are presented as mean ± SD. (B) Comparisons of testes weight between individual animal groups were performed using a two-tailed t-test, with the corresponding P-values displayed in the table.

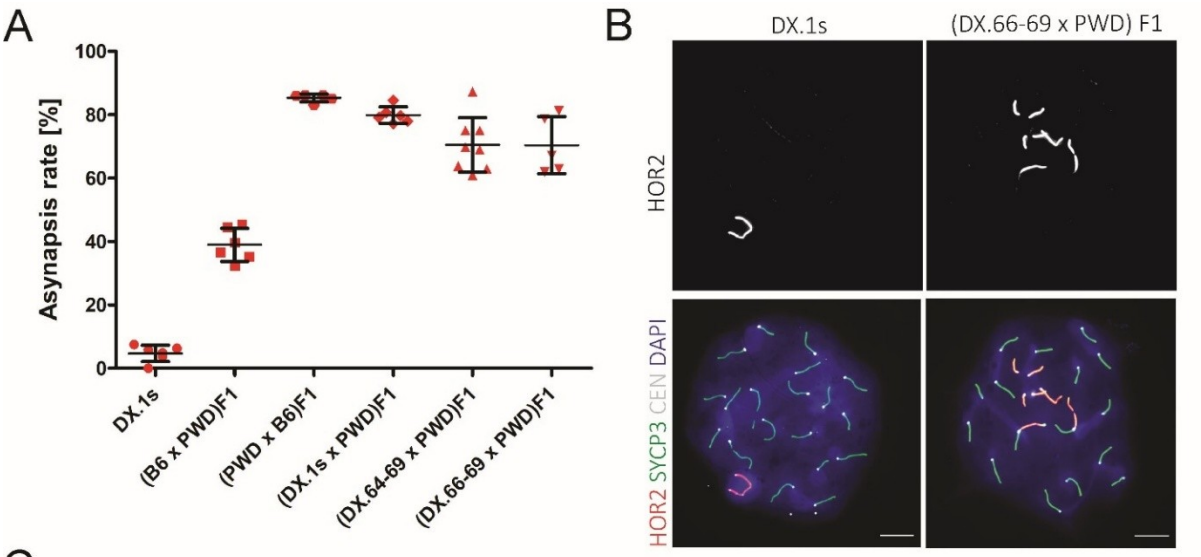

C

DX.1s	DX.1s				
(B6 x PWD)F1	< 0.001	(B6 x PWD)F1			
(PWD x B6)F1	< 0.001	< 0.001	(PWD x B6)F1		
(DX.1s x PWD)F1	< 0.001	< 0.001	0.0022	(DX.1s x PWD)F1	
(DX.64-69 x PWD)F1	< 0.001	< 0.001	0.0031	0.0248	(DX.64-69 x PWD)F1
(DX.66-69 x PWD)F1	< 0.001	< 0.001	0.0064	0.0352	0.9878

Figure 12. Chromosomal asynapsis of hybrid males.

(A) The mean asynapsis rate (± SD) in F1 hybrid males carrying different portions of X^{PWD} chroosome and B6.DX.1s were analyzed. Autosomal asynapsis (frequency of pachytene cells with at least one asynapsed autosome) was examined in 5–8 animals per genotype, with at least 50 pachytene nuclei scored per male. (B) Representative immunofluorescence micrographs show the HORMAD2-positive XY pair in a pachytene spermatocyte of B6.DX.1s congenic male, as well as asynapsed autosomes in (DX.66-69 x PWD)F1 hybrids. Asynapsed chromosome axes were immunostained with HORMAD2 antibody. SYCP3 visualized the lateral elements of synaptonemal complexes. CEN labeled centromeric heterochromatin, and DAPI stained nuclear DNA. Scale bar, 10 µm. (C) Comparisons of the asynapsis rates between individual animal groups were performed using two-tailed t-test, with P-values displayed in the table.

Meir1 controls global meiotic recombination rate

The *Meiotic recombination 1* (*Meir1*) gene was localized within the *Hstx2* interval and identified as the strongest transgressive modifier of meiotic recombination rate in B6.DX.1s males. The $Meir1^{PWD}$ allele, derived from the PWD strain with a naturally high recombination rate (29.3 ± 2.9 foci), lowered crossover frequency in a transgressive manner when introgressed into the B6 genome (Balcova et al., 2016).

Crossover frequency, determined by counting the MLH1 foci per pachytene spermatocyte, showed that both the 4.34 Mb interval (B6.DX.64-69, 22.0 ± 2.1 foci) and 2.70 Mb interval (B6.DX.66-69, 22.2 ± 2.0 foci) from the PWD genome reduced recombination compared to B6 (23.9 ± 2.3 foci) and B6.DX.1 (23.0 ± 2.2 foci). While these intervals acted similarly to *Meir1*, the reduction did not reach the level seen in B6.DX.1s (21.1 ± 1.8 foci) (Figure 13). We conclude that additional genetic elements in the proximal PWD sequence, beyond the 2.70 Mb interval, are required to fully replicate the *Meir1* phenotype.

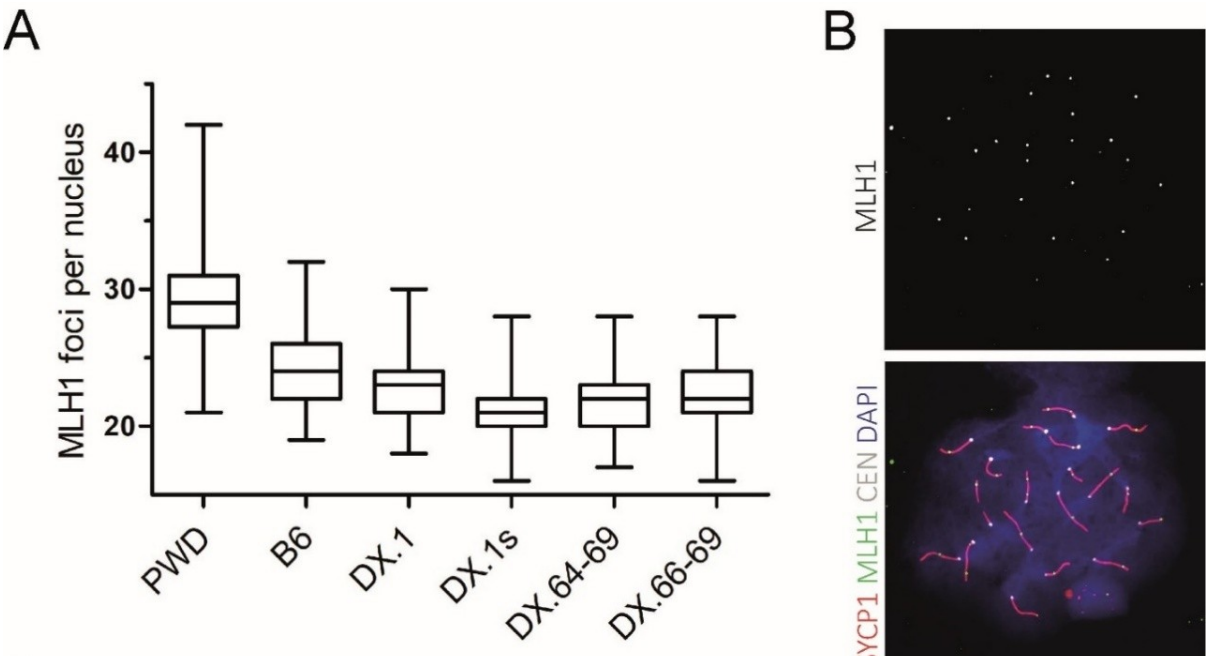

C

PWD	PWD				
B6	< 0.001	B6			
DX.1	< 0.001	< 0.001	DX.1		
DX.1s	< 0.001	< 0.001	< 0.001	DX.1s	
DX.64-69	< 0.001	< 0.001	< 0.001	< 0.001	DX.64-69
DX.66-69	< 0.001	< 0.001	< 0.001	< 0.001	0.4940

Figure 13. Transgressive effect of the *Hstx2*^{PWD} allele on crossover rate.

(A) The mean crossover rate values (± SD) are presented for subconsomic and congenic males carrying different portions of the X^{PWD} chromosome on the B6 genetic background. (B) A representative immunofluorescence micrograph shows crossing-over events immunostained with the MLH1 antibody, SYCP1 highlights the central elements of the synaptonemal complex, CEN labels centromeric heterochromatin, and DAPI stains nuclear DNA.

Scale bar, 10 µm. (C) Comparisons of recombination rates between individual animal groups were conducted using a two-tailed t-test, with P-values displayed in the table.

Analysis of the candidate genes

The newly defined 2.7 Mb long *Hstx2* locus contains 7 annotated protein-coding genes, 1 lncRNA and 21 microRNAs (GRCm38, Figure 9). From the available data, we selected candidate genes that are expressed in male germ cells, particularly during the early stages of prophase I when double-strand breaks (DSBs) and chromosome pairing occur. Additionally, we analyzed single nucleotide polymorphisms (SNPs) between the PWD and B6 strains. Only two protein-coding genes are expressed during the expected time, and only one of these genes has two nonsynonymous SNPs between the PWD and B6 parental strains (Table 12).

Gene Symbol	**X chromosome position [Mb]**	**Meiotic expression**	**SNPs (PWD/B6)**
Slitrk2	66.649-66.661	POST-meiotic	2
Gm1140	67.682-67.693	PRE-meiotic	7
Gm14692	67.695-67.706	PRE-meiotic	7
4933436I01Rik	67.919-67.921	RS	7
Fmr1os	68.667-68.678	n.d.	0
Fmr1	68.678-68.717	LEP, ZYG	0
Fmr1nb	68.761-68.804	LEP, ZYG	2
Gm6812	68.892-68.893	ES	n.d.

Table 11. List of protein-coding genes spanning the interval of the newly defined *Hstx2* locus (Chr X: 66.51–69.21 Mb, GRCm38), n.d. - not defined. LEP, ZYG - leptotene, zygotene, RS - round spermatids, ES - elongated spermatids.

RT-qPCR analysis was performed on testes from juvenile and adult males to confirm the expression of selected genes during the onset of meiosis and to compare their expression across different mouse strains and hybrids. *Fmr1nb* expression in the testes of 14 days postpartum (dpp) males did not differ significantly among B6, PWD, B6.DX.1s, or both hybrids ($P>0.05$, t-test) (Figure 14A). However, *Fmr1* expression was significantly higher in the testes of sterile (PWD x B6)F1 hybrid males compared to B6, PWD, B6.DX.1s, and fertile (B6 x PWD)F1 hybrids ($P<0.05$, t-test) (Figure 15A). In adult males, no significant difference

in *Fmr1nb* and *Fmr1* expression was observed between B6 and PWD strains. Both genes, however, were overexpressed in sterile adult (PWD x B6)F1 hybrid males compared to the B6 and PWD parental strains ($P<0.01$ for *Fmr1nb*, $P<0.001$ for *Fmr1*, t-test), likely due to the improper functioning of meiotic sex chromosome inactivation (MSCI) (Figure 14B, 15B).

Fluorescent immunolabeling on histological sections of testes confirmed the presence of FMR1NB and FMRP proteins in germ cells during early meiosis. Both proteins were detected in early meiotic stages, with the signal disappearing after prophase I (Figure 16).

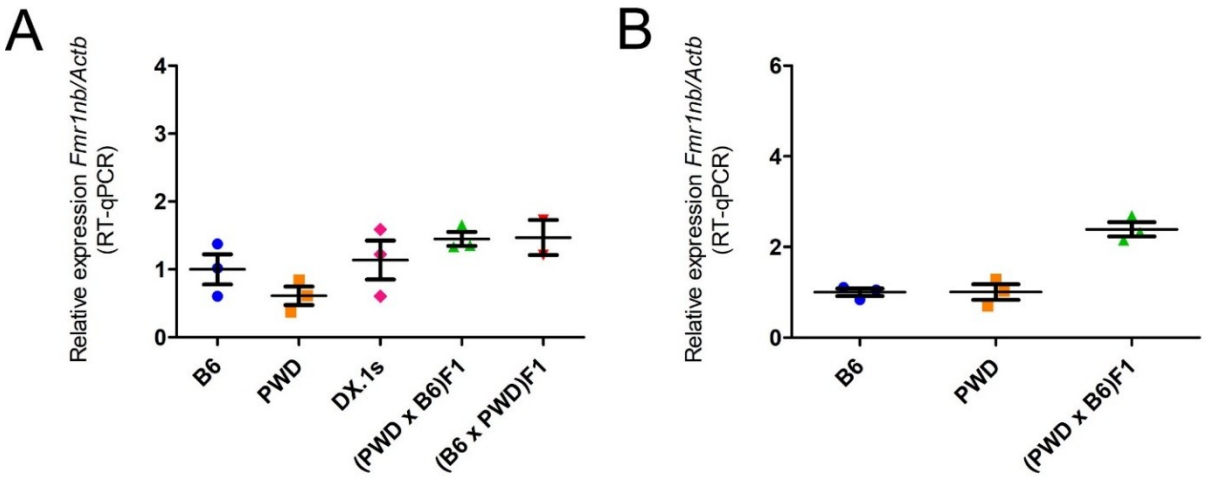

Figure 14. Relative *Fmr1nb* expression.

(A) *Fmr1nb* relative expression in the testes of 14 days postpartum (dpp) males. (B) *Fmr1nb* relative expression in the testes of adult males (> 8 weeks). Expression analyses were normalized to the *Actb* reference gene and presented as fold changes relative to B6 (with the average B6 expression set to 1). All results are expressed as mean ± SD, based on data from at least two different males per strain.

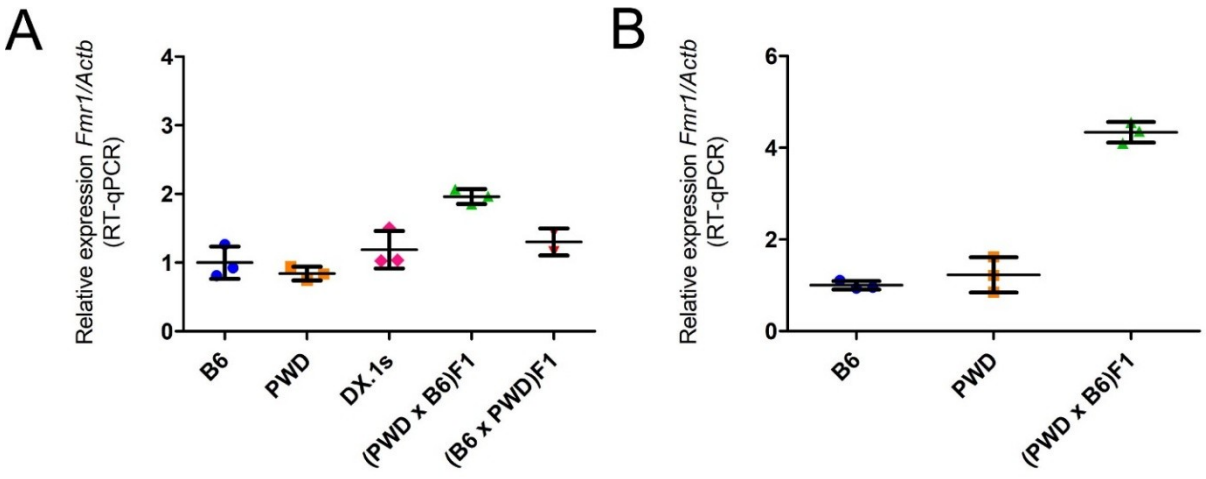

Figure 15. Relative *Fmr1* expression.

(A) *Fmr1* relative expression in the testes of 14 days postpartum (dpp) males. (B) *Fmr1* relative expression in the testes of adult males (> 8 weeks). Expression analyses were normalized to the *Actb* reference gene and presented

as fold changes relative to B6 (with the average B6 expression set to 1). All results are expressed as mean ± SD, based on data from at least two different males per strain.

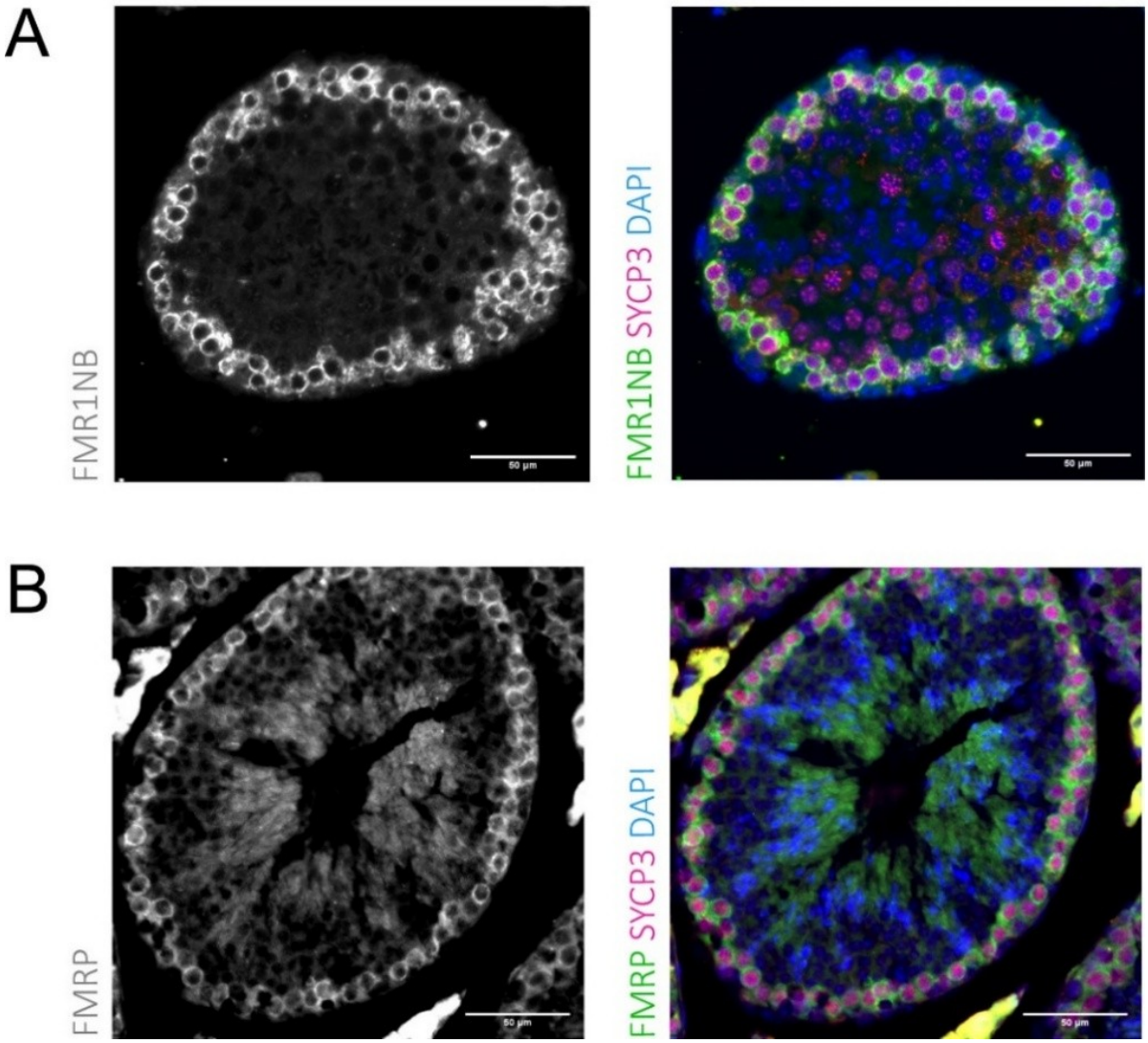

Figure 16. Immunolabeling of testes.

(A) Immunolabeling of FMR1NB and SYCP3 in histological sections of the testis from a B6.DX.1s male. FMR1NB is shown in green, SYCP3 in violet, and DAPI in blue. Scale bar, 50 µm. (B) Immunolabeling of FMRP and SYCP3 in histological sections of the testis from B6.DX.1s male. FMRP is shown in green, SYCP3 in violet, and DAPI in blue. Scale bar, 50 µm.

Western blot analysis of testicular protein samples from B6 and PWD strains revealed expression of three FMR1NB isoforms (Q80ZA7, UniProt), comprising 238, 192 and 166 amino acids, respectively. Notably, FMR1NB expression was lower in PWD than in B6. The most abundant isoform in the testes was isoform-3, which consists of 166 amino acids, while the other two isoforms were only weakly expressed in the B6 strain (Figure 18B). Two

nonsynonymous substitutions in *Fmr1nb* gene result in two amino acid exchanges: at position 31, Arginine^{PWD} is replaced by Threonine^{B6}, and at position 162, Leucine^{PWD} is replaced by Isoleucine^{B6}.

For FMRP (P35922, UniProt) only one isoform in the testes of B6 and PWD strains was detected by western blot, despite databases indicating 12 isoforms resulting from alternative splicing, ranging from 614 to 415 amino acids. We found no difference in FMRP expression between B6 and PWD strains. However, both proteins were overexpressed in sterile hybrids (PWD x B6)F1, likely due to the accumulation of early meiotic cells and the absence of post-pachytene stages (Figure 27B).

The *Hstx2* locus plays a crucial role in hybrid male sterility between PWD and B6 strains, and the differential expression of genes like *Fmr1* and *Fmr1nb* in hybrids compared to parental strains suggested that genetic elements within this interval may contribute to disrupted meiosis and sterility.

Generation and confirmation of the *Fmr1nb* deletion line

To investigate the effect of the *Fmr1nb* null allele on the *Hstx1/2* phenotypes, our colleagues from Transgenic and Archiving Module (TAM, IMG) generated a *Fmr1nb* deletion mutant line using TALEN nucleases. A 19 bp deletion was introduced into the PWD allele of the B6.DX.1s congenic strain. The deletion was detected by polymerase chain reaction (PCR) using a specific pair of primers (Table 1) and visualized on a 4 % agarose gel. The mutation was further confirmed by Sanger sequencing of the PCR product. The deletion affected the first exon, disrupting the ATG start codon, and resulted in the loss of the translation initiation site (Figure 17). The absence of the FMR1NB protein was verified by fluorescent immunolabelling of histological sections of testes and by western blot analysis (Figure 18B).

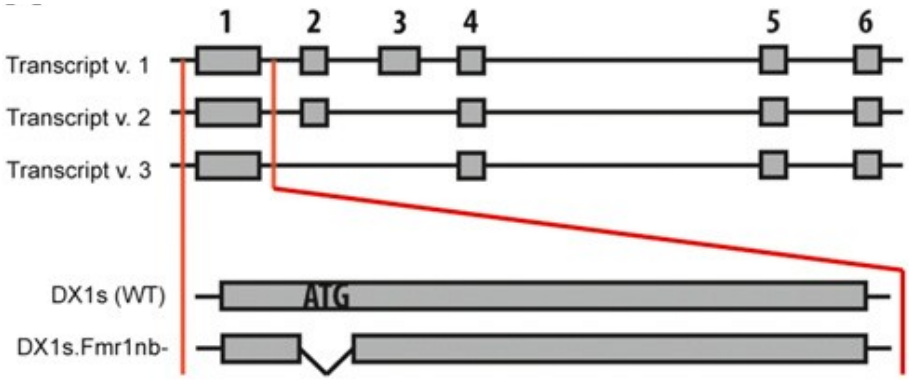

Figure 17. Generation of the *Fmr1nb* null allele.

The *Fmr1nb* transcript variants are depicted, comprising six, five, and four exons.

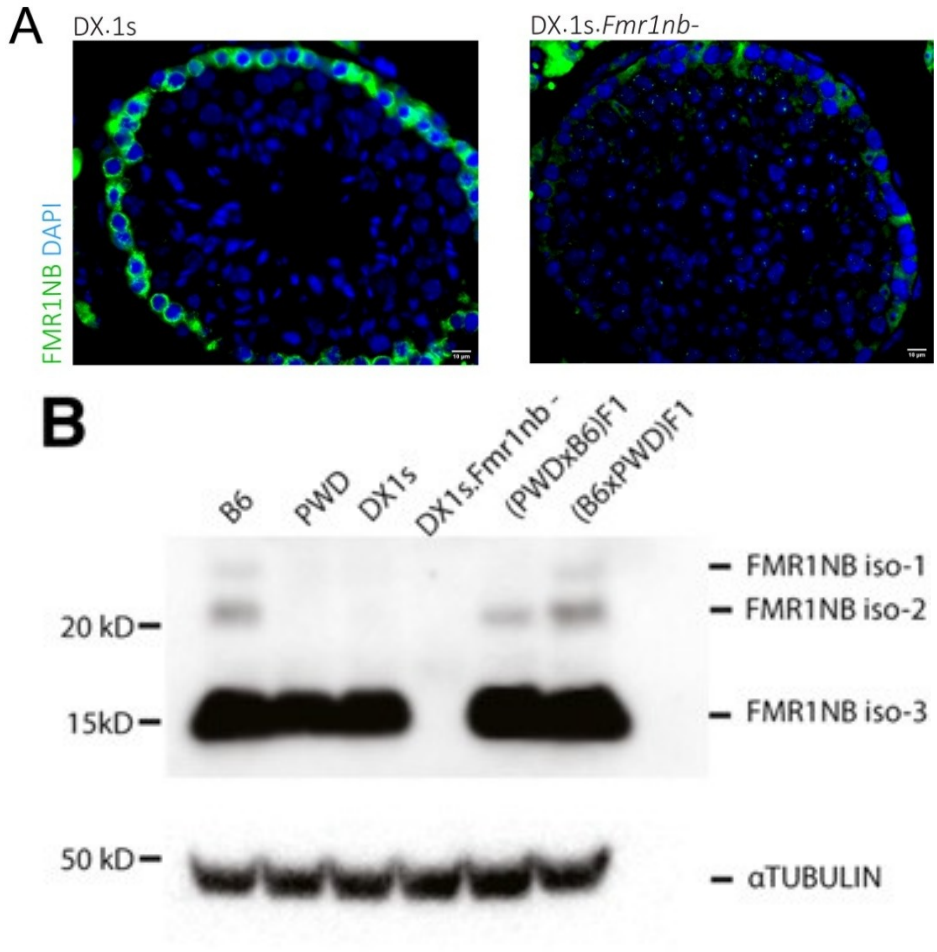

Figure 18. Confirmation of *Fmr1nb* knockout.

(A) Immunolabeling of FMR1NB in histological sections of testes from B6.DX.1s and B6.DX.1s$^{Fmr1nb-}$ males. FMR1NB is shown in green, DAPI in blue. Scale bar, 10 µm. (B) FMR1NB protein levels in the testes of males

with the indicated genotypes were assessed by western blot. None of the three FMR1NB isoforms were detectable in the B6.DX.1s$^{Fmr1nb-}$ strain. αTubulin was used as a loading control.

Phenotypes of B6.DX.1s$^{Fmr1nb-}$ males

The B6.DX.1s$^{Fmr1nb-}$ males successfully mated with either B6 or B6.DX.1s females. To evaluate fertility, three males were paired with B6 virgin females for 3 months, and the number of pups sired by B6.DX.1s$^{Fmr1nb-}$ and B6.DX.1s males was recorded. The results showed that the mean litter size for the *Fmr1nb* null mutant males was significantly lower than that of males carrying the wild-type allele (1.8 ± 0.8 vs. 5.0 ± 1.5, P<0.05, t-test) (Figure 19).

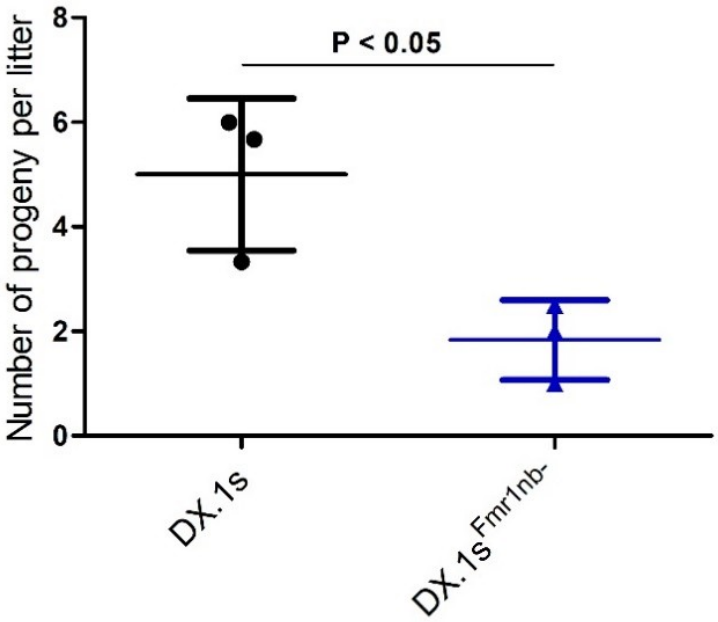

Figure 19. Number of progeny sired by B6.DX.1s and B6.DX.1s$^{Fmr1nb-}$ males.

Mean number of offspring per litter (± SD) born to B6 females. Three males from each strain were mated with B6 females for three months. Statistical comparison was performed using a two-tailed t-test.

To investigate the potential role of *Fmr1nb* in meiosis, we first focused on changes in testes weight and sperm count between B6.DX.1s$^{Fmr1nb-}$ and B6.DX.1s control males. The testes weight of B6.DX.1s$^{Fmr1nb-}$ males was significantly lower than of B6.DX.1s males (156.7 ± 19.6 mg vs. 167.8 ± 9.5 mg, P<0.01, t-test) (Figure 20A), but the sperm counts were not significantly different between the two groups (45.5 ± 12.7 x 10^{-6} vs. 48.0 ± 12.7 x 10^{-6}, P=0.4568, t-test) (Figure 20B).

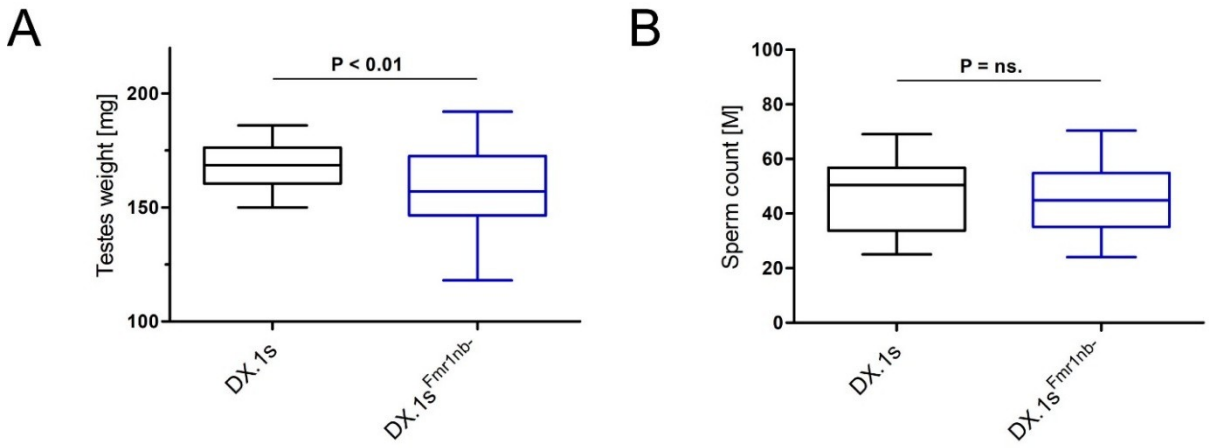

Figure 20. Fertility parameters of B6.DX.1s and B6.DX.1s$^{Fmr1nb-}$ males.

(A) The mean testes weight (in milligrams ± SD). (B) The mean sperm count (in millions per pair of epididymis ± SD) (P=0.4568). Statistical comparisons were performed using a two-tailed t-test.

To analyze the progression of spermatogenesis, we examined the morphology of the testes histological sections stained by hematoxylin and eosin. Spermatogenesis disruptions were not observed in B6.DX.1s$^{Fmr1nb-}$ males compared to B6.DX.1s controls (Figure 21). All stages of spermatogenesis were present, from spermatogonia to spermatozoa. However, fluorescence TUNEL labeling revealed a significantly higher number of apoptotic cells in the seminiferous tubules of B6.DX.1s$^{Fmr1nb-}$ males compared to B6.DX.1s controls (3.4 ± 0.2 vs. 1.5 ± 0.4, P<0.01, t-test) (Figure 22A, B)

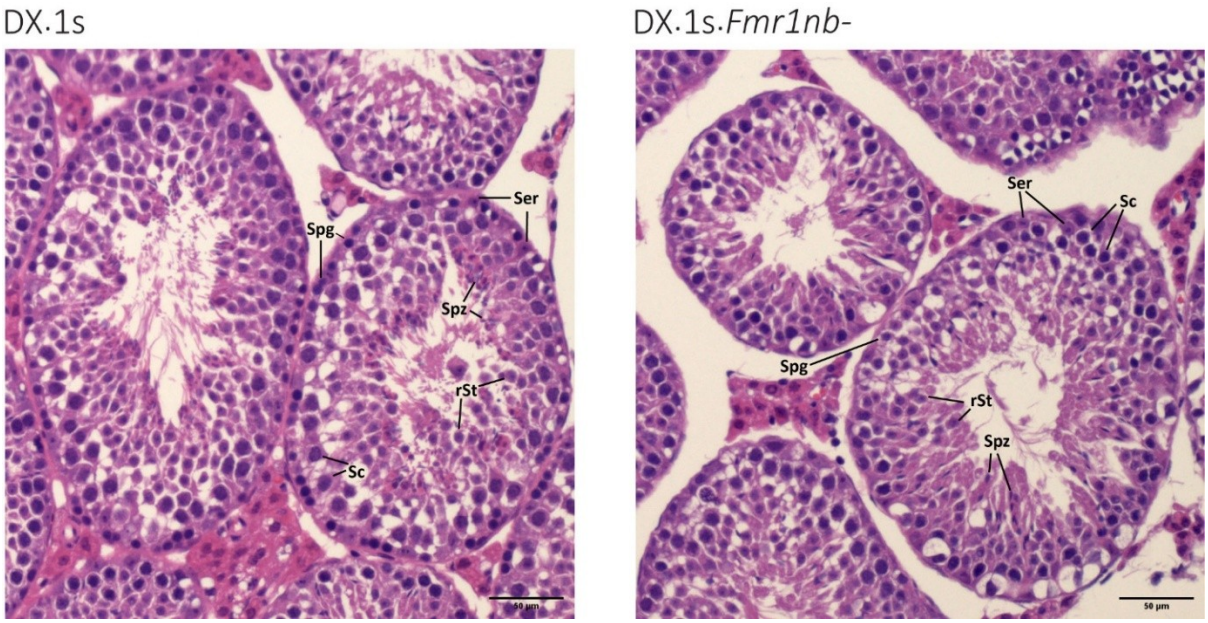

Figure 21. Histological sections of testes from B6.DX.1s and B6.DX.1s$^{Fmr1nb-}$ males.

Seminiferous tubules stained with hematoxylin and eosin showed no morphological changes or differences in the occurrence of meiotic cells. Labeled cell types: Ser, Sertoli cells; Spg, Spermatogonia; Sc, Spermatocytes; rSt, round Spermatids; Spz, Spermatozoa. Scale bar, 50 µm.

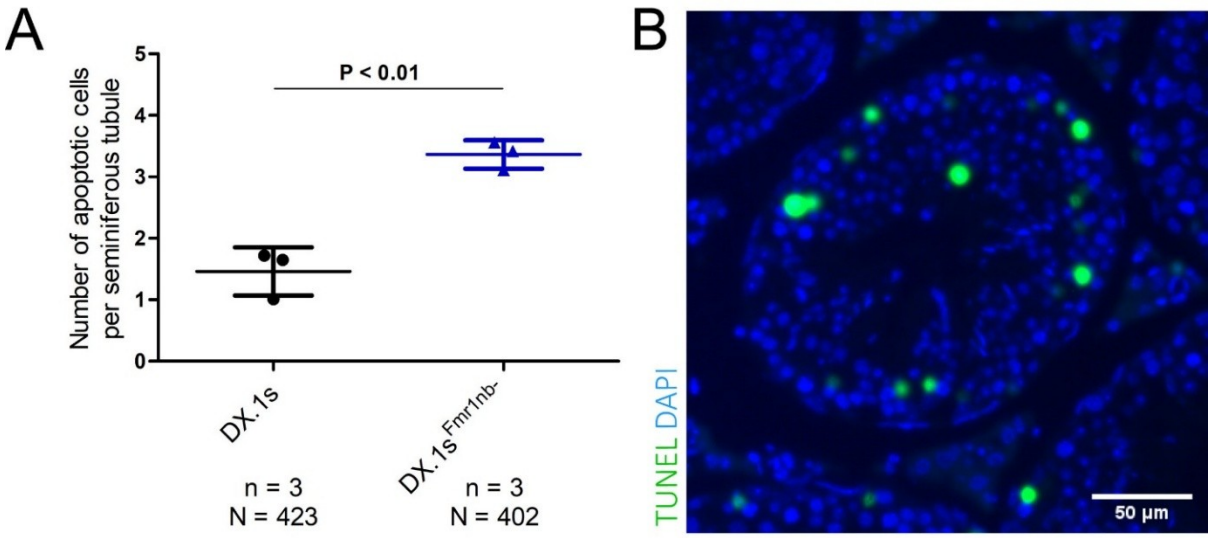

Figure 22. Apoptotic cells in the testes of B6.DX.1s and B6.DX.1s$^{Fmr1nb-}$ males.

(A) The mean number (± SD) of apoptotic cells per seminiferous tubule; *n* indicates the number of tested males, and *N* the number of seminiferous tubules examined. Statistical comparison was performed using a two-tailed t-test. (B) Seminiferous tubule stained by fluorescence TUNEL assay (green) and DAPI (blue). Scale bar, 50 µm.

We further analyzed progression through prophase I of meiosis, with an emphasis on meiotic chromosome synapsis and crossover formation. No disruptions were observed in synaptonemal complex formation or chromosome pairing. The rate of asynapsed autosomes

was 5.2 ± 2.1 % in B6.DX.1s$^{Fmr1nb-}$ males compared to 4.7 ± 2.6 % in B6.DX.1s males (P=0.7214, t-test) (Figure 23A). Similarly, there was no significant difference in the number of crossovers, as visualized by MLH1 staining (20.8 ± 1.7 for B6.DX.1s$^{Fmr1nb-}$ vs. 21.1 ± 1.8 for B6.DX.1s, P=0.0583, t-test) (Figure 23B). These results suggest that prophase I of spermatogenesis progresses normally in B6.DX.1s$^{Fmr1nb-}$ males.

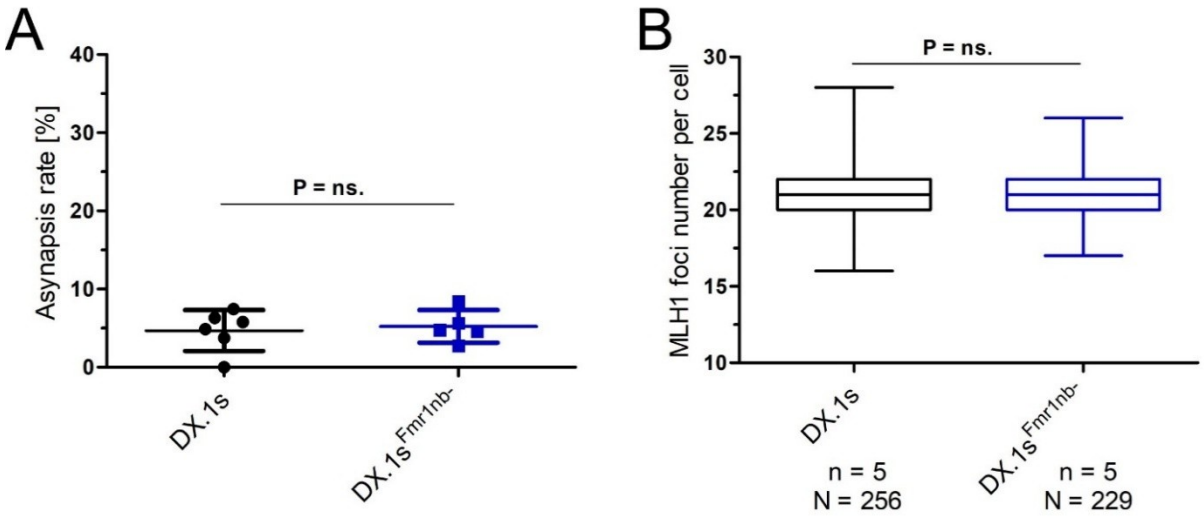

Figure 23. Progression through prophase I of meiosis in B6.DX.1s and B6.DX.1s$^{Fmr1nb-}$ males.

(A) The mean asynapsis rate (± SD) (P=0.7214) and (B) the crossover rate (± SD) (P=0.0583) in males of each genotype. Autosomal asynapsis frequency and crossover numbers were examined in at least five males per genotype, with at least 40 pachytene nuclei scored per male. *n* indicates the number of males, and *N* the number of pachytene nuclei. Statistical comparisons were performed using a two-tailed t-test.

To examine the effect of the *Fmr1nb* null allele on the *Hstx1* phenotype, we compared the morphology of spermatozoa from B6.DX.1s$^{Fmr1nb-}$ and B6.DX.1s males. B6.DX.1s$^{Fmr1nb-}$ males exhibited a significantly higher proportion of malformed sperm heads compared to B6.DX.1s controls (76.9 ± 8.0 % vs. 69.0 ± 7.3 %, P<0.05, t-test) (Figure 24). This finding is consistent with previous reports on the *Fmr1nb* null allele in a B6 background (Lustyk et al., 2019). However, the high proportion of malformed sperm heads in B6.DX.1s males suggests that *Fmr1nb* is not the sole modifier of sperm head morphology on chromosome X.

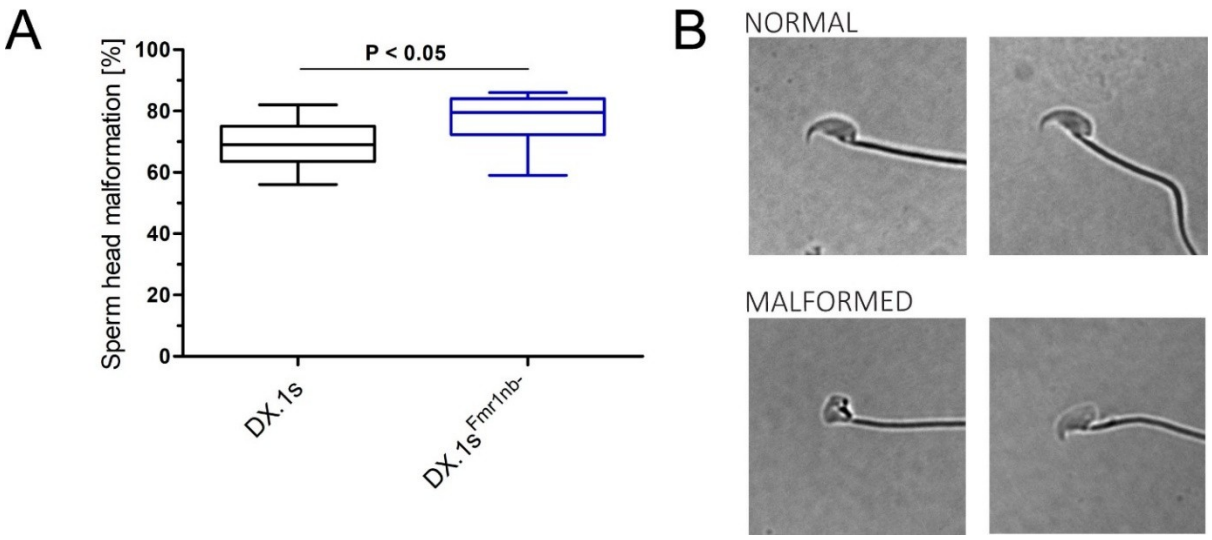

Figure 24. Effect of *Fmr1nb* null allele on the *Hstx1* phenotype.

(A) The mean freguency of sperm head malformations (percentage ± SD) for each genotype. Statistical comparison was performed using a two-tailed t-test. (B) Sample images showing normal and malformed sperm heads.

To investigate whether *Fmr1nb* interacts with the *Hstx2* phenotype, we analyzed hybrid males for testes weight and sperm count. No significant differences were observed in testes weight between (B6.DX.1s$^{Fmr1nb-}$ x PWD)F1 and control (B6.DX.1s x PWD)F1 males (61.8 ± 4.1 mg vs. 62.9 ± 2.9 mg, P=0.3284, t-test) (Figure 25A), nor in sperm count (0.03 ± 0.08 x 10^{-6} vs. 0.01 ± 0.02 x 10^{-6}, P=0.1887, t-test). Surprisingly, we observed a significantly lower percentage of asynapsed autosomes in (B6.DX.1s$^{Fmr1nb-}$ x PWD)F1 males compared to control (B6.DX.1s x PWD)F1 (75.1 ± 1.4 % vs. 79.8 ± 2.6 %, P<0.05, t-test) (Figure 25B). However, this reduction in autosomal asynapsis did not affect progression through meiosis, and the *Fmr1nb*^{PWD} null allele did not rescue the sterility of (B6.DX.1s.$^{Fmr1nb-}$ x PWD) F1 hybrid males.

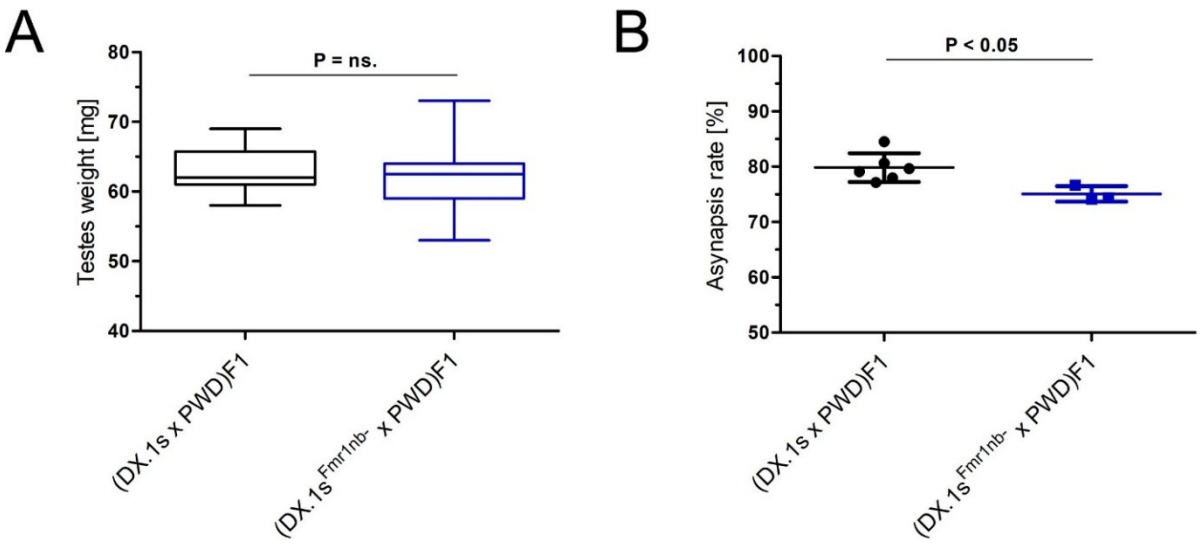

Figure 25. Effect of *Fmr1nb* null allele on the *Hstx2* phenotype.

(A) The mean testes weight (in milligrams ± SD) of (B6.DX.1s$^{Fmr1nb-}$ x PWD)F1 males and control (B6.DX.1s x PWD)F1 males (P=0.3284). (B) The mean autosomal asynapsis rate (± SD) in males of each genotype. Statistical comparisons were performed using a two-tailed t-test.

To conclude, the *Fmr1nb* gene is not essential for autosomal pairing or crossover formation during meiosis, but it plays a critical role in the normal course of spermiogenesis. In intersubspecific F1 hybrids, the absence of FMR1NB does not modify meiotic arrest or hybrid sterility, suggesting that *Fmr1nb* is not a major contributor to the *Hstx2*-associated hybrid sterility phenotype.

Generation and confirmation of the *Fmr1* null line

To investigate the role of *Fmr1* in the *Meir1* and *Hstx2* phenotypes, we generated an *Fmr1*^{PWD} null allele mutant line using the CRISPR-Cas9 method. To produce the B6.DX.1s.$^{Fmr+/-}$ line (in collaboration with colleagues from TAM, IMG), I designed gRNAs for *Fmr1* gene editing in the B6.DX.1s line, as described in the Methods section. Transgenic founder animals were tested for the presence of the edited *Fmr1* gene by specific PCR targeting the expected deletion. The amplicons were separated on a 4% agarose gel, which showed no length polymorphism between founders and wild-type controls. However, the founder PCR amplicons were Sanger sequenced to achieve single-nucleotide resolution, revealing a 2 bp insertion at the expected Cas9 nuclease cleavage site (Figure 26). In silico analysis indicated that the TT insertion caused a frameshift mutation, leading to the premature appearance of a stop codon. To confirm whether the 2 bp insertion in the first exon of *Fmr1* resulted in the

absence of FMRP protein, we performed fluorescent immunolabelling of histological sections of the testes and conducted a western blot analysis (Figure 27).

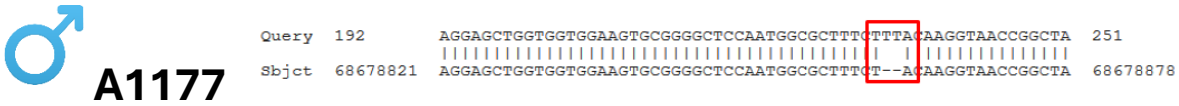

Figure 26. Visualization of TT Insertion.

The TT insertion is visualized in the target region, showing the location and impact of the 2 bp insertion. This causes a frameshift mutation, leading to the premature appearance of a stop codon. The analysis confirms the insertion's effect on gene function.

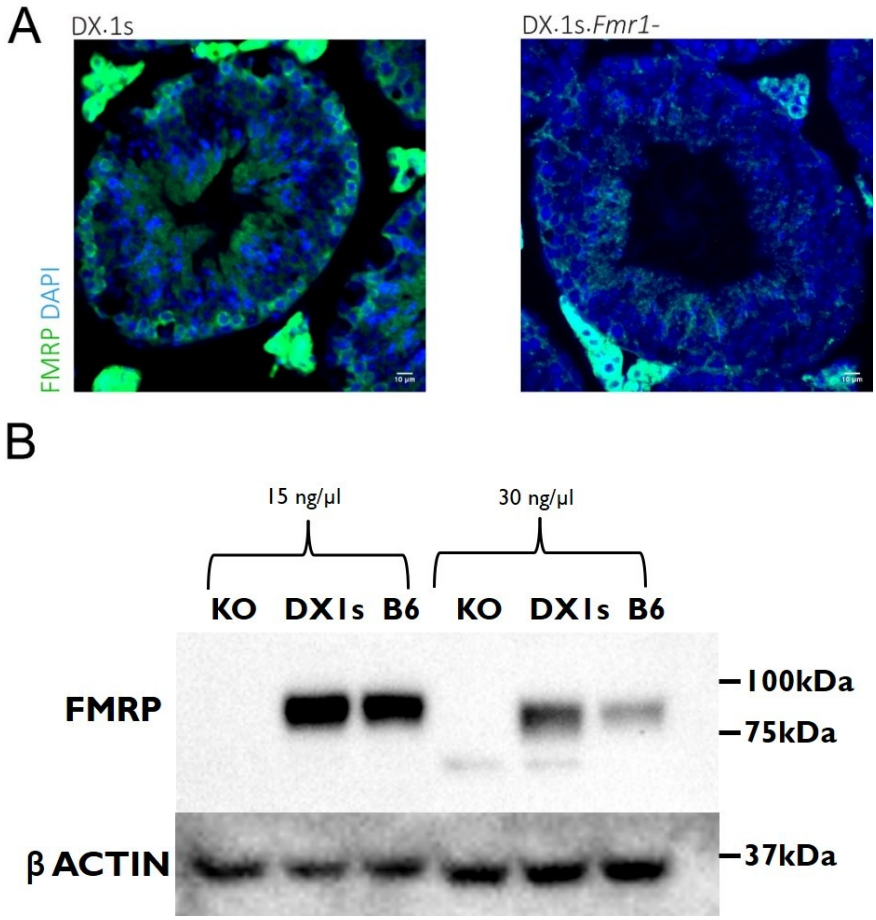

Figure 27. Confirmation of *Fmr1* knockout.

(A) Immunolabeling of FMRP in histological sections of testis from B6.DX.1s and B6.DX.1s^{Fmr1-} males. FMRP is shown in green, and DAPI is in blue. Scale bar, 10 µm. (B) FMRP levels in the testes of males with the indicated

genotypes, assessed bywWestern blot. FMRP was not detectable in the B6.DX.1s^{Fmr1-} strain. β-actin was used as a loading control.

Phenotypes of B6.DX.1s^{Fmr1-} males

To investigate the role of *Fmr1* in meiosis, we first compared testes weight and sperm count between B6.DX.1s^{Fmr1-} and B6.DX.1s males. We observed significant increase in the mean testes weight of B6.DX.1s^{Fmr1-} males compared to B6.DX.1s controls (199.7 ± 16.1 mg vs. 167.8 ± 9.5 mg, P<0.001, t-test) (Figure 28A), confirming previous findings that *Fmr1* knockout causes macroorchidism in humans (The Dutch-Belgian Fragile X Consortium, 1994). However, the sperm count in B6.DX.1s^{Fmr1-} males did not significantly differ from B6.DX.1s controls (49.1 x 10^{-6} ± 10.6 vs. 48.0 x 10^{-6} ± 12.7, P=0.8099, t-test) (Figure 28B).

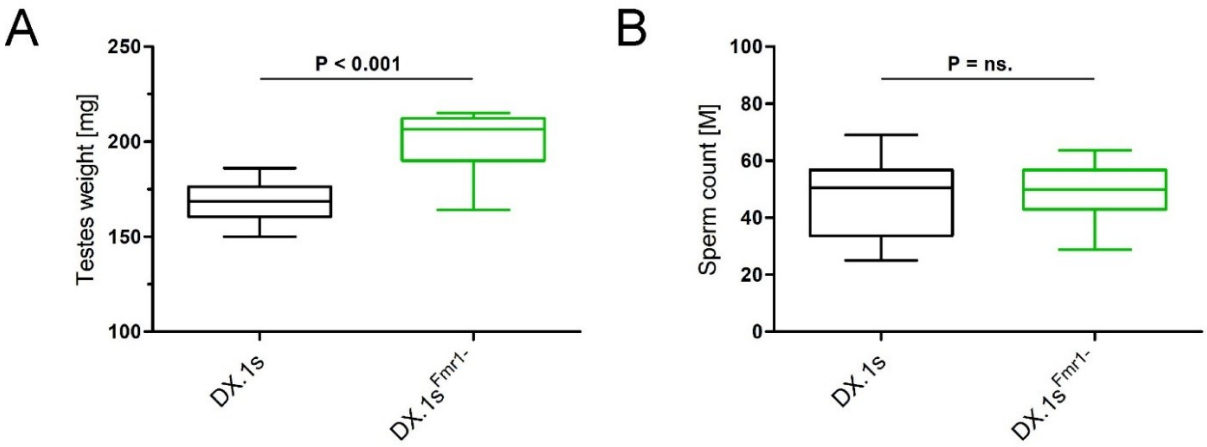

Figure 28. Fertility parameters of B6.DX.1s and B6.DX.1s^{Fmr1-} males.

(A) The mean testes weight (in milligrams ± SD). (B) The mean sperm count (in millions per pair of epididymis ± SD) (P=0.8099). Statistical comparisons were performed using a two-tailed t-test.

Next, we analyzed the progression of spermatogenesis. Cross-sections of testes stained with hematoxylin and eosin revealed no disruptions in spermatogenesis, and meiosis proceeded normally in B6.DX.1s^{Fmr1-} males (Figure 29). Additionally, we observed no morphological changes in the seminiferous tubules, suggesting that the observed macroorchidism could be due to an increased number or size of the interstitial cells, which we were unable to detect in this analysis.

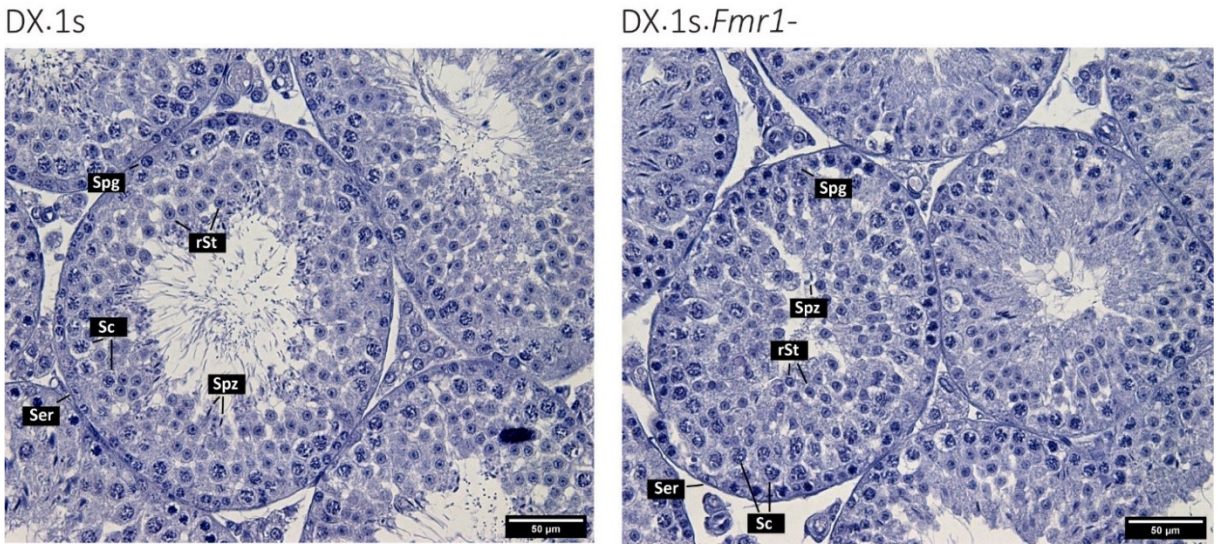

Figure 29. Histological sections of testes from B6.DX.1s and B6.DX.1s^{Fmr1-} males.

Seminiferous tubules stained with hematoxylin and eosin showed no morphological changes or differences in the occurrence of meiotic cells. Labeled cell types: Ser, Sertoli cells; Spg, Spermatogonia; Sc, Spermatocytes; rSt, round Spermatids; Spz, Spermatozoa. Scale bar, 50 µm.

We also examined the progression of prophase I of meiosis. Fluorescent immunostaining of synaptonemal complex proteins in spermatocyte spreads revealed no disruptions in autosomal pairing. The rate of asynapsed autosomes was 6.0 ± 2.3 % in B6.DX.1s^{Fmr1-} males compared to 4.7 ± 2.6 % in B6.DX.1s controls (P=0.4531, t-test) (Figure 30A). However, we observed a significantly increased number of crossovers, as indicated by MLH1 staining (21.7 ± 2.3 in B6.DX.1s^{Fmr1-} males vs. 21.1 ± 1.8 in B6.DX.1s controls, P<0.001, t-test) (Figure 30B). This finding contrasts with data published by Alpatov et al. (2014), who showed that, in the absence of FMRP, the resolution of single-strand DNA repair intermediates is delayed in meiotic germ cells, resulting in defective crossover formation. We conclude that autosomal pairing and synapsis progress correctly in B6.DX.1s^{Fmr1-} males, but crossover formation is disrupted, suggesting that *Fmr1* may function as a *Meiotic recombination 1* (*Meir1*) (Balcova et al., 2016).

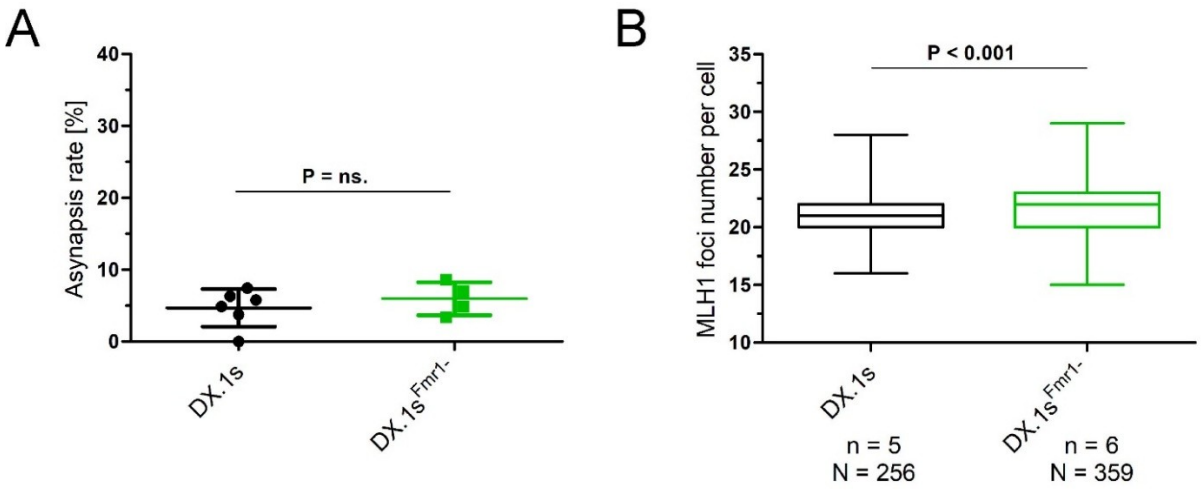

Figure 30. Progression through prophase I of meiosis in B6.DX.1s and B6.DX.1s^{Fmr1-} males.

(A) The mean asynapsis rate (± SD) (P=0.4531) and (B) the crossover rate (± SD) in males of each genotype. Autosomal asynapsis frequency and mature crossover numbers were examined in at least four males per genotype, with at least 40 pachytene nuclei scored per male; *n* indicates the number of males, and *N* the number of pachytene nuclei. Statistical comparisons were performed using a two-tailed t-test.

To assess whether *Fmr1* functions as a *Hstx2* modifier, we analyzed hybrid males for testes weight and sperm count. We observed a significant decrease in testes weight between (B6.DX.1s^{Fmr1-} x PWD)F1 and control (B6.DX.1s x PWD)F1 males (67.0 ± 4.72 mg vs. 62.85 ± 2.94 mg, P<0.01, t-test) (Figure 31A), although this did not affect sperm count (0.03 ± 0.06 x 10^{-6} vs. 0.01 ± 0.02 x 10^{-6}, P=0.2131, t-test). Furthermore, we observed no significant change in the rate of asynapsed autosomes when comparing (B6.DX.1s^{Fmr1-} x PWD)F1 males with controls (B6.DX.1s x PWD)F1 (83.46 ± 3.09 % vs. 79.84 ± 2.6 %, P=0.0640, t-test) (Figure 31B).

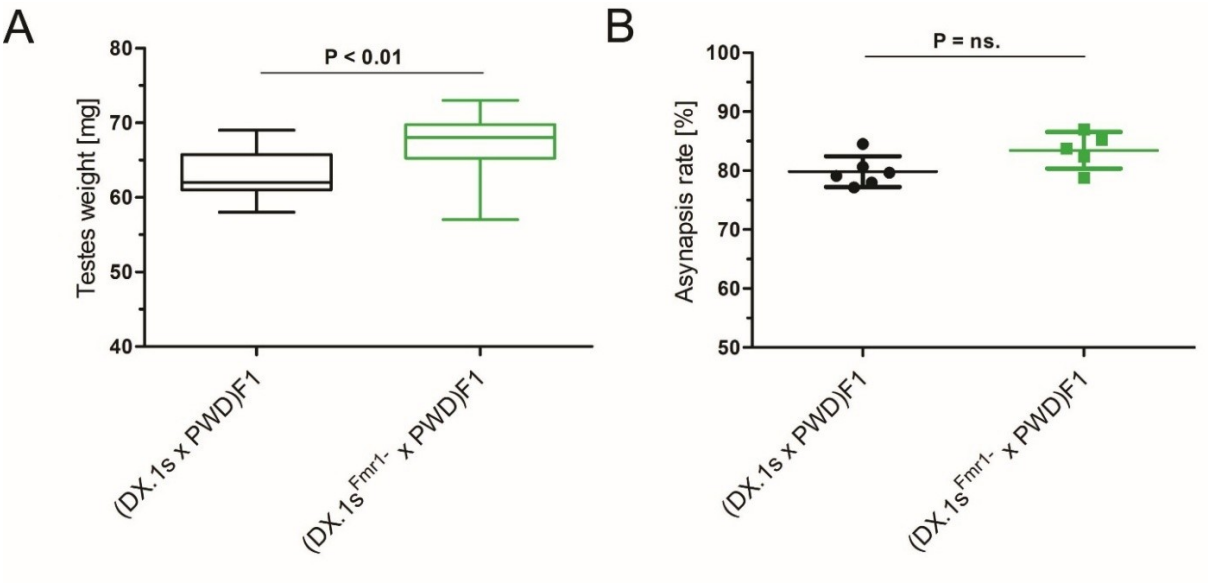

Figure 31. Effect of the *Fmr1* null allele on the *Hstx2* phenotype.

(A) The mean testes weight (in milligrams ± SD) of (B6.DX.1s^{Fmr1-} x PWD)F1 males and control (B6.DX.1s x PWD)F1 males. (B) The mean autosomal asynapsis rate (± SD) in males of each genotype. Statistical comparisons were performed using a two-tailed t-test.

We conclude that *Fmr1* is not required for autosomal pairing during prophase I of meiosis. However, the absence of the *Fmr1*^{PWD} allele on a B6 background significantly increased the number of crossovers, supporting the idea that *Fmr1* plays a role in crossover regulation, likely as a component of the *Meir1* pathway. Despite this, the increased crossover levels in B6.DX.1s^{Fmr1-} males (21.7 ± 2.3 MLH1 foci) are still significantly lower than those in B6 males (23.9 ± 2.3, $P < 0.001$, t-test), suggesting that FMRP may be part of a complex responsible for crossover formation. Moreover, another factor in the proximal region of the PWD X chromosome appears necessary to fully restore MLH1 foci levels in the B6 strain. In intersubspecific F1 hybrids, the absence of FMRP does not influence meiotic arrest of hybrids, indicating that *Fmr1* does not play a major role in hybrid sterility within the *Hstx2* locus context.

Tg(*Fmr1,Fmr1os,Fmr1nb)* transgenic lines phenotypes

To test whether *Fmr1nb*^{PWD} or *Fmr1*^{PWD} alleles are responsible for the sterile phenotype in (PWD x B6)F1 hybrid males, we first generated a B6 transgenic mouse line containing a randomly inserted extra copy of the *Fmr1nb*^{B6} and *Fmr1*^{B6} alleles. The hypothesis assumes that the extra B6 alleles of these genes will rescue the sterile phenotype caused by the PWD allele. We selected a BAC DNA clone (see Methods) containing the genomic DNA region of the B6

strain with *Fmr1*, *Fmr1os,* and *Fmr1nb* genes. The transgenic line was initially prepared in the B6 mouse strain, and the transgene was later transferred to the B6.DX.1s consomic strain through crossing. The B6.DX.1s.XC7 transgenic line contains the $Fmr1nb^{PWD}$ and $Fmr1^{PWD}$ genes from the X chromosome, along with an extra $Fmr1nb^{B6}$ and $Fmr1^{B6}$ transgenic copy randomly inserted into the genome. The presence of the transgene was confirmed by PCR with primers designed for BAC construct flanking regions (see Methods).

RNA extracts from the testes of 14dpp transgenic B6.XC7 and B6 control males were prepared. Relative expression analysis revealed no difference in *Fmr1nb* expression between the transgenic line and B6 ($P=1.0000$, t-test) (Figure 32A). However, *Fmr1* expression was 3.2-fold higher in B6.XC7 males ($P<0.01$, t-test) (Figure 32B). Overexpression of *Fmr1* was confirmed at the protein level by fluorescent immunolabelling of histological sections from adult testes using an antibody against FMRP (Figure 32C) and western blot analysis (Figure 33). Additionally, histological sections revealed no spermatozoa, despite the presence of round spermatids, suggesting possible issues during the spermiogenesis stage, likely in the maturation of spermatozoa. FMRP was detected in all types of meiotic cells in B6.XC7 males, suggesting that its additional expression comes from the randomly inserted autosomal transgene, not just from the X chromosome. Therefore, we focused on *Fmr1* as the primary driver of the transgenic phenotype, although we cannot completely exclude the roles of *Fmr1nb* and *Fmr1os*.

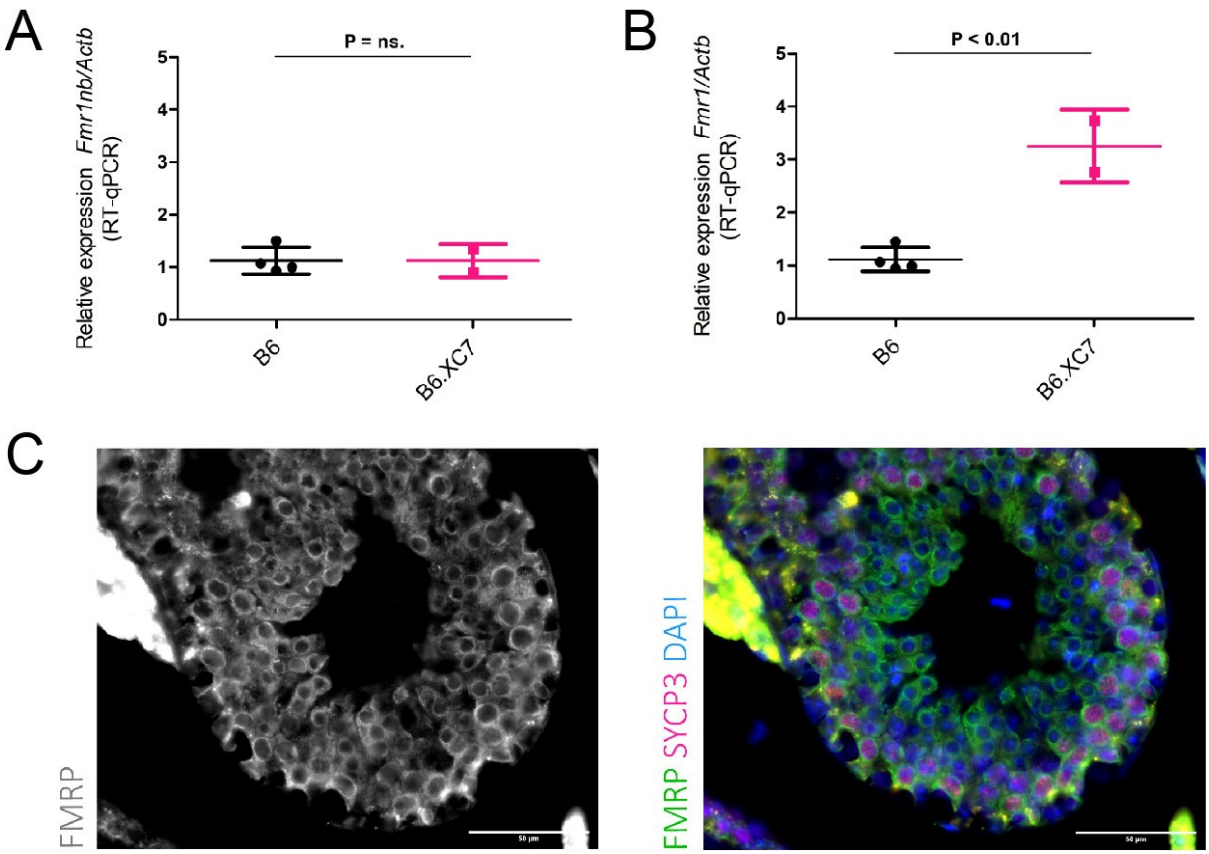

Figure 32. Gene expression in transgenic mouse line.

(A) *Fmr1nb* relative expression in the testes of 14dpp males. (B) *Fmr1* relative expression in the testes of 14dpp males. Expression analyses are normalized to *Actb* reference gene and presented as fold changes relative to B6 (with the average B6 expression set to 1). All results are calculated as mean ± SD from at least two males per strain. (C) Immunolabeling of FMRP in histological sections of the testis from B6.XC7 male. FMRP is shown in green, and DAPI in blue. Scalle bar, 50 µm.

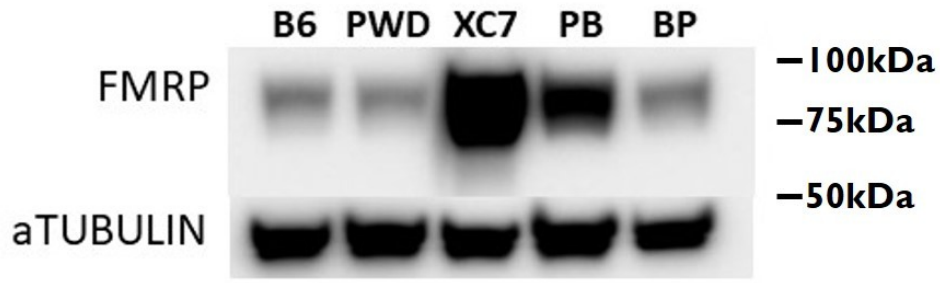

Figure 33. FMRP levels in the isolated germ cells of males with the indicated genotypes assessed by western blot.

FMRP was abbnormally observed in B6.XC7 transgenic line. α-tubulin was used as a loading control.

Next, we evaluated fertility parameters in transgenic males (B6.XC7 and B6.DX.1s.XC7) and controls (B6 and B6.DX.1s). The mean testes weights were significantly reduced in both transgenic lines (106.8 ± 10.5 mg for B6.XC7 and 113.3 ± 7.7 mg for

B6.DX.1s.XC7) compared to B6 and B6.DX.1s (176.8 ± 15.0 mg and 167.8 ± 9.5 mg, respectively; P < 0.001 for both, t-test) (Figure 34A). Furthermore, none of the transgenic line produced any spermatozoa (0.13 ± 0.12 x 10^{-6} for B6.XC7 and 0.07 ± 0.07 x 10^{-6} for B6.DX.1s.XC7) compared to control B6 (58.2 ± 14.8 x 10^{-6}) and B6.DX.1s (48.0 ± 12.7 x 10^{-6}) males (P<0.001 for both, t-test) (Figure 34B). Although we have not yet identified the cause of full sterility in XC7 transgenic males, it is likely that FMRP overexpression during later stages of meiosis disrupts sperm maturation.

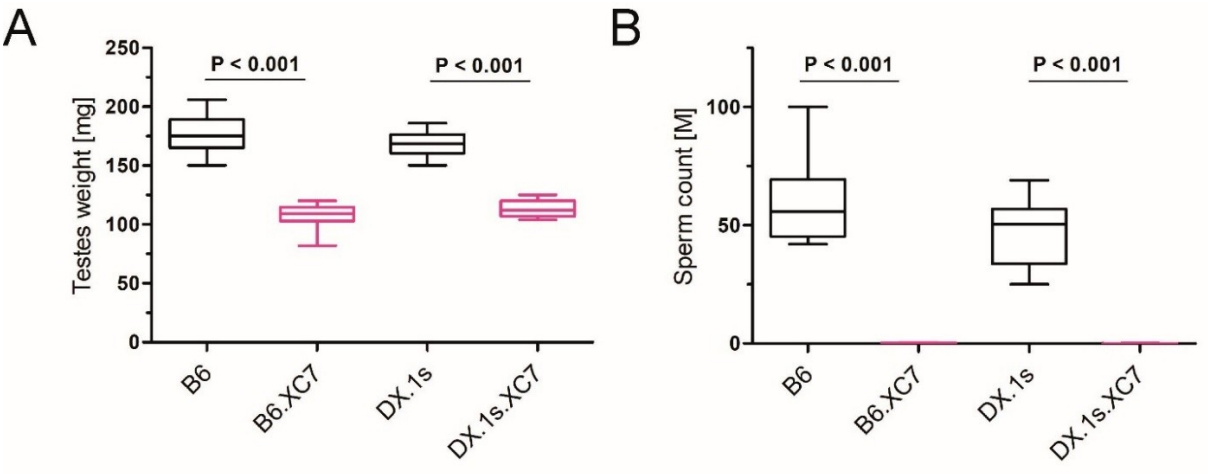

Figure 34. Fertility parameters of transgenic lines males and controls.

(A) The mean testes weight (in milligrams ± SD). (B) The mean sperm count (in millions per pair of epididymis ± SD) (P=0.8099). Statistical comparisons were performed using a two-tailed t-test.

We next investigated whether the additional *Fmr1*^{B6} allele acts as a potential MEIR1 putative protein (Balcova et al., 2016) by analyzing crossing-over events during prophase I of meiosis via fluorescent immunostaining of SYCP1 and MLH1 proteins. We observed a significantly increased number of crossovers (as indicated by MLH1 foci) in both transgenic lines, B6.XC7 and B6.DX.1s.XC7 (24.43 ± 0.14 and 23.59 ± 0.12, respectively), compared to B6 and B6.DX.1s (23.29 ± 0.16 and 21.13 ± 0.11, respectively; P<0.001 for both, t-test). Interestingly, the extra *Fmr1*^{B6} allele on the B6.DX.1s background restored the number of MLH1 foci to B6 levels (23.59 ± 0.12 and 23.29 ± 0.16; P=0.1289, t-test) (Figure 35). This suggests that the *Fmr1*^{PWD} allele may interfere with crossover formation, while an additional *Fmr1*^{B6} copy can rescue this process on the B6.DX.1s background. Moreover, the additional *Fmr1*^{B6} gene copy on autosomes is responsible for the higher number of crossovers, indicating that FMRP functions as a MEIR1 putative protein.

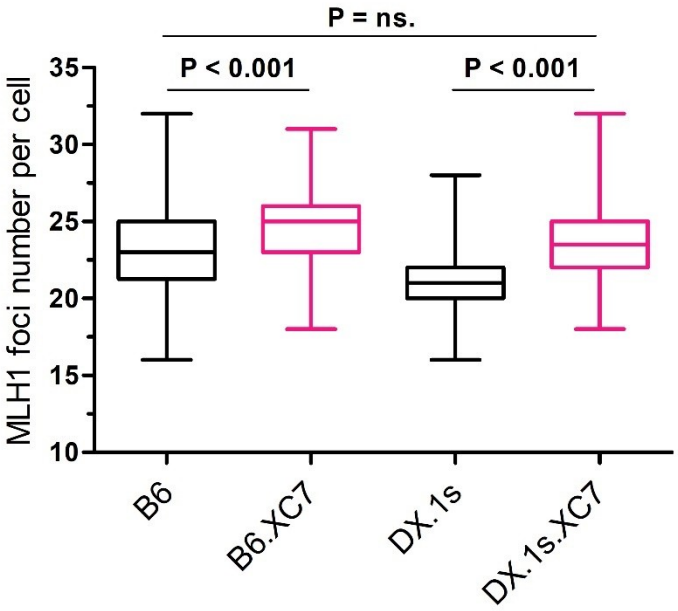

Figure 35. Frequency of crossing over in transgenic lines males and controls.

The mean crossover rate (± SD) in males of each genotype. Crossover numbers were examined in at least five males per genotype, with at least 40 pachytene nuclei scored per male. Statistical comparisons were performed using a two-tailed t-test.

To test whether the extra *Fmr1*^{B6} copy could rescue the sterile phenotype associated with *Hstx2*, hybrid males were analyzed for testes weight and sperm count. As in the pure transgenic models, we observed a significant decrease in testes weight between (B6.DX.1s.XC7 x PWD)F1 and control (B6.DX.1s x PWD)F1 males (56.45 ± 3.21 mg vs. 62.85 ± 2.94 mg, P<0.001, t-test) (Figure 36A), but no effect on sperm count (0.04 ± 0.06 x 10^{-6} vs. 0.01 ± 0.02 x 10^{-6}, P=0.2131, t-test), indicating that FMRP overexpression may disrupt spermatogenesis in the later stages. While we anticipated a decrease in autosomal asynapsis in transgenic hybrids, the observed reduction was not statistically significant, and the transgene containing *Fmr1*, *Fmr1os,* and *Fmr1nb* did not rescue the sterile phenotype in (B6.DX.1s.XC7 x PWD)F1 hybrids (73.1 ± 10.4 % vs. 79.8 ± 2.6 %, P=0.1554, t-test) (Figure 36B).

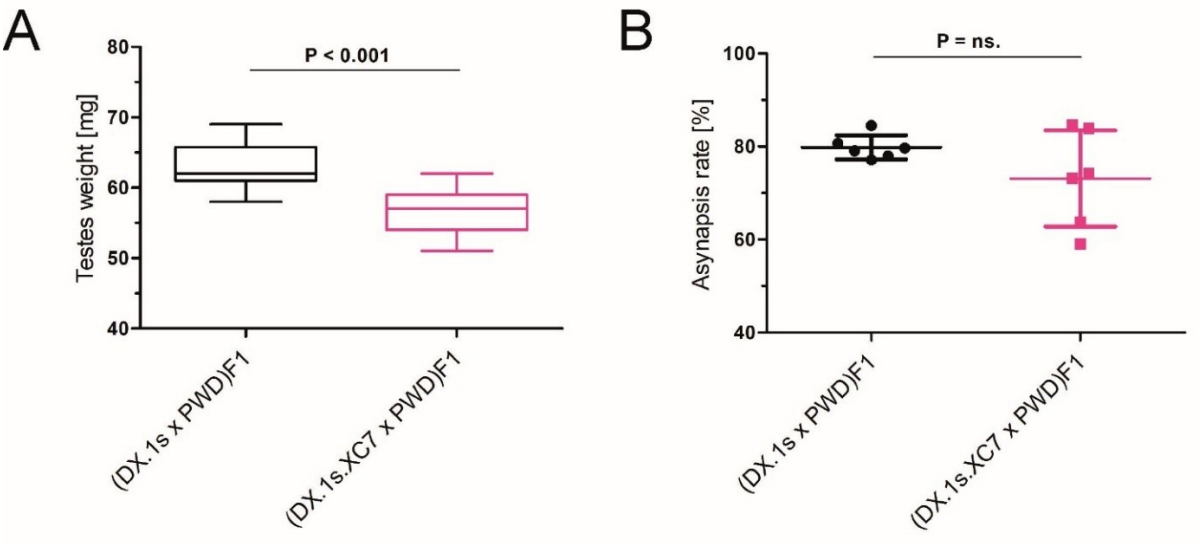

Figure 36. Effect of the transgene on the *Hstx2* phenotype.

(A) The mean the testes weight (in milligrams ± SD) of (B6.DX.1s.XC7 x PWD)F1 males and control (B6.DX.1s x PWD)F1 males. (B) The mean autosomal asynapsis rate (± SD) in males of each genotype (P=0.1554). Statistical comparisons were performed using a two-tailed t-test.

We conclude that the extra copies of *Fmr1*, *Fmr1os,* and *Fmr1nb* from the B6 strain, inserted randomly into the autosomes, are not necessary for autosomal pairing during prophase I, and none of these genes function as *Hstx2* modifiers in sterile hybrid males. However, the overexpression of FMRP from the transgene significantly increased the number of crossovers, suggesting that *Fmr1* plays a role in the *Meir1* pathway. Both transgenic lines, B6.XC7 and B6.DX.1s.XC7, showed higher MLH1 foci numbers compared to their wild-type counterparts, and the crossover numbers in B6.DX.1s.XC7 were restored to B6 levels. These findings indicate that FMRP may be part of a complex involved in crossover formation. However, despite its role in crossing-over, FMRP overexpression did not rescue the hybrid sterility phenotype in *Hstx2*-related hybrid males.

MicroRNA expression profiling

To investigate whether the microRNA cluster could be implicated as the *Hstx2,* we performed expression profiling of selected microRNAs in the testes of juvenile (Figure 37) and adult male mice (Figure 38). This approach should revel differences in expression between B6 and PWD alleles in both homozygous and heterozygous autosomal background. Indeed, we observed higher expression of the PWD allele for members of the miR-465 family microRNAs, represented by miR-465a. These finginds aligns with our work showing that the *Mir-465* cluster is duplicated in the PWD strain compared to B6 (Lustyk et al., 2019). To confirm miRNA

expression in the early stages of meiosis, we examined testes from 12dpp and 18dpp males. During the first wave of spermatogenesis, most spermatocytes in 12dpp males are in the zygotene/leptotene stages. As spermatogenesis progresses, spermatocytes in 18dpp males reach stages beyond pachytene. We detected the mature form of miR-465a in both 12dpp and 18dpp testes from B6, PWD strains and hybrids (PWD x B6)F1 and (B6 x PWD)F1. Interestingly, the expression of the PWD allele of miR-465a in the (PWD x B6)F1 hybrids was about 50% elevated over the expression in the PWD males (Figure 37). In adult males, we also confirmed a higher expression of the PWD allele of the miR-465 family, represented by miR-465a (Figure 38).

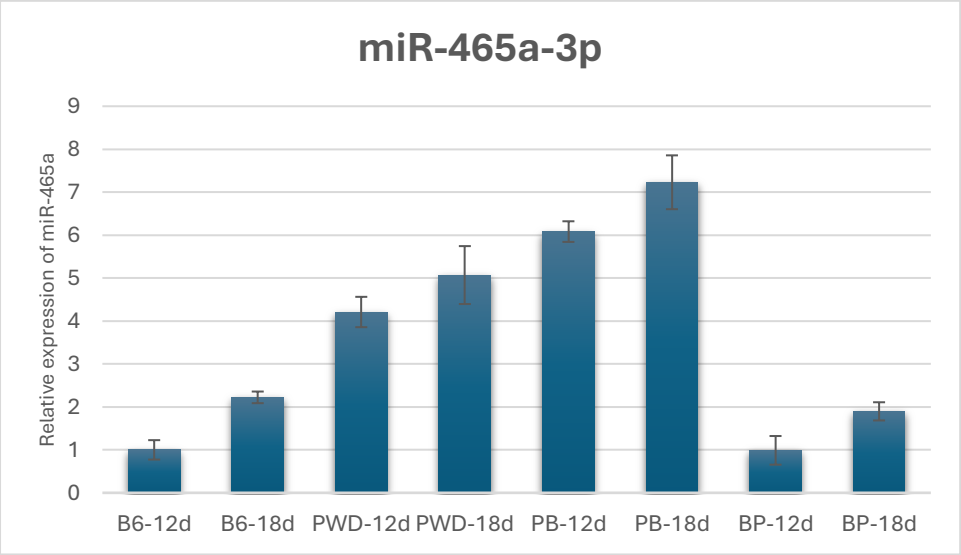

Figure 37. Relative expression of miR-465a in juvenile males.

Expression analyses were normalized to the let-7a reference and presented as fold changes relative to B6 (with the average B6 expression set to 1). All results are expressed as mean ± SD, based on data from three different males per strain.

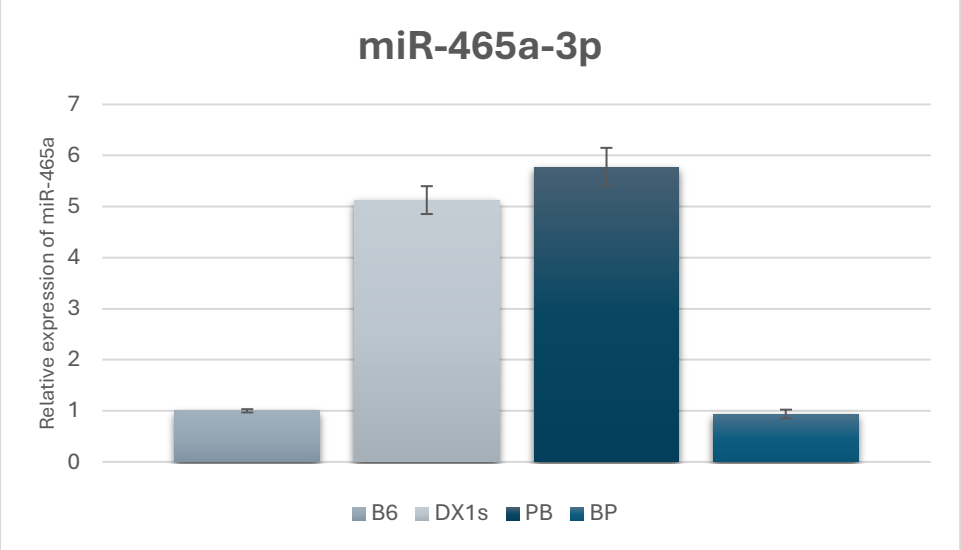

Figure 38. Relative expression of miR-465a in adult wild-type and hybrid males.

Expression analyses were normalized to the let-7a reference and presented as fold changes relative to B6 (with the average B6 expression set to 1). All results are expressed as mean ± SD, based on data from three different males per strain.

Summary of hypotheses and objectives

This study aimed to contribute to our understanding of the genetic basis of hybrid male sterility between the PWD and B6 mouse strains. Specifically, we focused on dissecting the role of *Hstx2* locus on the X chromosome and evaluating the contributions of the candidate genes *Fmr1nb* and *Fmr1*. Additionally, we investigated whether these genes also contribute to the *Hstx1* and *Meir1* loci. Furthermore, we performed microRNA expression profiling of Mir465, another *Hstx2* candidate, to assess differences between B6 and PWD alleles in juvenile and adult males.

Previous research established that the *Hstx2* locus significantly contributes to hybrid sterility, manifested as reduced testes wight, lower sperm count, and higher asynapsis of homologous chromosomes during prophase I of meiosis. However, the precise genetic elements and their interactions remained unclear.

Here, we applied classical genetics and CRISPR/Cas9 technology to develop two novel subconsomic strains, B6.DX.64-69 and B6.DX.66-69, carrying 4.34 Mb and 2.70 Mb segments of the PWD sequence, respectively. Both subconsomic (congenic) strains displayed reduced testes weight, increased frequency of malformed sperm heads (*Hstx1* phenotype), and decreased crossover frequency (*Meir1* phenotype). Importantly, (B6.DX.64-69 x PWD)F1 and (B6.DX.66-69 x PWD)F1 hybrids were sterile, with lower testes weight and elevated chromosome asynapsis rates (*Hstx2* phenotype). Although there was a slight reduction in the effect sizes across all phenotypes in the refined intervals, we concluded that the 2.70 Mb segment from the PWD strain carries the *Hstx2* candidate(s) and is both necessary and sufficient to induce the sterility phenotype in hybrid males.

Further investigation of the genetic factors inside the 2.70 Mb region responsible for sterility, including *Fmr1nb*, *Fmr1*, using genetically modified mouse lines, revealed their roles in hybrid male sterility, meiotic recombination, and their potential identification with the *Hstx1*, *Meir1*, and *Hstx2* loci.

Fmr1nb showed importance in spermiogenesis, particularly as a modifier of sperm head morphology associated with the *Hstx1* locus. In *Fmr1nb* knockout model, B6.DX.1s$^{Fmr1nb-}$ males showed an increased proportion of malformed sperm heads, suggesting that *Fmr1nb* contributes to proper sperm morphology. However, despite its role in sperm morphology,

Fmr1nb did not reverse meiotic arrest or hybrid sterility in hybrid males, suggesting that it is not a primary modifier of *Hstx2*-related sterility.

Fmr1 emerged as a key player in meiotic crossover regulation, likely as part of the *Meir1* pathway. The *Fmr1* knockout model showed an increase in crossover events, as indicated by elevated MLH1 foci, supporting *Fmr1* to be potential *Meir1* locus. However, the crossover increase in *Fmr1* knockout males did not reach the levels of wild-type B6, suggesting that FMRP likely acts within a complex regulating crossover. Moreover, in a transgenic mouse model with an additional $Fmr1^{B6}$ allele, MLH1 foci levels were restored to those of B6 controls, reinforcing *Fmr1*'s role in crossover regulation within the *Meir1* pathway.

Despite introducing additional copy of *Fmr1*, *Fmr1nb*, and *Fmr1os* by transgenesis, the transgenic lines did not reverse the sterility observed in hybrid males. Overexpression of *Fmr1* increased crossover events, particularly in the B6.XC7 and B6.DX.1s.XC7 transgenic lines, but it did not alleviate meiotic arrest or rescue hybrid sterility. These findings suggest that while *Fmr1* influence crossover formation, neither *Fmr1* nor *Fmr1nb* alone are sufficient to release the meiotic arrest which drives hybrid sterility.

In conclusion, our study provides critical insight into the genetic architecture of hybrid male sterility, pinpointing a specific 2.70 Mb segment on the PWD X chromosome that is essential and sufficient to reproduce the sterility phenotype. Although *Fmr1* and *Fmr1nb* play notable roles in crossover regulation and sperm morphology, respectively, they do not modify the hybrid sterility phenotype associated with meiotic arrest. Further exploration of other genetic factors within the *Hstx2* interval is needed to fully understand the molecular mechanisms underlying this sterility phenotype.

Discussion

Interplay between PRDM9 and *Hstx2* in hybrid sterility

Our model of male hybrid sterility in (PWD x B6)F1 males proposes that intersubspecific male hybrid sterility is primarily governed by three key components, the *Prdm9* gene, which produces the PRDM9 protein essential for initiating genetic recombination during meiosis, subspecies-specific heterozygosity of homologous autosomes, and the *Hstx2* locus on the X chromosome. This model offers a more straightforward explanation compared to other studies that suggest a complex genetic architecture controlling hybrid sterility in similar mouse subspecies combinations (Tucker et al., 1992; Payseur et al., 2004; Macholán et al., 2007, 2011).

PRDM9 is a crucial protein that directs DNA double-strand breaks (DSBs) at specific sites during prophase I of meiosis, essential for sperm cell development. In PWD and B6 hybrid mice, PRDM9 causes asymmetric distribution of recombination hotspots, with the $PRDM9^{B6}$ targeting predominantly the PWD chromosomes and vice versa. This asymmetry arises due to evolutionary divergence in PRDM9-binding sites, leading to improper chromosome pairing and repair during meiosis, ultimately causing infertility (Baker et al., 2015; Davies et al., 2016; Smagulova et al., 2016; Gregorova et al., 2018).

Despite having the same set of chromosomes and the same degree of PRDM9-induced asymmetry, reciprocal hybrids show differences in fertility (Bhattacharyya et al., 2013, 2014). The (PWD x B6)F1 males exhibit complete sterility due to meiotic arrest caused by persistent DSBs and chromosome asynapsis. In contrast, (B6 x PWD)F1 males show improved fertility compared to the reciprocal cross (Bhattacharyya et al., 2013). This difference suggests that the $Hstx2^{PWD}$ locus on the X chromosome is a key factor in modulating the effects of PRDM9-induced asymmetry.

We propose that *Hstx2* may help alleviate the problems caused by PRDM9-induced asymmetry in several ways:

1. **Extending repair time:** *Hstx2* might prolong the time in which cells have to repair DSBs, allowing for proper synapsis of homologous chromosomes.
2. **Reducing mismatch repair sensitivity:** *Hstx2* could make the DNA repair machinery less sensitive to differences between the DNA sequences. By modulating the repair

machinery, it could promote crossover formation and synapsis despite sequence heterology.

3. **Facilitating alternative repair pathways:** *Hstx2* may encourage the use of sister chromatids for repair instead of homologous chromosomes. This switch could help resolve persistent DSBs, preventing meiotic arrest.

By influencing these processes, *Hstx2* could enhance the ability of hybrid cells to repair DNA breaks and proceed through meiosis successfully, reducing sterility (Lustyk et al., 2019).

The significance of interactions between matching chromosomes is further highlighted by observations that in backcross males, the asymmetry in DNA breaks disappears in regions where chromosomes are from the same subspecies. This leads to normal pairing and successful meiosis in those regions, supporting the idea that chromosomes compatibility is crucial (Gregorova et al., 2018).

The understanding of how *Hstx2* interacts with PRDM9 provides valuable insight into hybrid sterility between PWD and B6 mice. By potentially modulating DNA repair mechanisms and chromosome pairing, *Hstx2* plays a key role in determining success or failure of meiosis resulting in fertile or sterile hybrids.

Hstx2 locus as a recombination cold spot

Genomic regions with suppressed recombination are often rearranged between the species and tend to accumulate genes related to reproductive isolation (Nachman and Payseur, 2012). The *Hstx2* locus aligns with this pattern, functioning both as a recombination cold spot and housing the *Meir1* locus, a modifier of meiotic recombination.

Our attempts to refine the *Hstx2* locus through backcrossing and CRISPR/Cas9-mediated recombination highlighted its nature as a recombination cold spot. We revealed the absence of recombination events within the *Hstx2* locus across the backcross population. Only one recombinant, reducing the *Hstx2* locus to 2.7MB, was obtained through a backcross facilitated by the CRISP/Cas9 system, notably occurring outside of the targeted site. The inability to induce recombination within *Hstx2*, even with CRISP/Cas9, underscore the locus' unique properties, possible species-specific chromosomal rearrangement(s), and its crucial role in hybrid male sterility.

Recombination cold spots are often associated with structural variations such as inversions or copy number variations, which may lead to alterations in chromatin structure

containing reproductive isolation genes, reducing their expression in germ cells (Coyne and Orr, 2004; Morgan et al., 2017; Fuller et al., 2018). We performed optical mapping (in collaboration with Max Planck Institute for Evolutionary Biology, Plön, Germany), which provided high-resolution optical maps of the *Hstx2* region in PWD and B6 genomes. Although no inversions were revealed, we observed PWD-specific structural variants involving a cluster of microRNA genes duplicated in the PWD genome, which can have functional implications related to *Hstx2* (Lustyk et al., 2019).

The confirmation of *Hstx2* as a recombination-resistant region strengthens the hypothesis that hybrid sterility loci may be maintained through restricted recombination, contributing to reproductive isolation.

Role of candidates' gene *Fmr1nb* and *Fmr1* in male fertility

We identified *Fmr1nb* as a *Hstx2* candidate gene applying two main criteria which are the expression during meiotic prophase I and the polymorphisms between PWD and B6 alleles (Bhattacharyya et al., 2014; Margolin et al., 2014; Lustyk et al., 2019). Our studies on knocked-out *Fmr1nb* revealed that it is primarily involved in spermiogenesis, significantly influencing sperm head morphology associated with the *Hstx1* locus. However, the elevated frequency of malformed sperm heads in B6.DX.1s males indicates that *Fmr1nb* is not the only factor on the X chromosome influencing this phenotype. However, since the absence of FMR1NB did not impact meiotic progression, crossover formation, or rescue hybrid sterility in *Hstx2*-related hybrids, we consider *Fmr1nb* an unlikely candidate for *Hstx2*. Its influence appears to be specific in post-meiotic stages of spermatogenesis.

Fmr1 emerges as another potential *Hstx2* candidate due to its expression during prophase I of meiosis (Margolin et al., 2014). Another reason to consider *Fmr1* as a *Hstx2* candidate was evidence published earlier about a delay in the repair of single-strand intermediates in the *Fmr1* knockout model, which resulted in impaired crossover formation. Furthermore, the spermatocytes lacking FMRP are unable to complete homologous chromosome synapsis during meiotic prophase I (Alpatov et al., 2014). Our *Fmr1* knockout model demonstrated an impact on crossover frequency, as indicated by an increase in MLH1 foci. Furthermore, an additional copy of the $Fmr1^{B6}$ allele in transgenic lines B6.XC7 and B6.DX.1s.XC7 also led to increased crossover frequency, suggesting that the $Fmr1^{PWD}$ allele acts as a crossover suppression factor, which can be alleviated either by knockout or by the addition of the B6 allele. Another reason of the elevated crossover number could be the high

expression of the transgenic *Fmr1*^{B6} allele located on the autosomes, which bypasses meiotic sex chromosome inactivation (MSCI). Additionally, due to FMRP accumulation in meiotic cells, these B6.XC7 males become sterile, with no sperm present. However, the exact mechanism of FMRP in crossover formation remains unknown. This suggests a potential role of *Fmr1* as a *Meir1*, likely functioning within a regulatory complex responsible for meiotic crossover formation.

While the *Fmr1*^{PWD} allele potentially functions as a crossover frequency suppressor, its knockout or the introduction of an additional B6 allele into the genome did not rescue the hybrids sterility phenotype. However, the asynapsis rate varies highly in transgenic hybrids, possibly due to *Fmr1* overexpression beyond pachytene stage of meiosis. Despite these variations, the hybrids remain completely sterile.

Mir465 cluster copy number variation within the *Hstx2* locus

Expression profiling revealed higher expression of the miR-465 family microRNAs from the PWD allele in both juvenile and adult mice. This aligns with our previous findings of higher expression and a *Mir-465* cluster duplication in the PWD strain (Bhattacharyya et al., 2014; Lustyk et al., 2019). Detection of mature miR-465 microRNAs in both early and later stages of spermatogenesis further supports a role for this microRNA cluster in meiosis, particularly in the context of hybrid sterility.

Our unpublished data on genetically modified mouse lines carrying a large genomic deletion of both allelic forms of the *Mir-465* cluster, namely B6.Mir-465$^{\text{B6-DEL}}$ mouse line (20 kb deletion) and DX.Mir-465$^{\text{PWD-DEL}}$ mouse line (40 kb deletion), show important results suggesting that *Mir-465* cluster is a possible key factor within *Hstx2*.

Conclusions

Our study advances the understanding of hybrid male sterility by refining the size of the *Hstx2* locus and evaluating the contributions of *Fmr1nb* and *Fm1*. The *Hstx2* locus emerges as a critical determinant of sterility in (PWD x B6)F1 hybrids, residing within a recombination cold spot and harboring genetic factors that cause meiotic arrest. While *Fmr1nb* influences sperm morphology associated with the *Hstx1* phenotype, it does not impact hybrid sterility linked to *Hstx2*. Similarly, *Fmr1* modulates crossover frequency but is not a primary modifier of sterility.

Our unpublished data suggests that the *Mir-465* cluster may be a major regulatory element within the *Hstx2* locus responsible for (PWD x B6)F1 hybrid sterility. Its copy number variation between PWD and B6 strains, differences in expression between reciprocal hybrids, and significant influence on meiotic chromosome synapsis in transgenic and knockout hybrid models support its role in hybrid sterility.

Our findings focused on the role of *Hstx2* locus highlight the complex interplay between genetic factors that can lead to reproductive isolation and speciation. However, further research is needed to fully understand the basis of the molecular mechanisms induced by the genetic interactions between *Prdm9* and *Hstx2*.

Publications and author contributions

1. Lustyk D, Kinský S, Ullrich KK, Yancoskie M, Kašíková L, Gergelits V, Sedlacek R, Chan YF, Odenthal-Hesse L, Forejt J, Jansa P. Genomic Structure of *Hstx2* Modifier of *Prdm9*-Dependent Hybrid Male Sterility in Mice. Genetics. 2019 Nov;213(3):1047-1063.

As the first author, I managed mouse breeding, prepared samples, performed microscopy and analysis, conducted gene and protein expression analysis, completed sequencing, and contributed to the writing of the manuscript.

2. Gregorova S, Gergelits V, Chvatalova I, Bhattacharyya T, Valiskova B, Fotopulosova V, Jansa P, Wiatrowska D, Forejt J. Modulation of *Prdm9*-controlled meiotic chromosome asynapsis overrides hybrid sterility in mice. Elife. 2018 Mar 14;7:e34282.

I prepared the samples, conducted RNA FISH microscopy and subsequent analysis.

3. Valiskova B, Gregorova S, Lustyk D, Šimeček P, Jansa P, Forejt J. Genic and chromosomal components of Prdm9-driven hybrid male sterility in mice (Mus musculus). Genetics. 2022 Aug 30;222(1):iyac116.

I prepared the samples, conducted microscopy and subsequent analysis, and contributed to discussions on the manuscript.

4. Papanikos F, Clément JAJ, Testa E, Ravindranathan R, Grey C, Dereli I, Bondarieva A, Valerio-Cabrera S, Stanzione M, Schleiffer A, Jansa P, Lustyk D, Fei JF, Adams IR, Forejt J, Barchi M, de Massy B, Toth A. Mouse ANKRD31 Regulates Spatiotemporal Patterning of Meiotic Recombination Initiation and Ensures Recombination between X and Y Sex Chromosomes. Mol Cell. 2019 Jun 6;74(5):1069-1085.e11.

I prepared the samples, conducted RNA FISH microscopy and subsequent analysis.

List of figures

Figure 1. Dobzhansky-Muller model of hybrid incompatibility (Wu and Ting, 2004). 11

Figure 2. Worldwide distribution of *Mus musculus* subspecies (Phifer-Rixey and Nachman, 2015). 14

Figure 3. A map of *Mus musculus* subspecies hybrid zone across Europe (Macholán et al., 2008) 15

Figure 4. Mouse crossing diagram for hybrid sterility between PWD and B6 strains. 16

Figure 5. Mammalian meiosis and gametogenesis (Handel and Schimenti, 2010). 18

Figure 6. Chromosome organization during meiotic prophase I (Baudat et al., 2013)..... 20

Figure 7. Schematic synaptonemal complex (Yang and Wang, 2009)..... 21

Figure 8. Model of molecular mechanism of the asymmetric formation of DSBs (Forejt and Jansa, 2023)..... 24

Figure 9. Mapping of hybrid male sterility at the *Hstx1* and *Hstx2* loci in subconsomic and congenic strains..... 42

Figure 10. Fertility parameters of subconsomic and congenic males. 45

Figure 11. Fertility parameters of hybrid males..... 47

Figure 12. Chromosomal asynapsis of hybrid males. 48

Figure 13. Transgressive effect of the $Hstx2^{PWD}$ allele on crossover rate. 49

Figure 14. Relative *Fmr1nb* expression. 51

Figure 15. Relative *Fmr1* expression. 51

Figure 16. Immunolabeling of testes. 52

Figure 17. Generation of the *Fmr1nb* null allele. 54

Figure 18. Confirmation of *Fmr1nb* knockout. 54

Figure 19. Number of progeny sired by B6.DX.1s and B6.DX.1s$^{Fmr1nb-}$ males. 55

Figure 20. Fertility parameters of B6.DX.1s and B6.DX.1s$^{Fmr1nb-}$ males. 56

Figure 21. Histological sections of testes from B6.DX.1s and B6.DX.1s$^{Fmr1nb-}$ males. 57

Figure 22. Apoptotic cells in the testes of B6.DX.1s and B6.DX.1s$^{Fmr1nb-}$ males. 57

Figure 23. Progression through prophase I of meiosis in B6.DX.1s and B6.DX.1s$^{Fmr1nb-}$ males. 58

Figure 24. Effect of *Fmr1nb* null allele on the *Hstx1* phenotype. 59

Figure 25. Effect of *Fmr1nb* null allele on the *Hstx2* phenotype. 60

Figure 26. Visualization of TT Insertion..... 61

Figure 27. Confirmation of *Fmr1* knockout. 61

Figure 28. Fertility parameters of B6.DX.1s and B6.DX.1s^{Fmr1-} males. 62

Figure 29. Histological sections of testes from B6.DX.1s and B6.DX.1s^{Fmr1-} males. 63
Figure 30. Progression through prophase I of meiosis in B6.DX.1s and B6.DX.1s^{Fmr1-} males. 64
Figure 31. Effect of the *Fmr1* null allele on the *Hstx2* phenotype 65
Figure 32. Gene expression in transgenic mouse line 67
Figure 33. FMRP levels in the isolated germ cells of males with the indicated genotypes assessed by western blot. 67
Figure 34. Fertility parameters of transgenic lines males and controls. 68
Figure 35. Frequency of crossing over in transgenic lines males and controls. 69
Figure 36. Effect of the transgene on the *Hstx2* phenotype. 70
Figure 37. Relative expression of miR-465a in juvenile males. 71
Figure 38. Relative expression of miR-465a in adult wild-type and hybrid males. 72

List of tables

Table 1. List of primers 30
Table 2. Conditions for quantitative real-time PCR for gene expression 31
Table 3. List of qPCR primers – design Universal Probe Library (Roche) 32
Table 4. Conditions for quantitative real-time PCR for microRNA expression 33
Table 5. List of microRNA specific LNA primers 34
Table 6. List of primary antibodies for western blot and immunocytochemistry 35
Table 7. List of secondary antibodies for immunocytochemistry 36
Table 8. Distribution of PWD/B6 recombination events along the X chromosome. 42
Table 10. *Hstx1* locus mapping. 44
Table 11. *Hstx2* locus mapping. 46
Table 12. List of protein-coding genes spanning the interval of the newly defined *Hstx2* locus (Chr X: 66.51– 69.21 Mb, GRCm38), n.d. - not defined. LEP, ZYG - leptotene, zygotene, RS - round spermatids, ES - elongated spermatids. 50

References

Alpatov, R., Lesch, B.J., Nakamoto-Kinoshita, M., Blanco, A., Chen, S., Stützer, A., Armache, K.J., Simon, M.D., Xu, C., Ali, M., Murn, J., Prisic, S., Kutateladze, T.G., Vakoc, C.R., Min, J., Kingston, R.E., Fischle, W., Warren, S.T., Page, D.C., Shi, Y., 2014. A chromatin-dependent role of the fragile X mental retardation protein FMRP in the DNA damage response. Cell 157, 869–881. https://doi.org/10.1016/j.cell.2014.03.040

Anderson, L.K., Reeves, A., Webb, L.M., Ashley, T., 1999. Distribution of crossing over on mouse synaptonemal complexes using immunofluorescent localization of MLH1 protein. Genetics 151, 1569–1579. https://doi.org/10.1093/genetics/151.4.1569

Baird, S.J.E., Macholán, M., 2012. What can the Mus musculus musculus/M. m. domesticus hybrid zone tell us about speciation?, in: Piálek, J., Macholán, M., Munclinger, P., Baird, S.J.E. (Eds.), Evolution of the House Mouse, Cambridge Studies in Morphology and Molecules: New Paradigms in Evolutionary Bio. Cambridge University Press, Cambridge, pp. 334–372. https://doi.org/10.1017/CBO9781139044547.016

Baker, C.L., Kajita, S., Walker, M., Saxl, R.L., Raghupathy, N., Choi, K., Petkov, P.M., Paigen, K., 2015. PRDM9 drives evolutionary erosion of hotspots in Mus musculus through haplotype-specific initiation of meiotic recombination. PLoS Genet. 11, e1004916. https://doi.org/10.1371/journal.pgen.1004916

Balcova, M., Faltusova, B., Gergelits, V., Bhattacharyya, T., Mihola, O., Trachtulec, Z., Knopf, C., Fotopulosova, V., Chvatalova, I., Gregorova, S., Forejt, J., 2016. Hybrid Sterility Locus on Chromosome X Controls Meiotic Recombination Rate in Mouse. PLoS Genet. 12, e1005906. https://doi.org/10.1371/journal.pgen.1005906

Ball, R.L., Fujiwara, Y., Sun, F., Hu, J., Hibbs, M.A., Handel, M.A., Carter, G.W., 2016. Regulatory complexity revealed by integrated cytological and RNA-seq analyses of meiotic substages in mouse spermatocytes. BMC Genomics 17, 628. https://doi.org/10.1186/s12864-016-2865-1

Barbash, D.A., Ashburner, M., 2003. A novel system of fertility rescue in Drosophila hybrids reveals a link between hybrid lethality and female sterility. Genetics 163, 217–226. https://doi.org/10.1093/genetics/163.1.217

Baudat, F., Buard, J., Grey, C., Fledel-Alon, A., Ober, C., Przeworski, M., Coop, G., de Massy, B., 2010. PRDM9 is a major determinant of meiotic recombination hotspots in humans and mice. Science 327, 836–840. https://doi.org/10.1126/science.1183439

Baudat, F., Imai, Y., de Massy, B., 2013. Meiotic recombination in mammals: localization and regulation. Nat. Rev. Genet. 14, 794–806. https://doi.org/10.1038/nrg3573

Bhattacharyya, T., Gregorova, S., Mihola, O., Anger, M., Sebestova, J., Denny, P., Simecek, P., Forejt, J., 2013. Mechanistic basis of infertility of mouse intersubspecific hybrids. Proc. Natl. Acad. Sci. U. S. A. 110. https://doi.org/10.1073/pnas.1219126110

Bhattacharyya, T., Reifova, R., Gregorova, S., Simecek, P., Gergelits, V., Mistrik, M., Martincova, I., Pialek, J., Forejt, J., 2014. X chromosome control of meiotic chromosome synapsis in mouse inter-subspecific hybrids. PLoS Genet. 10, e1004088. https://doi.org/10.1371/journal.pgen.1004088

Bolcun-Filas, E., Handel, M.A., 2018. Meiosis: the chromosomal foundation of reproduction. Biol. Reprod. 99, 112–126. https://doi.org/10.1093/biolre/ioy021

Bolcun-Filas, E., Schimenti, J.C., 2012. Genetics of meiosis and recombination in mice. Int. Rev. Cell Mol. Biol. 298, 179–227. https://doi.org/10.1016/B978-0-12-394309-5.00005-5

Boursot, P., Din, W., Anand, R., Darviche, D., Dod, B., Deimling, F.V., Talwar, G.P., Bonhomme, F., 1996. Origin and radiation of the house mouse: mitochondrial DNA phylogeny. J. Evol. Biol. 9, 391–415. https://doi.org/10.1046/J.1420-9101.1996.9040391.X

Buard, J., Barthès, P., Grey, C., de Massy, B., 2009. Distinct histone modifications define initiation and repair of meiotic recombination in the mouse. EMBO J. 28, 2616–2624. https://doi.org/10.1038/emboj.2009.207

Cabart, P., Chew, H.K., Murphy, S., 2004. BRCA1 cooperates with NUFIP and P-TEFb to activate transcription by RNA polymerase II. Oncogene 23, 5316–5329. https://doi.org/10.1038/sj.onc.1207684

Charlesworth, B., 2015. Causes of natural variation in fitness: evidence from studies of Drosophila populations. Proc. Natl. Acad. Sci. U. S. A. 112, 1662–1669. https://doi.org/10.1073/pnas.1423275112

Charlesworth, D., Schemske, D.W., Sork, V.L., 1987. The evolution of plant reproductive characters; sexual versus natural selection. Experientia. Suppl. 55, 317–335. https://doi.org/10.1007/978-3-0348-6273-8_14

Cohen, P.E., Pollack, S.E., Pollard, J.W., 2006. Genetic Analysis of Chromosome Pairing, Recombination, and Cell Cycle Control during First Meiotic Prophase in Mammals. Endocr. Rev. 27, 398–426. https://doi.org/10.1210/er.2005-0017

Coyne, J.A., Orr, H.A., 2004. Speciation. Oxford University Press, Oxford, New York.

Coyne, J.A., Orr, H.A., 1998. The evolutionary genetics of speciation. Philos. Trans. R. Soc. Lond. B. Biol. Sci. 353, 287–305. https://doi.org/10.1098/rstb.1998.0210

Darwin, C., 1859. The Origin of Species. Literary Classics, Inc., New York.

Davies, B., Hatton, E., Altemose, N., Hussin, J.G., Pratto, F., Zhang, G., Hinch, A.G., Moralli, D., Biggs, D., Diaz, R., Preece, C., Li, R., Bitoun, E., Brick, K., Green, C.M., Camerini-Otero, R.D., Myers, S.R., Donnelly, P., 2016. Re-engineering the zinc fingers of PRDM9 reverses hybrid sterility in mice. Nature 530, 171–176. https://doi.org/10.1038/nature16931

Didion, J.P., de Villena, F.P.-M., 2013. Deconstructing Mus gemischus: advances in understanding ancestry, structure, and variation in the genome of the laboratory mouse. Mamm. Genome Off. J. Int. Mamm. Genome Soc. 24, 1–20. https://doi.org/10.1007/s00335-012-9441-z

Dobzhansky, T., 1937. Genetics and the Origin of Species. Columbia University Press.

Dobzhansky, T., 1936. Studies on Hybrid Sterility. II. Localization of Sterility Factors in Drosophila Pseudoobscura Hybrids. Genetics 21, 113–135. https://doi.org/10.1093/genetics/21.2.113

Dobzhansky, T., 1935. A Critique of the Species Concept in Biology. Philos. Sci. 2, 344–355. https://doi.org/10.1086/286379

Dzur-Gejdosova, M., Simecek, P., Gregorova, S., Bhattacharyya, T., Forejt, J., 2012. Dissecting the genetic architecture of F1 hybrid sterility in house mice. Evol. Int. J. Org. Evol. 66, 3321–3335. https://doi.org/10.1111/j.1558-5646.2012.01684.x

Ernst, C., Eling, N., Martinez-Jimenez, C.P., Marioni, J.C., Odom, D.T., 2019. Staged developmental mapping and X chromosome transcriptional dynamics during mouse spermatogenesis. Nat. Commun. 10, 1251. https://doi.org/10.1038/s41467-019-09182-1

Forejt, J., 1996. Hybrid sterility in the mouse. Trends Genet. TIG 12, 412–417. https://doi.org/10.1016/0168-9525(96)10040-8

Forejt, J., Gregorová, S., 1977. Meiotic studies of translocations causing male sterility in the mouse. I. Autosomal reciprocal translocations. Cytogenet. Cell Genet. 19, 159–179. https://doi.org/10.1159/000130806

Forejt, J., Iványi, P., 1974. Genetic studies on male sterility of hybrids between laboratory and wild mice (Mus musculus L.). Genet. Res. 24, 189–206. https://doi.org/10.1017/s0016672300015214

Forejt, J., Jansa, P., 2023. Meiotic Recognition of Evolutionarily Diverged Homologs: Chromosomal Hybrid Sterility Revisited. Mol. Biol. Evol. 40, msad083. https://doi.org/10.1093/molbev/msad083

Forejt, J., Jansa, P., Parvanov, E., 2021. Hybrid sterility genes in mice (Mus musculus): a peculiar case of PRDM9 incompatibility. Trends Genet. TIG 37, 1095–1108. https://doi.org/10.1016/j.tig.2021.06.008

Forejt, J., Piálek, J., Trachtulec, Z., 2012. Hybrid male sterility genes in the mouse subspecific crosses, in: Piálek, J., Macholán, M., Munclinger, P., Baird, S.J.E. (Eds.), Evolution of the House Mouse, Cambridge Studies in Morphology and Molecules: New Paradigms in Evolutionary Bio. Cambridge University Press, Cambridge, pp. 482–503. https://doi.org/10.1017/CBO9781139044547.021

Fuller, Z.L., Leonard, C.J., Young, R.E., Schaeffer, S.W., Phadnis, N., 2018. Ancestral polymorphisms explain the role of chromosomal inversions in speciation. PLoS Genet. 14, e1007526. https://doi.org/10.1371/journal.pgen.1007526

Gavrilets, S., 1997. Evolution and speciation on holey adaptive landscapes. Trends Ecol. Evol. 12, 307–312. https://doi.org/10.1016/S0169-5347(97)01098-7

Geraldes, A., Basset, P., Gibson, B., Smith, K.L., Harr, B., Yu, H.-T., Bulatova, N., Ziv, Y., Nachman, M.W., 2008. Inferring the history of speciation in house mice from autosomal, X-linked, Y-linked and mitochondrial genes. Mol. Ecol. 17, 5349–5363. https://doi.org/10.1111/j.1365-294X.2008.04005.x

Good, J.M., Dean, M.D., Nachman, M.W., 2008. A complex genetic basis to X-linked hybrid male sterility between two species of house mice. Genetics 179, 2213–2228. https://doi.org/10.1534/genetics.107.085340

Gray, S., Cohen, P.E., 2016. Control of Meiotic Crossovers: From Double-Strand Break Formation to Designation. Annu. Rev. Genet. 50, 175–210. https://doi.org/10.1146/annurev-genet-120215-035111

Gregorová, S., Divina, P., Storchova, R., Trachtulec, Z., Fotopulosova, V., Svenson, K.L., Donahue, L.R., Paigen, B., Forejt, J., 2008. Mouse consomic strains: exploiting genetic

divergence between Mus m. musculus and Mus m. domesticus subspecies. Genome Res. 18, 509–515. https://doi.org/10.1101/gr.7160508

Gregorová, S., Forejt, J., 2000. PWD/Ph and PWK/Ph inbred mouse strains of Mus m. musculus subspecies--a valuable resource of phenotypic variations and genomic polymorphisms. Folia Biol. (Praha) 46, 31–41.

Gregorova, S., Gergelits, V., Chvatalova, I., Bhattacharyya, T., Valiskova, B., Fotopulosova, V., Jansa, P., Wiatrowska, D., Forejt, J., 2018. Modulation of Prdm9-controlled meiotic chromosome asynapsis overrides hybrid sterility in mice. eLife 7, e34282. https://doi.org/10.7554/eLife.34282

Gregorová, S., Mnuková-Fajdelová, M., Trachtulec, Z., Capková, J., Loudová, M., Hoglund, M., Hamvas, R., Lehrach, H., Vincek, V., Klein, J., Forejt, J., 1996. Sub-milliMorgan map of the proximal part of mouse Chromosome 17 including the hybrid sterility 1 gene. Mamm. Genome Off. J. Int. Mamm. Genome Soc. 7, 107–113. https://doi.org/10.1007/s003359900029

Haldane, J.B.S., 1922. Sex ratio and unisexual sterility in hybrid animals. J. Genet. 12, 101–109. https://doi.org/10.1007/BF02983075

Hamer, G., Gell, K., Kouznetsova, A., Novak, I., Benavente, R., Höög, C., 2006. Characterization of a novel meiosis-specific protein within the central element of the synaptonemal complex. J. Cell Sci. 119, 4025–4032. https://doi.org/10.1242/jcs.03182

Handel, M.A., Schimenti, J.C., 2010. Genetics of mammalian meiosis: regulation, dynamics and impact on fertility. Nat. Rev. Genet. 11, 124–136. https://doi.org/10.1038/nrg2723

Homolka, D., Ivanek, R., Capkova, J., Jansa, P., Forejt, J., 2007. Chromosomal rearrangement interferes with meiotic X chromosome inactivation. Genome Res. 17, 1431–1437. https://doi.org/10.1101/gr.6520107

Hunter, N., 2015. Meiotic Recombination: The Essence of Heredity. Cold Spring Harb. Perspect. Biol. 7, a016618. https://doi.org/10.1101/cshperspect.a016618

Isabelle, M., Moreel, X., Gagné, J.-P., Rouleau, M., Ethier, C., Gagné, P., Hendzel, M.J., Poirier, G.G., 2010. Investigation of PARP-1, PARP-2, and PARG interactomes by affinity-purification mass spectrometry. Proteome Sci. 8, 22. https://doi.org/10.1186/1477-5956-8-22

Janoušek, V., Wang, L., Luzynski, K., Dufková, P., Vyskočilová, M.M., Nachman, M.W., Munclinger, P., Macholán, M., Piálek, J., Tucker, P.K., 2012. Genome-wide architecture of reproductive isolation in a naturally occurring hybrid zone between Mus musculus musculus and M. m. domesticus. Mol. Ecol. 21, 3032–3047. https://doi.org/10.1111/j.1365-294X.2012.05583.x

Jung, M., Wells, D., Rusch, J., Ahmad, S., Marchini, J., Myers, S.R., Conrad, D.F., 2019. Unified single-cell analysis of testis gene regulation and pathology in five mouse strains. eLife 8, e43966. https://doi.org/10.7554/eLife.43966

Keane, T.M., Goodstadt, L., Danecek, P., White, M.A., Wong, K., Yalcin, B., Heger, A., Agam, A., Slater, G., Goodson, M., Furlotte, N.A., Eskin, E., Nellåker, C., Whitley, H., Cleak, J., Janowitz, D., Hernandez-Pliego, P., Edwards, A., Belgard, T.G., Oliver, P.L., McIntyre, R.E., Bhomra, A., Nicod, J., Gan, X., Yuan, W., van der Weyden, L., Steward, C.A., Bala, S., Stalker, J., Mott, R., Durbin, R., Jackson, I.J., Czechanski, A., Guerra-Assunção, J.A., Donahue, L.R., Reinholdt, L.G., Payseur, B.A., Ponting, C.P., Birney,

E., Flint, J., Adams, D.J., 2011. Mouse genomic variation and its effect on phenotypes and gene regulation. Nature 477, 289–294. https://doi.org/10.1038/nature10413

Keeney, S., Giroux, C.N., Kleckner, N., 1997. Meiosis-specific DNA double-strand breaks are catalyzed by Spo11, a member of a widely conserved protein family. Cell 88, 375–384. https://doi.org/10.1016/s0092-8674(00)81876-0

Kwan, K.Y., Moens, P.B., Wang, J.C., 2003. Infertility and aneuploidy in mice lacking a type IA DNA topoisomerase III beta. Proc. Natl. Acad. Sci. U. S. A. 100, 2526–2531. https://doi.org/10.1073/pnas.0437998100

Laurie, C.C., 1997. The weaker sex is heterogametic: 75 years of Haldane's rule. Genetics 147, 937–951. https://doi.org/10.1093/genetics/147.3.937

Lustyk, D., Kinský, S., Ullrich, K.K., Yancoskie, M., Kašíková, L., Gergelits, V., Sedlacek, R., Chan, Y.F., Odenthal-Hesse, L., Forejt, J., Jansa, P., 2019. Genomic Structure of Hstx2 Modifier of Prdm9-Dependent Hybrid Male Sterility in Mice. Genetics 213, 1047–1063. https://doi.org/10.1534/genetics.119.302554

Macholán, M., Baird, S.J.E., Dufková, P., Munclinger, P., Bímová, B.V., Piálek, J., 2011. Assessing multilocus introgression patterns: a case study on the mouse X chromosome in central Europe. Evol. Int. J. Org. Evol. 65, 1428–1446. https://doi.org/10.1111/j.1558-5646.2011.01228.x

Macholán, M., Baird, S.J.E., Munclinger, P., Dufková, P., Bímová, B., Piálek, J., 2008. Genetic conflict outweighs heterogametic incompatibility in the mouse hybrid zone? BMC Evol. Biol. 8, 271. https://doi.org/10.1186/1471-2148-8-271

Macholán, M., Vyskocilová, M., Bonhomme, F., Krystufek, B., Orth, A., Vohralík, V., 2007. Genetic variation and phylogeography of free-living mouse species (genus Mus) in the Balkans and the Middle East. Mol. Ecol. 16, 4774–4788. https://doi.org/10.1111/j.1365-294X.2007.03526.x

Mack, K.L., Nachman, M.W., 2017. Gene Regulation and Speciation. Trends Genet. TIG 33, 68–80. https://doi.org/10.1016/j.tig.2016.11.003

Mahadevaiah, S.K., Turner, J.M., Baudat, F., Rogakou, E.P., de Boer, P., Blanco-Rodríguez, J., Jasin, M., Keeney, S., Bonner, W.M., Burgoyne, P.S., 2001. Recombinational DNA double-strand breaks in mice precede synapsis. Nat. Genet. 27, 271–276. https://doi.org/10.1038/85830

Maheshwari, S., Barbash, D.A., 2011. The genetics of hybrid incompatibilities. Annu. Rev. Genet. 45, 331–355. https://doi.org/10.1146/annurev-genet-110410-132514

Margolin, G., Khil, P.P., Kim, J., Bellani, M.A., Camerini-Otero, R.D., 2014. Integrated transcriptome analysis of mouse spermatogenesis. BMC Genomics 15, 39. https://doi.org/10.1186/1471-2164-15-39

Masly, J.P., Jones, C.D., Noor, M.A.F., Locke, J., Orr, H.A., 2006. Gene transposition as a cause of hybrid sterility in Drosophila. Science 313, 1448–1450. https://doi.org/10.1126/science.1128721

Mayr, E., 1963. Animal Species and Evolution. Belknap Press of Harvard University Press.

McDonough, Y., Ruzicka, F., Connallon, T., 2024. Reconciling theories of dominance with the relative rates of adaptive substitution on sex chromosomes and autosomes. Proc. Natl. Acad. Sci. U. S. A. 121, e2406335121. https://doi.org/10.1073/pnas.2406335121

Mihola, O., Trachtulec, Z., Vlcek, C., Schimenti, J.C., Forejt, J., 2009. A mouse speciation gene encodes a meiotic histone H3 methyltransferase. Science 323, 373–375. https://doi.org/10.1126/science.1163601

Morgan, A.P., Gatti, D.M., Najarian, M.L., Keane, T.M., Galante, R.J., Pack, A.I., Mott, R., Churchill, G.A., de Villena, F.P.-M., 2017. Structural Variation Shapes the Landscape of Recombination in Mouse. Genetics 206, 603–619. https://doi.org/10.1534/genetics.116.197988

Morimoto, K., Numata, K., Daitoku, Y., Hamada, Y., Kobayashi, K., Kato, K., Suzuki, H., Ayabe, S., Yoshiki, A., Takahashi, S., Murata, K., Mizuno, S., Sugiyama, F., 2020. Reverse genetics reveals single gene of every candidate on Hybrid sterility, X Chromosome QTL 2 (Hstx2) are dispensable for spermatogenesis. Sci. Rep. 10, 9060. https://doi.org/10.1038/s41598-020-65986-y

Mukaj, A., Piálek, J., Fotopulosova, V., Morgan, A.P., Odenthal-Hesse, L., Parvanov, E.D., Forejt, J., 2020. Prdm9 Intersubspecific Interactions in Hybrid Male Sterility of House Mouse. Mol. Biol. Evol. 37, 3423–3438. https://doi.org/10.1093/molbev/msaa167

Muller, H.J., 1942. Isolating Mechanisms, Evolution and Temperature., in: Biol. Symp. 6; 71-125.

Myers, S., Bowden, R., Tumian, A., Bontrop, R.E., Freeman, C., MacFie, T.S., McVean, G., Donnelly, P., 2010. Drive against hotspot motifs in primates implicates the PRDM9 gene in meiotic recombination. Science 327, 876–879. https://doi.org/10.1126/science.1182363

Nachman, M.W., Payseur, B.A., 2012. Recombination rate variation and speciation: theoretical predictions and empirical results from rabbits and mice. Philos. Trans. R. Soc. Lond. B. Biol. Sci. 367, 409–421. https://doi.org/10.1098/rstb.2011.0249

Naveira, H.F., 1998. The genetics of hybrid male sterility in Drosophila. Endless Forms 330–338.

Neale, M.J., Pan, J., Keeney, S., 2005. Endonucleolytic processing of covalent protein-linked DNA double-strand breaks. Nature 436, 1053–1057. https://doi.org/10.1038/nature03872

Orr, H.A., 1995. The population genetics of speciation: the evolution of hybrid incompatibilities. Genetics 139, 1805–1813. https://doi.org/10.1093/genetics/139.4.1805

Orr, H.A., 1993. Haldane's rule has multiple genetic causes. Nature 361, 532–533. https://doi.org/10.1038/361532a0

Orr, H.A., Presgraves, D.C., 2000. Speciation by postzygotic isolation: forces, genes and molecules. BioEssays News Rev. Mol. Cell. Dev. Biol. 22, 1085–1094. https://doi.org/10.1002/1521-1878(200012)22:12<1085::AID-BIES6>3.0.CO;2-G

Osoegawa, K., Tateno, M., Woon, P.Y., Frengen, E., Mammoser, A.G., Catanese, J.J., Hayashizaki, Y., de Jong, P.J., 2000. Bacterial artificial chromosome libraries for mouse sequencing and functional analysis. Genome Res. 10, 116–128.

Parvanov, E.D., Petkov, P.M., Paigen, K., 2010. Prdm9 controls activation of mammalian recombination hotspots. Science 327, 835. https://doi.org/10.1126/science.1181495

Payseur, B.A., Krenz, J.G., Nachman, M.W., 2004. Differential patterns of introgression across the X chromosome in a hybrid zone between two species of house mice. Evol. Int. J. Org. Evol. 58, 2064–2078. https://doi.org/10.1111/j.0014-3820.2004.tb00490.x

Phadnis, N., Orr, H.A., 2009. A single gene causes both male sterility and segregation distortion in Drosophila hybrids. Science 323, 376–379. https://doi.org/10.1126/science.1163934

Phifer-Rixey, M., Nachman, M.W., 2015. Insights into mammalian biology from the wild house mouse Mus musculus. eLife 4, e05959. https://doi.org/10.7554/eLife.05959

Presgraves, D.C., 2013. Hitchhiking to speciation. PLoS Biol. 11, e1001498. https://doi.org/10.1371/journal.pbio.1001498

Presgraves, D.C., 2008. Sex chromosomes and speciation in Drosophila. Trends Genet. TIG 24, 336–343. https://doi.org/10.1016/j.tig.2008.04.007

Presgraves, D.C., 2003. A fine-scale genetic analysis of hybrid incompatibilities in Drosophila. Genetics 163, 955–972. https://doi.org/10.1093/genetics/163.3.955

Royo, H., Polikiewicz, G., Mahadevaiah, S.K., Prosser, H., Mitchell, M., Bradley, A., de Rooij, D.G., Burgoyne, P.S., Turner, J.M.A., 2010. Evidence that meiotic sex chromosome inactivation is essential for male fertility. Curr. Biol. CB 20, 2117–2123. https://doi.org/10.1016/j.cub.2010.11.010

Schilthuizen, M., Giesbers, M.C.W.G., Beukeboom, L.W., 2011. Haldane's rule in the 21st century. Heredity 107, 95–102. https://doi.org/10.1038/hdy.2010.170

Schmekel, K., Daneholt, B., 1995. The central region of the synaptonemal complex revealed in three dimensions. Trends Cell Biol. 5, 239–242. https://doi.org/10.1016/s0962-8924(00)89017-0

She, J.X., Bonhomme, F., Boursot, P., Thaler, L., Catzeflis, F., 1990. Molecular phylogenies in the genus Mus: Comparative analysis of electrophoretic, scnDNA hybridization, and mtDNA RFLP data. Biol. J. Linn. Soc. 41, 83–103. https://doi.org/10.1111/j.1095-8312.1990.tb00823.x

Skarnes, W.C., Rosen, B., West, A.P., Koutsourakis, M., Bushell, W., Iyer, V., Mujica, A.O., Thomas, M., Harrow, J., Cox, T., Jackson, D., Severin, J., Biggs, P., Fu, J., Nefedov, M., de Jong, P.J., Stewart, A.F., Bradley, A., 2011. A conditional knockout resource for the genome-wide study of mouse gene function. Nature 474, 337–342. https://doi.org/10.1038/nature10163

Slegtenhorst-Eegdeman, K.E., de Rooij, D.G., Verhoef-Post, M., van de Kant, H.J., Bakker, C.E., Oostra, B.A., Grootegoed, J.A., Themmen, A.P., 1998. Macroorchidism in FMR1 knockout mice is caused by increased Sertoli cell proliferation during testicular development. Endocrinology 139, 156–162. https://doi.org/10.1210/endo.139.1.5706

Smagulova, F., Brick, K., Pu, Y., Camerini-Otero, R.D., Petukhova, G.V., 2016. The evolutionary turnover of recombination hot spots contributes to speciation in mice. Genes Dev. 30, 266–280. https://doi.org/10.1101/gad.270009.115

Smagulova, F., Gregoretti, I.V., Brick, K., Khil, P., Camerini-Otero, R.D., Petukhova, G.V., 2011. Genome-wide analysis reveals novel molecular features of mouse recombination hotspots. Nature 472, 375–378. https://doi.org/10.1038/nature09869

Storchová, R., Gregorová, S., Buckiová, D., Kyselová, V., Divina, P., Forejt, J., 2004. Genetic analysis of X-linked hybrid sterility in the house mouse. Mamm. Genome Off. J. Int. Mamm. Genome Soc. 15, 515–524. https://doi.org/10.1007/s00335-004-2386-0

Tarsounas, M., Morita, T., Pearlman, R.E., Moens, P.B., 1999. RAD51 and DMC1 form mixed complexes associated with mouse meiotic chromosome cores and synaptonemal complexes. J. Cell Biol. 147, 207–220. https://doi.org/10.1083/jcb.147.2.207

Teeter, K.C., Thibodeau, L.M., Gompert, Z., Buerkle, C.A., Nachman, M.W., Tucker, P.K., 2010. The variable genomic architecture of isolation between hybridizing species of house mice. Evol. Int. J. Org. Evol. 64, 472–485. https://doi.org/10.1111/j.1558-5646.2009.00846.x

The Dutch-Belgian Fragile X Consortium, 1994. Fmr1 knockout mice: a model to study fragile X mental retardation. Cell 78, 23–33.

Ting, C.T., Tsaur, S.C., Wu, M.L., Wu, C.I., 1998. A rapidly evolving homeobox at the site of a hybrid sterility gene. Science 282, 1501–1504. https://doi.org/10.1126/science.282.5393.1501

Truett, G.E., Heeger, P., Mynatt, R.L., Truett, A.A., Walker, J.A., Warman, M.L., 2000. Preparation of PCR-quality mouse genomic DNA with hot sodium hydroxide and tris (HotSHOT). BioTechniques 29, 52, 54. https://doi.org/10.2144/00291bm09

Tucker, P.K., Sage, R.D., Warner, J., Wilson, A.C., Eicher, E.M., 1992. Abrupt cline for sex chromosomes in a hybrid zone between two species of mice. Evol. Int. J. Org. Evol. 46, 1146–1163. https://doi.org/10.1111/j.1558-5646.1992.tb00625.x

Turelli, M., Orr, H.A., 2000. Dominance, epistasis and the genetics of postzygotic isolation. Genetics 154, 1663–1679. https://doi.org/10.1093/genetics/154.4.1663

Turelli, M., Orr, H.A., 1995. The dominance theory of Haldane's rule. Genetics 140, 389–402. https://doi.org/10.1093/genetics/140.1.389

Turner, J.M.A., 2015. Meiotic Silencing in Mammals. Annu. Rev. Genet. 49, 395–412. https://doi.org/10.1146/annurev-genet-112414-055145

Turner, J.M.A., 2007. Meiotic sex chromosome inactivation. Dev. Camb. Engl. 134, 1823–1831. https://doi.org/10.1242/dev.000018

Valiskova, B., Gregorova, S., Lustyk, D., Šimeček, P., Jansa, P., Forejt, J., 2022. Genic and chromosomal components of Prdm9-driven hybrid male sterility in mice (Mus musculus). Genetics 222, iyac116. https://doi.org/10.1093/genetics/iyac116

Vyskočilová, M., Trachtulec, Z., Forejt, J., Piálek, J., 2005. Does geography matter in hybrid sterility in house mice? Biol. J. Linn. Soc. Volume 84, Issue 3.

Wang, L., Valiskova, B., Forejt, J., 2018. Cisplatin-induced DNA double-strand breaks promote meiotic chromosome synapsis in PRDM9-controlled mouse hybrid sterility. eLife 7, e42511. https://doi.org/10.7554/eLife.42511

Waterston, R.H., Lindblad-Toh, K., Birney, E., Rogers, J., Abril, J.F., Agarwal, P., Agarwala, R., Ainscough, R., Alexandersson, M., An, P., Antonarakis, S.E., Attwood, J., Baertsch, R., Bailey, J., Barlow, K., Beck, S., Berry, E., Birren, B., Bloom, T., Bork, P., Botcherby, M., Bray, N., Brent, M.R., Brown, D.G., Brown, S.D., Bult, C., Burton, J., Butler, J., Campbell, R.D., Carninci, P., Cawley, S., Chiaromonte, F., Chinwalla, A.T., Church, D.M., Clamp, M., Clee, C., Collins, F.S., Cook, L.L., Copley, R.R., Coulson, A., Couronne, O., Cuff, J., Curwen, V., Cutts, T., Daly, M., David, R., Davies, J., Delehaunty, K.D., Deri, J., Dermitzakis, E.T., Dewey, C., Dickens, N.J., Diekhans, M., Dodge, S., Dubchak, I., Dunn, D.M., Eddy, S.R., Elnitski, L., Emes, R.D., Eswara, P., Eyras, E., Felsenfeld, A., Fewell, G.A., Flicek, P., Foley, K., Frankel, W.N., Fulton,

L.A., Fulton, R.S., Furey, T.S., Gage, D., Gibbs, R.A., Glusman, G., Gnerre, S., Goldman, N., Goodstadt, L., Grafham, D., Graves, T.A., Green, E.D., Gregory, S., Guigó, R., Guyer, M., Hardison, R.C., Haussler, D., Hayashizaki, Y., Hillier, L.W., Hinrichs, A., Hlavina, W., Holzer, T., Hsu, F., Hua, A., Hubbard, T., Hunt, A., Jackson, I., Jaffe, D.B., Johnson, L.S., Jones, M., Jones, T.A., Joy, A., Kamal, M., Karlsson, E.K., Karolchik, D., Kasprzyk, A., Kawai, J., Keibler, E., Kells, C., Kent, W.J., Kirby, A., Kolbe, D.L., Korf, I., Kucherlapati, R.S., Kulbokas, E.J., Kulp, D., Landers, T., Leger, J.P., Leonard, S., Letunic, I., Levine, R., Li, J., Li, M., Lloyd, C., Lucas, S., Ma, B., Maglott, D.R., Mardis, E.R., Matthews, L., Mauceli, E., Mayer, J.H., McCarthy, M., McCombie, W.R., McLaren, S., McLay, K., McPherson, J.D., Meldrim, J., Meredith, B., Mesirov, J.P., Miller, W., Miner, T.L., Mongin, E., Montgomery, K.T., Morgan, M., Mott, R., Mullikin, J.C., Muzny, D.M., Nash, W.E., Nelson, J.O., Nhan, M.N., Nicol, R., Ning, Z., Nusbaum, C., O'Connor, M.J., Okazaki, Y., Oliver, K., Overton-Larty, E., Pachter, L., Parra, G., Pepin, K.H., Peterson, J., Pevzner, P., Plumb, R., Pohl, C.S., Poliakov, A., Ponce, T.C., Ponting, C.P., Potter, S., Quail, M., Reymond, A., Roe, B.A., Roskin, K.M., Rubin, E.M., Rust, A.G., Santos, R., Sapojnikov, V., Schultz, B., Schultz, J., Schwartz, M.S., Schwartz, S., Scott, C., Seaman, S., Searle, S., Sharpe, T., Sheridan, A., Shownkeen, R., Sims, S., Singer, J.B., Slater, G., Smit, A., Smith, D.R., Spencer, B., Stabenau, A., Stange-Thomann, N., Sugnet, C., Suyama, M., Tesler, G., Thompson, J., Torrents, D., Trevaskis, E., Tromp, J., Ucla, C., Ureta-Vidal, A., Vinson, J.P., Von Niederhausern, A.C., Wade, C.M., Wall, M., Weber, R.J., Weiss, R.B., Wendl, M.C., West, A.P., Wetterstrand, K., Wheeler, R., Whelan, S., Wierzbowski, J., Willey, D., Williams, S., Wilson, R.K., Winter, E., Worley, K.C., Wyman, D., Yang, S., Yang, S.-P., Zdobnov, E.M., Zody, M.C., Lander, E.S., 2002. Initial sequencing and comparative analysis of the mouse genome. Nature 420, 520–562. https://doi.org/10.1038/nature01262

Wojtasz, L., Cloutier, J.M., Baumann, M., Daniel, K., Varga, J., Fu, J., Anastassiadis, K., Stewart, A.F., Reményi, A., Turner, J.M.A., Tóth, A., 2012. Meiotic DNA double-strand breaks and chromosome asynapsis in mice are monitored by distinct HORMAD2-independent and -dependent mechanisms. Genes Dev. 26, 958–973. https://doi.org/10.1101/gad.187559.112

Wu, C.-I., Ting, C.-T., 2004. Genes and speciation. Nat. Rev. Genet. 5, 114–122. https://doi.org/10.1038/nrg1269

Yang, F., Wang, P.J., 2009. The Mammalian synaptonemal complex: a scaffold and beyond. Genome Dyn. 5, 69–80. https://doi.org/10.1159/000166620

Zhang, F., Zhang, Y., Lv, X., Xu, B., Zhang, H., Yan, J., Li, H., Wu, L., 2019. Evolution of an X-Linked miRNA Family Predominantly Expressed in Mammalian Male Germ Cells. Mol. Biol. Evol. 36, 663–678. https://doi.org/10.1093/molbev/msz001

Zickler, D., Kleckner, N., 2023. Meiosis: Dances Between Homologs. Annu. Rev. Genet. 57, 1–63. https://doi.org/10.1146/annurev-genet-061323-044915

Zickler, D., Kleckner, N., 2015. Recombination, Pairing, and Synapsis of Homologs during Meiosis. Cold Spring Harb. Perspect. Biol. 7, a016626. https://doi.org/10.1101/cshperspect.a016626

Zickler, D., Kleckner, N., 1999. Meiotic chromosomes: integrating structure and function. Annu. Rev. Genet. 33, 603–754. https://doi.org/10.1146/annurev.genet.33.1.603